Title

Electronic Structure Theory for Radicaloid Systems and Intermolecular Interactions

Permalink

https://escholarship.org/uc/item/2j85c1vr

Author

Kurlancheek, Westin

Publication Date

2011

Peer reviewed|Thesis/dissertation

Electronic Structure Theory for Radicaloid Systems and Intermolecular Interactions

by

Westin Kurlancheek

A dissertation submitted in partial satisfaction of the
requirements for the degree of
Doctor of Philosophy

in

Chemistry

in the

Graduate Division
of the
University of California, Berkeley

Committee in charge:
Professor Head-Gordon, Chair
Professor William H. Miller
Professor Jhih-Wei Chu

Spring 2011

Electronic Structure Theory for Radicaloid Systems and Intermolecular Interactions

Abstract

Electronic Structure Theory for Radicaloid Systems and Intermolecular Interactions

by

Westin Kurlancheek

Doctor of Philosophy in Chemistry

University of California, Berkeley

Professor Head-Gordon, Chair

A radical molecule contains one or more electrons that are unpaired. A radicaloid may be defined as a molecule in which there are that are partially unpaired. As a result, the electronic structure of the radicaloid can be quite complicated for a variety of reasons. For a singlet biradicaloid, the singlet and triplet wavefunction can be quite close energetically which can lead to problems when trying to describe the system with a single determinant. The simplest solution to this problem is to allow the wavefunction to break spin-symmetry in order to get a lower energy. Unfortunately this action can lead to wavefunctions that are no longer eigenfunctions of the $\langle S^2 \rangle$ operator.

In the second chapter we investigate a distannyne which has a biradicaloid resonance structure. By examining the orbital Hessian, it is discovered that the spin-symmetric solution is a saddle-point in wavefunction space and is structurally different than the spin-polarized solution. We then increase the complexity of the model system and see that the spin-symmetric solution is only a minimum for the exact experimental system and not for a simplified model system in which bulky organic substituents are replaced by simpler phenyl groups. Therefore, the breaking of spin-symmetry is absolutely critical in the small model systems and the full substituents play a non-trivial role.

However, the breaking of the spin-symmetry can have consequences for physical quantities when correlated methods are used. At the point of spin polarization or unrestriction the orbital Hessian will have one eigenvalue which is zero. Since the relaxed density matrix in correlated methods like Second-Order Møller-Plesset theory (MP2) depend on the inverse of the Hessian, at the unrestriction point this quantity will be undefined. Some unphysical artifacts are identified as a direct consequence of this fact. First, discontinuities in first order molecular properties such as the dipole moment are seen at the geometries associated with unrestriction. Second, the relaxed density matrix itself fails to be N-representable, with natural orbital occupation numbers less than zero and greater than one. Therefore, it is desirable to use a method that is not dependent on the inverse of the Hessian like orbital optimized MP2 (O2).

Another system which requires the use of orbital optimization is a neutral soliton on a polyacetylene chain. In this system, the Hartree-Fock reference suffers from severe spin-polarization making the wavefunction physically unreasonable unless a very sophisticated

treatment of electron correlation is used to correct this problem. Originally, it was found that computationally expensive methods like CCSD(T) and CASSCF could adequately describe small model chain but not the full system. The O2 method is found to be an dramatic improvement over traditional MP2 which can be feasibly applied to polyenyl chains long enough to characterize the soliton. It is also discovered that density functionals are generally inadequate in describing the half-width of the soliton.

Finally, the last chapter takes a slightly different perspective and focuses on the addition of correlation energy to a successful energy decomposition analysis based on absolutely localized molecular orbitals. It is discovered that the resulting new method can adequately describe systems with dispersive intermolecular interactions and large amounts of charge transfer. This scheme is then applied to the water dimer systems and it is found that all of the intermolecular interactions similar in size with the electrostatic interaction being the largest and the dispersive interaction being the smallest. This method is also contrasted with other EDA schemes.

To those who did what was considered wrong in order to do what they knew was right.

Contents

Bibliography   **88**

List of Figures

List of Tables

Acknowledgments

Throughout the journey that we call graduate school, I have had some invaluable help from excellent people, and I would like to take this space to thank them. First and foremost I would need to thank Keith Lawler. Keith has been a mentor for me ever since I first stepped foot on the UC Berkeley campus. Keith was my sponsor when I first came here for visiting weekend and he has literally been helping me ever since that time. From helping me get started with a copy of Q-Chem to helping me create an effective outline for this thesis, Keith has constantly been willing to help me with anything work-related or not and I am truly grateful. I would also like to thank my other longtime office mate Eric Sundstrom. Eric, much like Keith, has always been willing to help me debug code in late night sessions and more over Eric has been a good friend throughout my time here in grad school. Of course, the journey to becoming a doctor would not have been possible without my advisor Martin Head-Gordon. Martin is a constant source of brilliant ideas and insightful criticism. Even during the times where I have been frustrated with any given project, Martin would have unique ability to inject new life into a stale project and reignite my interest in the investigation. Martin's attention to detail and rigor has prepared me well for moving on into my career. I would especially like to thank Martin for being supportive of my move from academia to the realm of science policy. In talking to other students making the same transition, I hear horror stories of advisors not being supportive and I am truly thankful that Martin has always giving me his full support in my future endeavors.

On a more personal level I would like to thank my friends and family for always being there for me. Although the questions of 'So how many papers do you need to graduate?' got a little tiresome, my family has always been positive force during my Ph.D. Since both of my parents are not scientists, they have provided invaluable training in trying to fully explain high-level science, a skill that I will be useful in science policy. I would also like the thank my girlfriend LeighAnn who is living proof that the people at metal shows are awesome. Knowing that I will be able to spend more time with her has provided a nice bit of extra motivation to power through the writing process.

Chapter 1

Introduction

1.1 Quantum Mechanics

Toward the turn of the 20th century, several physics experiments started to yield unexpected results. [1, 2, 3, 4] Based on the theories of classical physics, these empirical results could not be explained or reasoned but could be repeated. It became abundantly clear that a new theory was necessary to describe the inherent physics of matter at the atomic level. From the dual realization that particles are also waves and that quantities are quantized, came the new theory of Quantum Mechanics.[5, 6, 7, 8, 9, 10, 11, 12, 13, 14, 15] These two disparate concepts provide a mathematical framework in which to study small systems. The resulting equation for the quantum mechanical energy in a time-independent system is the time-independent Schrödinger equation, where the energy is the eigenvalue of the Hamiltonian total energy operator

$$\hat{H}|\Psi\rangle = E|\Psi\rangle \tag{1.1}$$
$$\hat{H} = \hat{T} + \hat{V} \tag{1.2}$$

The Hamiltonian includes operator expressions for the potential energy, $\hat{V}$, and the kinetic energy, $\hat{T}$. If the focus is shifted to systems that include a nucleus and electrons, which would be classified as systems that chemists would care about, the kinetic energy operator would include terms accounting for the motion of electrons and the nucleus. The potential energy would include interactions between electrons and the nucleus, electrons and electrons, and multiple nuclei. The following equation is the molecular Hamiltonian for the time-independent Schrödinger equation in atomic units.

$$\hat{H} = -\sum_{i=1}^{N} \frac{1}{2}\nabla_i^2 - \sum_{A=1}^{M} \frac{1}{2M_A}\nabla_A^2 - \sum_{i=1}^{N}\sum_{A=1}^{M} \frac{Z_A}{r_{iA}} + \sum_{j>i}^{N} \frac{1}{r_{ij}} + \sum_{B>A}^{M} \frac{Z_A Z_B}{R_{AB}} \tag{1.3}$$

In this previous equation the letters $A, B, \ldots$ refer to nuclear quantities and $i, j, \ldots$ refer to electronic quantities. The first two terms refer to the kinetic energy of the electrons and the nucleus respectively. The third term refers to the Coulomb attraction between the nucleus and the electrons. The final two terms describe the same particle charge repulsion from electrons and nuclei respectively.

The Born-Oppenheimer approximation simplifies the time-independent Schrödinger equation so that the electronic variables and the nuclear variables are fully separated.[16] A qualitative justification for neglecting the direct influence of the nucleus on the surrounding electrons is dependent on the difference in mass between the electron and the particles in the nucleus. The mass of a proton or a neutron is about 2000 times more massive than an electron. To a good approximation, the electrons move much faster than the nucleons. Therefore, the electrons are moving in the field of the nuclei. Furthermore, the nuclei can be thought of as fixed with respect to the motion of the electrons. This approximation greatly simplifies equation 1.3 to only the electronic hamiltonian which includes the electron kinetic energy, nuclear-electron attraction, and electron-electron repulsion.

$$\hat{H}_{el} = -\sum_i \frac{1}{2}\nabla_i^2 - \sum_i \sum_A \frac{Z_A}{r_{iA}} + \sum_i \sum_{j>i} \frac{1}{r_{ij}} \tag{1.4}$$

$$\hat{H}_{el}\Psi_{el} = E_{el}\Psi_{el} \tag{1.5}$$

The eigenvalue equation 1.5 gives the electronic energy and the electronic wavefunction for a given system of clamped nuclei and electrons. Solving this equation is the purpose of quantum chemistry, specifically the field of electronic structure theory. In order to solve this equation generally, the wavefunction must accommodate an arbitrary number of electrons, N. However, it is extremely difficult to solve for the large number of degrees of freedom inherent in systems with a large N. It would therefore be ideal to represent the total N electron wavefunction as a product of 1-electron wavefunctions. These 1-electron wavefunctions contain both a spatial component and a spin angular momentum component and are commonly referred to as spin orbitals.

$$\chi_i(r_1) = \psi_i(r_1)\alpha(\omega_1)$$
$$\chi_i(r_1) = \psi_i(r_1)\beta(\omega_1) \tag{1.6}$$

Furthermore, the spin angular momentum functions of the spin orbital are characterized by the variable ω_1 and are also orthonormal. Therefore the inner product of an alpha spin orbital and a beta spin orbital is zero.

$$\langle\alpha|\alpha\rangle = 1$$
$$\langle\beta|\beta\rangle = 1$$
$$\langle\alpha|\beta\rangle = 0. \tag{1.7}$$

The spatial wavefunctions depend on the position variable r_1, and are further approximated as the linear combinations of atomic orbitals. These atomic orbitals, $\phi_\mu(r_1)$, are optimized to capture specific properties or to have other convenient properties.

$$\psi_i(r_1) = \sum_\mu c_{\mu i}\phi_\mu(r_1). \tag{1.8}$$

It should be noted that the Roman letters, i, will be used to refer to the molecular orbital (MO) indices and the Greek letters, μ, will be used to refer to the atomic orbital indices.

Since these orbitals may contain electrons, the total wavefunction made up of orbitals must reflect the physical properties of electrons. Specifically, since electrons are fermions, the

total wavefunction must be anti-symmetric under exchange of parameters. This constraint is known as the Pauli Exclusion Principle and has the following property,[17]

$$|\chi_1(r_1)\chi_2(r_2)...\rangle = -|\chi_1(r_2)\chi_2(r_1)...\rangle. \tag{1.9}$$

When trying to encapsulate the Pauli Exclusion Principle within a mathematical construct, it becomes clear that a simple direct product will not create the appropriate anti-symmetry relation. In order to ensure this relation, a determinant of the spin orbitals is formed. Thanks to the properties of determinants, the Pauli Exclusion Principle will be satisfied by definition. This specific determinant is called a Slater Determinant, and the multi-electron wavefunction follows.[18, 19]

$$
\begin{aligned}
|\Psi_{HF}(r_1, r_2, \ldots, r_N)\rangle &= |\chi_1(r_1), \chi_2(r_2), \ldots, \chi_N(r_N)\rangle \\
&= \frac{1}{\sqrt{N!}}
\begin{vmatrix}
\chi_1(r_1) & \chi_2(r_1) & \cdots & \chi_N((r_1) \\
\chi_1(r_2) & \chi_2(r_2) & \cdots & \chi_N(r_2) \\
\vdots & \vdots & \ddots & \vdots \\
\chi_1(r_N) & \chi_2(r_N) & \cdots & \chi_N(r_N)
\end{vmatrix}
\end{aligned} \tag{1.10}
$$

Since our wavefunction only includes products of one-electron orbitals, there are no electron-electron correlations as will be evident in the following section. Correlations can be included in the wavefunction through the inclusion of some additional Slater Determinants for instance through the use of perturbation theory. Some of these techniques will be examined in the following sections.

1.2 Ab Initio Quantum Mechanics

1.2.1 Hartree-Fock Theory

One of the simplest approximations is the mean-field approximation which assumes that an electron only interacts with the mean-field created from the charge density of the other electrons.[20, 21, 22, 23, 24] This approximation is also called the Hartree-Fock approximation and is the backbone of Hartree-Fock theory (HF). Within this approximation the energy can be solved as the expectation value of the electronic Hamiltonian in the basis of the N-electron Slater Determinant.

$$
\begin{aligned}
E_{HF} &= \langle \Psi_{HF}|\hat{H}|\Psi_{HF}\rangle \\
E_{HF} &= \sum_i^{occ} \langle \chi_i|\hat{h}|\chi_i\rangle + \frac{1}{2}\sum_i^{occ}\sum_j^{occ} \left[\langle \chi_i\chi_j|\frac{1}{r_{ij}}|\chi_i\chi_j\rangle - \langle \chi_i\chi_j|\frac{1}{r_{ij}}|\chi_j\chi_i\rangle \right]
\end{aligned} \tag{1.11}
$$

The MO coefficients from equation 1.8 will be optimized using the variational theorem [25] in order to obtain the lowest possible energy and HF wavefunction. The major constraint on the HF wavefunction is that the individual orbitals are orthonormal, $\langle \chi_i|\chi_j\rangle = \delta_{ij}$. In electronic structure theory, the inner product of two functions is known as an overlap. The overlap matrix in the AO basis is defined thusly,

$$S_{\mu\nu} = \langle \phi_\mu(r)|\phi_\nu(r)\rangle. \tag{1.12}$$

Due to the constraint on the molecular orbitals in HF theory, the overlap matrix in the MO basis will simply be the identity matrix.

The Hartree Fock wavefunction in the MO basis contains spin orbitals that are either occupied or unoccupied (virtual). For example, in a finite AO basis of size K with N electrons, the HF wavefunction will contain N occupied orbitals (denoted $i, j, k...$) and $2K - N$ virtual orbitals (denoted $a, b, c, ...$). The number of basis functions K needs to be greater than $N/2$ so that there are enough orbitals to accommodate for each orbital to containing two electrons. The lowest energy orbitals will be the orbitals that the electrons will fill first and by definition the occupied orbitals. As the number of basis functions becomes larger than $N/2$, the Hartree-Fock energy becomes lower and the quality of the MOs increases. If the number of basis functions approaches infinity, then the Hartree-Fock energy will be the lowest possible energy for a single Slater Determinant for the given electronic Hamiltonian. This energy is referred to as the Hartree-Fock limit and the basis set is known as the complete basis set (CBS). For other methods like perturbation theory, the corresponding energy in the CBS is referred to as the CBS limit.

The main advantage of HF theory is that the multi-electron Schrödinger equation reduces to a coupled set of one electron eigenvalue equations for each spin orbital:

$$\hat{f}(r_1)\chi_1(r_1) = \varepsilon_i\chi_i(r_1)$$

$$\hat{f}(r_1) = \hat{h}(r_1) + \sum_{j \neq i} \hat{J}_j(r_1) - \sum_{j \neq i} \hat{K}_j(r_1)$$

$$\hat{h}(r_1) = -\sum_i \frac{1}{2}\nabla_i^2 - \sum_i \sum_A \frac{Z_A}{r_{iA}}$$

$$\hat{J}_j(r_1)\chi_i(r_1) = \left[\int dr_2 |\chi_j(r_2)|^2 \frac{1}{r_{ij}} \right] \chi_i(r_1)$$

$$\hat{K}_j(r_1)\chi_i(r_1) = \left[\int dr_2 \chi_j(r_2) \frac{1}{r_{ij}} \chi_i(r_2) \right] \chi_j(r_1) \tag{1.13}$$

In order to get the lowest possible HF energy, the eigenvalue equations are solved for each orbital, the orbitals are updated, and then the eigenvalue equations are solved again. This process continues until the energy is the lowest and the orbitals are no longer changing. This procedure is known as a self-consistent field approach for optimizing orbitals and obtaining the lowest possible HF energy. The resulting orbitals are used to form a Slater Determinant, which become the HF wavefunction. The HF wavefunction is used as a starting point or a reference for many higher-order methods.

In these higher-order methods, including perturbative methods, the Fock operator, $\hat{f}$, is used as the zeroth-order Hamiltonian. The expectation value of the Fock operator in the canonical HF MO basis will be a diagonal matrix because of the orthonormal MO orbitals with the diagonal values being,

$$\varepsilon_{pq} = \langle \chi_p(r_1) | \hat{f}(r_1) | \chi_q(r_1) \rangle$$

$$\varepsilon_p = \varepsilon_{pq}\delta_{pq}. \tag{1.14}$$

It should be noted that the HF energy is not simply the addition of all of the occupied orbital

energies, $E_{HF} \neq \sum\limits_{i=1}^{occ} \varepsilon_i$. This formulation would be double counting the the coulomb, $\hat{J}_j(r_1)$, and exchange, $\hat{K}_j(r_1)$, quantities since each orbital energy contains the full value. Therefore a factor of $\frac{1}{2}$ needs to be placed in front of these quantities to ensure the correct HF energy.

In the AO basis the Fock matrix is no longer a diagonal matrix and each element can be written as follows,

$$F_{\mu\nu} = \langle \phi_\mu(r_1)|\hat{f}(r_1)|\phi_\nu(r_1)\rangle. \tag{1.15}$$

The Fock matrix in a finite AO basis forms a generalized eigenvalue equation referred to as the Roothaan equations.[26] These equations are necessary for solving for the HF energy and wavefunction.

$$\mathbf{FC} = \mathbf{SC}\varepsilon$$

$$\sum_\nu F_{\mu\nu}c_{\nu i} = \varepsilon_i \sum_\nu S_{\mu\nu}c_{\nu i} \tag{1.16}$$

The generalized eigenvector equation is to solve for the MO coefficients, however the dependence of the Fock matrix on the MO coefficients requires the HF energy to be solved self-consistently. This generalized eigenvalue expression is ideal for a computer to solve and is why they are used in this field. When the spatial portion of the spin orbitals are allowed to be different for both the allowed spin eigenfunctions, then a different set of equations known as the Pople-Nesbet equations are solved.[27] This slightly different method is referred to as unrestricted Hartree-Fock (UHF). If the spatial portions are different for an α and β spin, then this is known as spin-polarization and the need for doing this type of procedure will be discussed further in the following sections.

1.2.2 Orbital Rotations

The procedure to optimize the orbitals for Hartree-Fock involves the repeated diagonalization of a matrix or through making an initial guess and updating by a series of unitary orbital rotations. These orbital rotations are the unitary mixing of the existing orbitals amongst each other. An orbital rotations can be represented by a unitary matrix, $\mathbf{U}$, with the special property that the adjoint is the inverse.

$$\mathbf{UU}^\dagger = \mathbb{1} \tag{1.17}$$

Since the orbital rotation unitary matrix is real-valued, it is classified as an orthogonal matrix. Orthogonal matrices have the convenient property of maintaining the inner product such that,

$$\mathbf{M}^\dagger\mathbf{M} = (\mathbf{UM})^\dagger(\mathbf{UM}) = \mathbf{M}^\dagger\mathbf{U}^\dagger\mathbf{UM} = \mathbf{M}^\dagger\mathbf{M}. \tag{1.18}$$

One way to form an unitary matrix is to take the exponential of an anti-Hermitian matrix:

$$\mathbf{U} = e^\theta$$
$$\theta^\dagger = -\theta. \tag{1.19}$$

If the matrix $\mathbf{U}$ is an orthogonal matrix, then the anti-Hermitian matrix becomes anti-symmetric and the adjoint becomes the transpose.

Another property of orthogonal matrices is that the full set of eigenvalues must have a modulus of 1, meaning that the eigenvalues lie on the unit circle. One possible way to view this property is to think of an orthogonal matrix as a rotation through any given angle between element p into element q, θ_{pq}. In fact all rotation matrices that are norm-preserving are orthogonal matrices. The two-dimension representation of this anti-symmetric matrix is as follows,

$$\theta = \left[\begin{array}{cc} 0 & \theta_{pq} \\ -\theta_{pq} & 0 \end{array} \right].$$

Exponentiating this matrix yields a rotation matrix, a specific type of orthogonal matrix.

$$\mathbf{G}(\theta_{\mathbf{pq}}) = e^\theta = \left[\begin{array}{cc} cos(\theta_{pq}) & sin(\theta_{pq}) \\ -sin(\theta_{pq}) & cos(\theta_{pq}) \end{array} \right]$$

For the general N-dimensional Givens rotation, the two-by-two rotation matrix is projected into a N-dimensional identity matrix.[28] Therefore the non-zero elements of the Givens rotation matrix will be the diagonal elements, and the elements containing elements consisting of entirely i and j.

$$
\begin{aligned}
g_{nn} &= 1 \quad \text{for } n \neq i, j \\
g_{ii} &= \cos \theta_{pq} \\
g_{jj} &= \cos \theta_{pq} \\
g_{ij} &= \sin \theta_{pq} \\
g_{ji} &= -\sin \theta_{pq} \quad \text{for } i > j
\end{aligned}
\tag{1.20}
$$

Any $N \times N$ rotation matrix can be represented as a product of a maximal $n(n-1)/2$ number of Givens rotation matrices. The resulting rotation matrix will also be an orthogonal matrix.

$$\mathbf{U} = \prod_p^N \prod_q^N \mathbf{G}(\theta_{\mathbf{pq}}). \tag{1.21}$$

The main advantage to these rotation matrices is that they can simplify orbital optimization problems in quantum chemical methods. The MO coefficients can always be decomposed as the product of the guess MO coefficients and an orthogonal matrix.

$$\mathbf{C} = \mathbf{C}_0 \prod_i^{N_{iter}} \mathbf{U}_i \tag{1.22}$$

The MO coefficients can be optimized through a series of orbital rotations from the initial guess MO coefficients. After a series of rotation iterations the MO coefficients will be optimized within a certain threshold with respect to the energy. Procedurally, orbital optimizations are performed until the gradient of the energy with respect to the MO coefficients reaches zero or some near zero threshold.

$$\frac{\partial E}{\partial \theta_{pq}} = \sum_\mu \left[\frac{\partial E}{\partial C_{\mu p}} C_{\mu q} - \frac{\partial E}{\partial C_{\mu q}} C_{\mu p} \right] = 0 \tag{1.23}$$

There are three types of orbital rotations that can be applied to the MO coefficients. The first type is a rotation between virtual orbitals. Since the Hartree-Fock energy is a modified sum of the occupied orbital energies and not dependent on the virtual orbital energies, the Hartree-Fock energy must be invariant to virtual-virtual rotations. The second type of orbital rotation is between occupied orbitals. However, if any two occupied orbitals are mixed, the individual orbital energies might change, but the overall sum of the two orbital energies would remain unchanged. Expanding this concept to the entire occupied space, any rotations between occupied orbitals will leave the Hartree-Fock energy unchanged, meaning that the Hartree-Fock energy is invariant to occupied-occupied rotations. Therefore the only type of orbital rotations that need to be considered are the occupied-virtual orbital rotations.

$$
\begin{aligned}
\frac{\partial E}{\partial \theta_{ij}} &= 0 \\
\frac{\partial E}{\partial \theta_{ab}} &= 0 \\
\frac{\partial E}{\partial \theta_{ia}} &= 0 \quad \text{only when the energy is converged} \quad (1.24)
\end{aligned}
$$

There are a variety of mathematical techniques used to solve this optimization problem in a computationally feasible manner[29, 30]. However, the discussion of these techniques is not within the scope of this thesis.

1.2.3 The Need for Spin-Unrestriction

The need to allow for different spatial orbitals corresponding to the α and β spins becomes apparent when examining the dissociation of H_2 in a minimal basis. At equilibrium, the system can be described accurately while maintaining that the two spin orbitals need to only differ by the spin eigenfunction and not the spatial component.

$$
\begin{aligned}
\chi_1(r_1) &= \psi_1(r_1)\alpha(\omega) \\
\chi_2(r_1) &= \psi_1(r_1)\beta(\omega) \\
\chi_3(r_2) &= \psi_2(r_2)\alpha(\omega) \\
\chi_4(r_2) &= \psi_2(r_2)\beta(\omega) \quad (1.25)
\end{aligned}
$$

In this system, ψ_1 describes the bonding σ_g orbital while ψ_2 represents the σ_u^* anti-bonding orbital at equilibrium. As the distance between the two hydrogen atoms increases, the spatial orbitals will eventually become degenerate, each representing a doubly occupied orbital on each of the hydrogen atoms. However, this is not the lowest energy dissociation behavior nor does it represent the symmetry of the system. Physically, this would accurately describe the heterolytic cleavage of the hydrogen molecule into a proton and a hydride. The lowest possible energy would be to have an electron on each of the the two hydrogens with the freedom to smoothly transition from the singlet of the equilibrium ground state to the infinitely separated singlet. For this to occur, the spin-symmetry must be broken so that the α electron and the β electron can reside in separate spatial orbitals.

$$
\chi_1(r_1) = \psi_{1\alpha}(r_1)\alpha(\omega)
$$

$$\chi_2(r_1) \quad = \quad \psi_{1\beta}(r_1)\beta(\omega) \tag{1.26}$$

The splitting of a spatial orbital into two separate spatial orbitals for each spin will allow for the correct asymptotic behavior in that there in an electron on each hydrogen atom. However, this splitting has the consequence that the wavefunction will no longer be a pure singlet. In fact, at dissociation the physical picture that emerges is that there is a superposition of the singlet and the triplet, since these two spin states are degenerate at $1/\mathrm{R}_{HH} \to \infty$, with the expectation value of the spin squared operator being equal to one.

$$\langle \Psi_{UHF}|\hat{S}^2|\Psi_{UHF}\rangle = \frac{1}{2} \cdot 0(0+1) + \frac{1}{2} \cdot 1(1+1) = 1 \tag{1.27}$$

Therefore obtaining the lowest variational energy creates a wavefunction that incorporates the unphysical triplet.

It should be noted that the if the initial guess for any system is a restricted wavefunction, the converged wavefunction will not become spin-polarized unless something perturbs the wavefunction away from this symmetry.[24] This symmetry becomes a problem because the restricted Hartree-Fock wavefunction is typically a saddle point when bonds are broken as in the H_2 example, being a minimum with respect to all coordinates except for the distortion or spin-polarization coordinate. If researchers are using a quantum chemical programs like a 'black box' method, then they would not suspect that a restricted calculation might be a saddle point. The resolution is that a converged restricted HF solution should be subject to stability analysis. If the derivative of the Hartree-Fock energy with respect to the orbital rotations (θ_{ai}) is zero and the second derivative has positive semidefinite character, then the solution is a local minimum and not a saddle point. [31]

$$\frac{\partial E_{HF}}{\partial \theta_{ai}} \quad = \quad 0$$
$$\frac{\partial^2 E_{HF}}{\partial \theta_{ai}\partial \theta_{bj}} \quad = \quad \mathcal{H}$$
$$\mathcal{H} \quad = \quad V\epsilon V^\dagger$$
$$\epsilon_{ij} \quad = \quad h_i\delta_{ij}$$
$$h_i \quad > \quad 0 \tag{1.28}$$

When one of the eigenvalues of the Hessian matrix is negative, signifying a saddle point, then a step should be taken in the direction of the corresponding eigenvector. This step usually breaks spin-symmetry and perturbs the system away from the restricted solution. Since this procedure is typically at least doubles the cost relative to the SCF optimization procedure, it should only be used in situations where it would be necessary. These situations include multi-reference systems, biradicaloid species, and stretched bonds.[32, 33, 34] An example of a multi-reference system would be polyacetylene or the distannyne containing complexes to be studied in depth in later chapters. In fact every except the last chapter contains a complex that requires the use of the procedure outlined above.

1.3 Density Functional Theory

It is also possible to form an energy from an electron density instead of trying to directly solve for the wavefunction. This strategy became known as Density Functional Theory (DFT) and allows the inclusion of electron correlation without a significant increase in computational cost versus HF theory.

The general concept of density functional theory is to replace the complicated wavefunction with a simpler quantity like the electron density. Essentially we replace an N-electron wavefunction with 3N spatial coordinates with a quantity that only has only has 3 spatial components. The electron density can be derived from a wavefunction as follows,

$$n(r_1) = N \int \cdots \int |\Psi(r_1, r_2, \ldots, r_N)|^2 ds_1 dr_2 \ldots dr_N \tag{1.29}$$

where ds refers to the spin coordinate with dr referring to the spatial coordinates. In order to accomplish this task, we take advantage of the Hohenberg-Kohn (HK) theorem which states that there is a 1-to-1 correspondence between the electron density and the ground state Hamiltonian, $\Psi \leftrightarrow n$, along with the fact that the electron density can be used to solve for the ground state energy. [35]

$$
\begin{aligned}
E\left[n\right] &\equiv \varepsilon\left[\Psi\left[n\right]\right] = F_{HK}\left[n\right] + \int dr v_{ext} n \\
F_{HK}\left[n\right] &\equiv \langle \Psi\left[n\right] | \hat{T} + \hat{V}_{ee} | \Psi\left[n\right] \rangle \\
\hat{T} &= -\sum_{i=1}^{N} \frac{1}{2} \nabla_i^2, \\
\hat{V}_{ee} &= \frac{1}{2} \sum_{i \neq j=1}^{N} \frac{1}{|r_i - r_j|}
\end{aligned} \tag{1.30}
$$

It is noted that atomic units are used which implies that $m_e = e^2 = \hbar = 1$. The HK theorem also states that the ground state density can be obtained variationally, i.e. the variational principle can be applied to the ground state density. [35]

$$
\begin{aligned}
E_0 &\leq E[\tilde{n}] \\
E_0 &= \min_{n \to N} \left(F[n] + \int n(r) V_{Ne} dr \right) \\
F[n(r)] &= T[n(r)] + J[n(r)] + E_{ncl}[n(r)]
\end{aligned} \tag{1.31}
$$

In the above equation the $\tilde{n}$ is used to represent a trial density. For the universal functional, F, the electron-electron interaction term is split into two parts: the classical Coulomb interaction, J, and the non-classical portion, E_{ncl}.[36] The non-classical term includes a self-interaction correction, exchange (from the anti-symmetry of fermions), and electron correlation effects. Unfortunately, the explicit form for both the kinetic energy functional and the electron-electron interaction functional are unknown, and will arguably never be known. Therefore, there is a need for approximations to take this theory from an intellectual curiosity to a usable computational approach.

Taking inspiration from HF theory, the first approximation will be to create a density based on a system of N non-interacting electrons.[37] For this type of system it is known that the exact wavefunction corresponding to this fictitious potential (uncharged fermions) is a Slater determinant.

$$\Theta_S = \frac{1}{\sqrt{N!}} \begin{vmatrix} \phi_1(r_1) & \phi_2(r_1) & \cdots & \phi_N((r_1) \\ \phi_1(r_2) & \phi_2(r_2) & \cdots & \phi_N(r_2) \\ \vdots & \vdots & \ddots & \vdots \\ \phi_1(r_N) & \phi_2(r_N) & \cdots & \phi_N(r_N) \end{vmatrix} \tag{1.32}$$

By making this approximation the exact kinetic energy is the same as the Hartree-Fock kinetic energy.

$$T_S = -\frac{1}{2} \sum_i^N \langle \phi_i | \nabla^2 | \phi_i \rangle \tag{1.33}$$

From this wavefunction a density can be constructed via equation 1.29. However the non-interacting kinetic energy and the interacting kinetic energy are in principle slightly different so a correction is needed. The non-classical electron interactions need to be accounted for as well. The functional designed by Kohn and Sham accomplishes this goal by grouping these two terms into a exchange-correlation in term in the following functional, F.[37]

$$\begin{aligned} F[n(r)] &= T_S[n(r)] + J[n(r)] + E_{XC}[n(r)] \\ E_{XC}[n] &\equiv (T[n] - T_S[n]) + (E_{ee}[n] - J[n]) = T_C[n] + E_{ncl}[n] \end{aligned} \tag{1.34}$$

It is noted that the above equation does not contain any approximations merely a splitting of the kinetic energy into a (presumably dominant) non-interacting part and an interacting correction. If the exact form of the E_{XC} functional was known, then DFT would be an exact theory with no more development necessary. However, the exact form of this functional is not known and like the full Hohenberg-Kohn functional, F_{HK}, is unlikely ever to be known. Therefore it is necessary to formulate an approximate exchange-correlation functional to closely model the true exchange-correlation function.

One popular approximation is to model the exchange and correlation via the uniform electron gas. In order to solve for the local exchange exactly, it is necessary to split the E_{XC} into an exchange term and a correlation term. This approximation leads to a local potential for the exchange portion of E_{XC} and when combined with the analogous treatment of correlation for the uniform electron gas is termed the local density approximation (LDA). Functionals based solely on this approximation tend to yield acceptably accurate results for systems like metal solids and some other regular periodic systems.[38] Essentially, any time the total electron density resembles a uniform electron gas these functionals perform well. However, on most molecular systems, which do not resemble the uniform electron gas, these functionals perform quite poorly with very large errors.[39]

The next level of complexity for functionals includes information about the gradient of the local density. This scheme is referred to as the generalized gradient approximation (GGA).[40] Since the gradient contains information about more than just the local density, the method tends to perform better for realistic molecular systems.[41]

However, the exact exchange for any given molecular system is known, and it is simply the Hartree-Fock exchange. Therefore it could be prudent to mix in an amount of exact exchange with the exchange functionals developed using the GGA approach.[42] Functionals containing this mixture of exact and approximate exchange are called hybrid functionals. Currently, the most popular density functional, B3LYP, is a hybrid functional.[42] All hybrid functionals contain semi-empirical parameters used to determine the amount of exact exchange and the amount of approximate exchange to include. These methods thrive because of a convenient cancellation of errors present in various terms used to form the E_{XC} functional. The B3LYP functional has proven to have generally very satisfying chemical accuracy when used to optimize a molecular geometry.[43] The performance of B3LYP for relative energies is also quite good with errors typically reduced by a factor of about two versus GGA's. When this is still inadequate, B3LYP is frequently used to find a suitable geometry and other *ab initio* methods are used to calculate relative energetics.

However, there are still problems with these hybrid functionals when there is a long-range interaction, specifically when an odd electron bond is dissociated. When the H_2^+ molecule is cleaved, the correct limit would be a degenerate ground state with an electron on either H atom having the exact same energy. Yet, when this limit is calculated with the B3LYP functional, the result is an unphysical half-electron on each H atom associated with a spurious energy lowering of ~50 kcal/mol. The unphysicality is a result of using an approximate exchange functional which leads to incomplete cancellation of the classical self-interaction and thus electrons partially interacting with themselves.[44, 45] One strategy to deal with this unfortunate consequence is to further decompose the exchange into long-range exchange and short-range exchange.[46, 47] Short-range exchange would be of the local variety whereas the long-range exchange would be the exact Hartree-Fock exchange. The range-separated functionals come much closer to capturing the correct dissociation limit for H_2^+ since at dissociation there would be only exact exchange.

Once the choice of E_{XC} functional has been made, the vaunted Kohn-Sham equations can be solved for the orbitals akin to the Roothaan equations for HF:[37]

$$
\begin{aligned}
\hat{h}_S(r)\,\phi_i(r) &= \varepsilon_i \phi_i(r), \\
\hat{h}_S(r) &\equiv -\frac{1}{2}\nabla^2 + \int \frac{\rho(r_2)}{r_{12}} dr_2 + \frac{\partial E_{XC}}{\partial \rho} - \sum_A^M \frac{Z_{1A}}{r_{1A}}
\end{aligned}
\tag{1.35}
$$

These equations are solved self-consistently in order to minimize the energy functional in equation 1.34.

One problem with density functional theory is that there is not a way to systematically improve the exchange-correlation functional. Therefore for difficult electronic structure problems, there would be no way to improve potentially poor results. Also since the exchange-correlation functional is approximate, the ground state energy can be lower than the exact ground state energy. In order to mitigate both of these issues, we will return our focus to wavefunction-based methods and the ability to add in correlation in a systematic fashion.

1.4   Correlated Methods

1.4.1   Møller-Plesset Perturbation Theory

Hartree-Fock theory is often qualitatively correct but it does not have quantitative accuracy. This inaccuracy stems from the fact that HF is a mean-field theory and does not incorporate instant electron-electron interactions. The difference between the exact and the restricted Hartree-Fock energy is referred to as the correlation energy in a given basis.

$$E_{exact} - E_{RHF} = E_{corr} \tag{1.36}$$

The exact wave function can be solved for by creating a wavefunction out of all of the possible determinants in a given basis. [48, 49, 50, 51] This method is known as full configuration interaction (FCI) and scales factorially. Yet, when compared to the mean-field energy, the correlation energy is quite small with the mean-field energy being about 95-99% of the exact energy.[24] Without including correlation energy it is impossible to capture some fundamental interactions like dispersion interactions. And in chemical transformations, such as bond-breaking, the correlation contribution does not cancel. For even $H_2 \rightarrow 2H$, there is an error of $\sim$25 kcal/mol.

One less computationally expensive way to capture the correlation is through the use of low order perturbation theory. This theory is based on the partitioning of the Hamiltonian and the Taylor expansion of the eigenvectors and eigenvalues. The Hamiltonian is split into a known part $\hat{H}_0$ and a small correction $\hat{H}_1$ which together make the total Hamiltonian difficult to solve. The known portion of the Hamiltonian is referred to as such because the eigenvalues and eigenvectors are required to be known.

$$\begin{aligned} \hat{H}|\Phi_i\rangle &= (\hat{H}_0 + \hat{H}_1)|\Phi_i\rangle = \epsilon_i|\Phi_i\rangle \\ \hat{H}_0|i\rangle &= E_i^{(0)}|i\rangle \end{aligned} \tag{1.37}$$

In order to keep track of order, a parameter λ will be introduced to the power series of the eigenfunctions and eigenvalues along with the small correction $\hat{H}_1$.

$$\begin{aligned} (\hat{H}_0 + \lambda\hat{H}_1)|\Phi\rangle &= \epsilon|\Phi\rangle \\ \epsilon_i &= E_i^{(0)} + \lambda E_i^{(1)} + \lambda^2 E_i^{(2)} + \dots \\ |\Phi_i\rangle &= |i^{(0)}\rangle + \lambda|i^{(1)}\rangle + \lambda^2|i^{(2)}\rangle + \dots \end{aligned} \tag{1.38}$$

Expanding the entire Schrödinger equation in terms of the order parameter yields,

$$\begin{aligned} (\hat{H}_0 + \lambda\hat{H}_1)(|i^{(0)}\rangle + \lambda|i^{(1)}\rangle + \lambda^2|i^{(2)}\rangle + \dots) \\ = (E_i^{(0)} + \lambda E_i^{(1)} + \lambda^2 E_i^{(2)} + \dots) \quad (|i^{(0)}\rangle + \lambda|i^{(1)}\rangle + \lambda^2|i^{(2)}\rangle + \dots). \end{aligned} \tag{1.39}$$

Since the eigenvectors are orthonormal, the first-order energy can be solved for by left projecting equation 1.39 by the zeroth order wavefunction.

$$E_i^{(1)} = \langle i^{(0)}|\hat{H}_1|i^{(0)}\rangle \tag{1.40}$$

If instead all of terms with a first order order parameter are gathered for equation 1.39, then the resulting equation is,

$$\hat{H}_0|i^{(1)}\rangle + \hat{H}_1|i^{(0)}\rangle = E_i^{(0)}|i^{(1)}\rangle + E_i^{(1)}|i^{(0)}\rangle. \tag{1.41}$$

By gathering terms and inserting the resolution of the identity for the zeroth-order wavefunction, $|k^{(0)}\rangle$, the first-order wavefunction can be defined as,

$$|i^{(1)}\rangle = \sum_{k \neq i} \frac{\langle k^{(0)}|V|i^{(0)}\rangle}{E_i^{(0)} - E_k^{(0)}}|i^{(0)}\rangle. \tag{1.42}$$

In continuing this procedure the second-order energy is defined as:

$$E_i^{(2)} = \sum_{k \neq i} \frac{|\langle k^{(0)}|V|i^{(0)}\rangle|^2}{E_i^{(0)} - E_k^{(0)}} \tag{1.43}$$

Although the above equations are simply formalism, one can see that this method would be perfectly suited to the electronic correlation problem. The correlation energy is difficult to obtain and important, yet it is small in magnitude compared to the non-interacting energy. Therefore, we will set the Fock operator as the zeroth-order Hamiltonian in this case and the difference between the full Hamiltonian and the Fock operator as the perturbing Hamiltonian.

$$\begin{aligned} \hat{H}_0 &= \hat{F} \\ \hat{H}_1 &= \hat{H} - \hat{F} \end{aligned} \tag{1.44}$$

By choosing the Fock operator as the zeroth-order Hamiltonian, the wavefunction becomes the eigenvalues and eigenfunctions of this operator. From equation 1.14, it is known that these quantities are the molecular orbitals and their corresponding energies. It should be noted that for our purposes, we only care about the corrections to the energy and not the corrections to the wavefunction. The zeroth-order energy would then be the sum of all of the orbital energies. The first order energy correction is the correction from the sum of all orbital energies to the Hartree-Fock energy.

$$E_i^{(0)} + E_i^{(1)} = \langle\Psi_{HF}|\hat{F}|\Psi_{HF}\rangle + \langle\Psi_{HF}|\hat{H} - \hat{F}|\Psi_{HF}\rangle = \langle\Psi_{HF}|\hat{H}|\Psi_{HF}\rangle = E_{HF} \tag{1.45}$$

To obtain an energy correction to the Hartree-Fock energy, the power series must be taken to second order. Therefore plugging in the specific elements into equation 1.43 along with using the Slater-Condon rules yields the Møller-Plesset Second-Order energy expression:[52, 24]

$$E_{MP2} = \frac{1}{4}\sum_{i,j}^{occ}\sum_{a,b}^{virt} \frac{|\langle\Psi_{ref}|\hat{H}|\Psi_{ij}^{ab}\rangle|^2}{\varepsilon_i + \varepsilon_j - \varepsilon_a - \varepsilon_b} = \frac{1}{4}\sum_{i,j}^{occ}\sum_{a,b}^{virt} \frac{|\langle ij||ab\rangle|^2}{\varepsilon_i + \varepsilon_j - \varepsilon_a - \varepsilon_b}. \tag{1.46}$$

The double bar integrals are the anti-symmetric two-electron integrals:

$$\langle ij||ab\rangle = \langle\chi_i(r_1)\chi_j(r_2)|\frac{1}{r_{12}}|\chi_a(r_1)\chi_b(r_2)\rangle - \langle\chi_i(r_1)\chi_j(r_2)|\frac{1}{r_{12}}|\chi_b(r_1)\chi_a(r_2)\rangle. \tag{1.47}$$

The MP2 energy expression scales with the fifth-order of system size, meaning that MP2 is more computationally demanding than both HF and DFT. There are several ways to reduce the scaling of this method. One of the more successful methods is to split the MP2 energy into same spin and opposite spin portions and then individually rescaling them.[53]

$$E_{MP2} = c_{SS}E_{SS} + c_{OS}E_{OS}$$

$$E_{SS} = \sum_{i,j}^{occ} \sum_{a,b}^{virt} \frac{\langle ij|ab\rangle\langle ab|ij\rangle - \langle ij|ab\rangle\langle ab|ji\rangle}{\varepsilon_i + \varepsilon_j - \varepsilon_a - \varepsilon_b}$$

$$E_{OS} = \sum_{i,j}^{occ} \sum_{a,b}^{virt} \frac{\langle ij|ab\rangle\langle ab|ij\rangle}{\varepsilon_i + \varepsilon_j - \varepsilon_a - \varepsilon_b} \tag{1.48}$$

Since the opposite-spin term is generally larger than the same-spin term, we can further approximate the MP2 energy by omitting the same-spin-term and scaling the opposite spin term.[54] Furthermore, the opposite-spin term can be approximated by a Laplace transform along with decomposing the four-center integrals into three-center integrals via the insertion of the resolution of the identity. These approximations reduce the formal scaling to only fourth order.[54]

However it must be noted that this perturbation method (like all such methods) is not variational, meaning that this energy could be lower than the exact energy. This can occur when there is a small HOMO-LUMO gap, because the denominator approaches zero yielding a very large energy. Also the MP2 energy only includes double excitations from the reference Slater determinant, $|\Psi_{ij}^{ab}\rangle$, whereas the exact energy would include all possible excitations in a given basis.

A further variant of MP2 theory is used in conjunction with DFT by using the KS orbitals instead of the HF orbitals.[55] The MP2-like correlation energy is added to the functional energy after the energy has converged and is commonly referred to as 'double-hybrids.' [56] Double-hybrid functionals can be formally justified using Gorling-Levy perturbation theory.[55] These functionals are promising because the results are generally improved from hybrid functionals and these functionals correctly describe dispersion complexes because of the MP2-like correction.[57] As will be demonstrated later, this theory has the same problems that are inherent in MP2 theory.

1.4.2 Coupled Cluster Theory

In order to approximate higher-level excitations a slightly different approach will be taken by exponentiating an excitation operator. This theory is known as Coupled Cluster theory (CC).[58, 59, 60, 61, 62, 63, 64, 65, 66, 67]

Coupled-Cluster theory is based on an exponential ansatz for the excitation operator. When the excitation operator acts on the reference Slater determinant (usually the Hartree-Fock reference), it produces a linear combination of excited Slater determinants.

$$|\Psi_{CCSD}\rangle = e^{\hat{T}}|\Psi_{HF}\rangle \tag{1.49}$$

The excitation operator, which will be further referred to as the cluster operator, can be conveniently expressed as a sum of creation and annihilation operators with a corresponding

amplitude. The cluster operator is split into levels of excitation, i.e. $\hat{T}_2$ will contain all possible doubles excitations. When the $\hat{T}_1$ operates on the HF reference it produces all of the singly excited Slater determinants.

$$
\begin{aligned}
\hat{T} &= \hat{T}_1 + \hat{T}_2 + \hat{T}_3 + \cdots \\
\hat{T}_1 &= \sum_i \sum_a t_i^a \hat{a}_i \hat{a}_a^\dagger
\end{aligned}
\tag{1.50}
$$

The most popular cluster operator usually contains the singles and doubles excitations (CCSD) because the inclusion of higher excitations is computationally demanding. All other possible excitations are then taken as products of the doubles and singles operator.[66] This fact can be seen by taking the Taylor series of the exponential.

$$
\begin{aligned}
\hat{T} &= \hat{T}_1 + \hat{T}_2 \\
e^T &= 1 + \hat{T}_1 + \hat{T}_2 + \frac{\hat{T}_1^2}{2} + \hat{T}_1 \hat{T}_2 + \frac{\hat{T}_1^3}{3!} + \cdots
\end{aligned}
\tag{1.51}
$$

In order to solve for the amplitudes in the cluster operator the following set of equations must be solved.

$$
\begin{aligned}
\langle \Psi_{HF} | e^{-\hat{T}} \hat{H} e^{\hat{T}} | \Psi_{HF} \rangle &= E_{CCSD} \\
\langle \Psi_S | e^{-\hat{T}} \hat{H} e^{\hat{T}} | \Psi_{HF} \rangle &= 0 \\
\langle \Psi_D | e^{-\hat{T}} \hat{H} e^{\hat{T}} | \Psi_{HF} \rangle &= 0
\end{aligned}
\tag{1.52}
$$

In the above equation Ψ_S is all singly excited determinants and Ψ_D is all doubly excited determinants. Once these equations are solved self-consistently the CCSD energy is obtained. By approximating all of the higher excitations as products of the lower excitations, this method does a very good job of capturing large amounts of the correlation energy.[68]

The CCSD method also does not suffer from the degeneracy problems inherent in the MP2 denominator. However, the major drawback of this theory is the computational cost that scales as sixth-order with system size coupled with the fact that this method is iterative (in order to solve the non-linear eq. 1.52), unlike MP2 theory. CC theory can be used as a benchmark, but it is too computationally demanding to use on large molecules or systems where large basis sets are crucial. Indeed, to achieve so-called 'chemical accuracy' CCSD itself is still generally inadequate and at least a perturbative estimate of the additional energy lowering due to triple substitutions is needed.[69] This is most commonly done via the CCSD(T) method. [70, 71]

Brueckner orbitals

These orbitals are defined to be the orbitals for which a single determinant has the largest overlap with the FCI wavefunction.[72, 73] Since the FCI wavefunction is impossible to solve except for small molecules, the Brueckner orbitals are also defined as the orbitals that yield a zero singles coefficient. These orbitals can be obtained by rotating the orbitals self-consistently until the singles coefficient is zero or by simply removing all of the singles determinants before the calculation and then minimizing the energy without them. In the

context of CC theory, Brueckner orbitals are optimized so that the singles excitation operator is zero.[74]

$$\hat{T}_1|\Psi_{BO}\rangle = 0 \tag{1.53}$$

While this optimization could be done with any level of CC theory, the simplest would be CC doubles where the cluster operator is simply the doubles excitation operator.[74] This theory is referred to as Bruecker Doubles (BD) theory and has been shown to yield properties like an aversion to breaking spin-symmetry which can be useful for multi-reference systems, biradicaloid species, and stretched bonds mentioned earlier.[75, 76] Essentially, the main advantage of these orbitals are that they are not HF orbitals and therefore do not have the same problems as HF orbitals. This issue will be crystallized in the later chapters when orbital-optimized MP2 will be used to fix some of the inherent problems of the Hartree-Fock reference.

1.5 Intermolecular Interactions

All of the *ab initio* theories can accurately describe the ground state of a group of molecules. However, it is significantly more difficult to decompose the intermolecular interactions between these molecules, which would be of interest to organic chemists looking to optimize certain interactions. This section will focus on the decomposition of the binding interactions between molecules.

Intermolecular interactions occur between two separated molecular species. There are several different types of interactions that can occur between these two species. Ion-ion, dipole-ion, and dipole-dipole are several types of electrostatic interactions that can occur between two molecules. These interactions involve a localized charge which will only depend on the set distance and orientation between the two molecules. Generally these are the strongest type of intermolecular interactions. These interactions range in strength from 250 kJ/mol for ion-ion interactions all the way down to 2 kJ/mol for weak dipole-dipole interactions.[77] Another way of presenting this point is that these forces do not depend on the field of the other molecule changing and therefore these interactions can be classified as permanent electrostatic interactions. Each of these interactions is dependent on the distance separating the two charges. Ion-ion interactions are the longest range interaction with the potential being proportional to inverse distance, and the ion-dipole potential being proportional to $\frac{1}{r^2}$. The dipole-dipole potential is proportional to $\frac{1}{r^3}$ if the dipoles are stationary, but averages to $\frac{1}{r^6}$ as the dipoles start rotating in the field of each other.[77]

Another interaction between molecules is the repulsive (Pauli) interaction between filled orbitals. This effect aries from the Pauli exclusion principle which mandates that there are only two electrons per spatial orbital.[17] However, as two atoms or molecules get close together, more than two electrons would be occupying similar orbitals which cannot happen because of the Pauli exclusion principle. The energetic consequence of this effect will be known as Pauli repulsion and it is a significant intermolecular effect. This effect is indistinguishable from the permanent electrostatic interaction and will therefore be grouped with it.

The next type of interaction is the dipole-induced dipole interaction. This interaction is based on the fact that a charge will cause the electrons in a different molecule to rearrange so

as to minimize the binding energy. When there is a small energy penalty for rearranging the electrons in a molecule, the molecule is referred to as polarizable. Therefore, this induced electrostatic energy will be referred to as the polarization energy and will generally be smaller in magnitude than the permanent electrostatic energy.[77]

Another type of binding energy is the induced dipole-induced dipole. This type of interaction is purely quantum mechanical and originates from quantum fluctuations in one molecule creating a field, inducing an interaction in the other molecule. London dispersion is another name for this type of dispersive interaction. Both of these potentials are proportional to $\frac{1}{r^6}$. The amount of interaction energy stemming from these interactions are dependent on the size of the two molecules involved. As the two molecules get bigger, the magnitude of these interactions increase significantly and can be larger than electrostatic interactions.

The final type of intermolecular interaction is charge transfer between an electron donor and an electron acceptor. This type of interaction is governed by the Hamiltonian between the donor and the acceptor and the rate can be explicitly calculated through the Generalized Mulliken-Hush theory pioneered by Cave and Newton.[78] This interaction is proportional to e^{-r} and will be the most sensitive to orientation and orbital shape. It should be noted that when the charge transfer interaction is over relatively long distance that DFT methods tend to perform quite poorly.[79]

In order to calculate each of these components a clever partitioning scheme will be used taking advantage of the unique form of the absolutely localized molecular orbitals (ALMO).[80] These orbitals are unique because there is no charge transfers between molecular fragments that are inherent in systems that contain multiple molecules. This partitioning is accomplished by restricting the MOs to be formed solely from the AOs on that particular fragment.

$$
C^{\mu}_{\bullet\ i} =
\begin{bmatrix}
C^{\mu_A}_{\bullet\ i_A} & 0 & 0 & \cdots & 0 \\
0 & C^{\mu_B}_{\bullet\ i_B} & 0 & \cdots & \vdots \\
0 & 0 & C^{\mu_C}_{\bullet\ i_C} & \cdots & \vdots \\
\vdots & \vdots & \vdots & \ddots & \vdots \\
0 & 0 & 0 & \cdots & C^{\mu_F}_{\bullet\ i_F}
\end{bmatrix}
\tag{1.54}
$$

Because of this restriction, the resulting MOs are now non-orthogonal and necessitates the use of the covariant and contravariant Einstein notation. This notation creates a dual-space between the covariant space and contravariant space through making the metric the overlap matrix.[81]

$$
|\phi^i\rangle = \sum_j |\phi_j\rangle (S^{-1})^{ji}
\tag{1.55}
$$

Therefore the following scheme can be used to calculate these intermolecular contributions. If there are two fragments, A and B, then the first step would be to calculate the energy of each fragment separately. Next calculate the one SCF cycle or KS cycle to calculate the HF or DFT energy but do not allow the orbitals to change from the separate calculations. This allows for all of the electrostatic interactions mentioned earlier.

The next step is to allow the orbitals to relax in response to the field created by the fragments. However the restriction of Eq. 1.54 must be maintained in order to restrict any

charge transfer. Therefore, only orbital rotations within each fragment are allowed so as to eliminate any charge transfer interaction. This will allow for the electrons to polarize with the difference between this relaxed ALMO energy and the one step energy being the polarization energy.

Finally the restriction on the orbitals is dropped and the orbitals are allowed to relax to the final SCF/KS orbitals. The difference between the SCF/DFT energy and the relaxed ALMO energy will be the charge transfer energy, the final contribution. In this scheme it is not possible to partition out the dispersive energy or the charge transfer contribution from adding a correlation functional which will be further investigated in chapter 5. All of the energy contributions add together to be equivalent to the binding energy between the two molecules and this will need to be maintained when the correlation energy is incorporated.

1.6   Outline of this Work

1.6.1   Effects of ligands and spin-polarization on the preferred conformation of distannynes

The importance of spin-polarization can be seen when experimental and theoretical evidence has shown that distannynes, RSnSnR, can adopt either a singly bonded or a multiply bonded structure. Within calculations on small models, such as MeSnSnMe, apparently dramatic differences in conformational preference have been reported. We show that these differences arise due to the treatment of spin-polarization in density functional theory (DFT), and review stability analysis; a diagnostic for the need to include spin-polarization. The low-energy singly bonded structure can only be reached when spin polarization is allowed. Additional DFT calculations on PhSnSnPh show that the singly bonded structure is the global minimum, leading to a flat torsional potential. The role of electronic effects is further probed by changing the donor-acceptor properties of R. Implications for the structural preference of experimentally synthesized species are discussed. This chapter has been published in Dalton Transactions.[82]

1.6.2   Violations of N-representability from Spin-Unrestricted Orbitals in Møller-Plesset Perturbation Theory and Related Double-Hybrid Density Functional Theory

At the unrestriction point problems can arise in MP2 theory. By examining the natural orbital occupation numbers, it was discovered that unrestricted Møller-Plesset perturbation theory (MP2) can violate N-representability by having natural occupation numbers greater than 2 or less than 0, even though the energy appears well-behaved. Analytically, this problem stems from the fact that the MP2 effective one-particle density matrix is dependent on the inverse of the orbital hessian matrix (A'). When a molecular system goes through the point where spin-restricted orbitals become unstable to unrestriction, one of the eigenvalues of the A' matrix will become 0, making it a singular matrix, thereby causing problems in the relaxed one-particle density matrix and discontinuities in the first order properties such as nuclear forces and dipole moments. Since the new 'double-hybrid' density functionals also

involve a second-order perturbation expression for correlation using Kohn-Sham orbitals, these functionals also exhibit similar issues near the unrestriction point. The unphysical orbital occupations can be eliminated and the first derivative discontinuities removed by optimizing orbitals with inclusion of the second order correlation energy. Connections to the second derivative discontinuities in Hartree-Fock and Kohn-Sham density functional theory are also discussed. This chapter has been published in Molecular Physics.[83]

1.6.3 Exploring the competition between localization and delocalization of the neutral soliton defect in polyenyl chains with the orbital optimized second order opposite spin method

In a manner similar to Brueckner Orbitals, orbital optimized MP2 is greatly improved over traditional MP2 with the HF reference. Theory and implementation of the analytic nuclear gradient is presented for orbital optimized scaled opposite-spin perturbation theory (O2). Evaluation of the O2 analytical gradient scales with the 4th power of molecular size, like the O2 energy. Since the O2 method permits optimization of the orbitals in the presence of wave-function-based electron correlation, it is suitable for problems where correlation effects determine the competition between localization and delocalization of an odd electron, or hole. One such problem is the description of a neutral soliton defect on an all-trans polyacetylene chain with an odd number of carbon atoms. For this problem, standard density functional theory methods are known to not describe the length of the soliton wave correctly. By contrast, we find that O2 approximately reproduces accurate coupled cluster results for small chains, and can also be applied to larger chains where such calculations are not feasible. Applied to $C_{41}H_{43}$, O2 calculations yield a soliton length of about 9 carbon atoms, which is in reasonable agreement with experimental estimates. These results are compared with a variety of density functional methods, including the ωB97x-D range-separated hybrid. This chapter has been submitted to the Journal of Chemical Physics.

1.6.4 Second order Møller-Plesset energy decomposition analysis for intermolecular interactions with applications to the ethylene dimer, He-BeO complex, and the water dimer

Finally, the principles of MP2 theory are applied to intermolecular interactions so as to capture dispersive interactions and correlated charge transfer. An existing absolutely localized molecular orbital energy decomposition analysis (ALMO EDA) that was defined at the self-consistent field (Hartree-Fock or Kohn-Sham density functional theory) is extended to include non-local correlation at the second order Møller-Plesset (MP2) level. Correlation contributions to frozen density interactions, polarization and charge transfer are individually obtained. This new correlated MP2 EDA is illustrated on the ethylene dimer, He-BeO complex, and water dimer, and shown to be adequately stable with respect to basis set extensions. This chapter will be published in the Journal of Chemical Physics.

Bibliography

[1] M. PLANCK, *Archives Neerlandaises des Sciences Exactes et Naturelles* , 164 (1900).

[2] M. PLANCK, *Archives Neerlandaises des Sciences Exactes et Naturelles* , 55 (1901).

[3] M. PLANCK, *Annalen Der Physik* **6**, 818 (1906).

[4] A. EINSTEIN, *Annalen Der Physik* **1**, 180 (1906).

[5] E. SCHRÖDINGER, *Annalen Der Physik* **77**, 43 (1925).

[6] E. SCHRÖDINGER, *Annalen Der Physik* **79**, 361 (1926).

[7] E. SCHRÖDINGER, *Annalen Der Physik* **79**, 489 (1926).

[8] E. SCHRÖDINGER, *Annalen Der Physik* **79**, 734 (1926).

[9] E. SCHRÖDINGER and V. FOCK, *Zeitschrift Fur Physik* , 808 (1931).

[10] A. KRAMERS and W. HEISIENBERG, *Zeitschrift Fur Physik* **31**, 681 (1925).

[11] W. HEISIENBERG, *Zeitschrift Fur Physik* **31**, 617 (1925).

[12] W. HEISIENBERG, *Zeitschrift Fur Physik* **35**, 557 (1926).

[13] W. HEISIENBERG, *Zeitschrift Fur Physik* , 587 (1933).

[14] P. DIRAC, *Proc. Royal Soc. London* , 621 (1927).

[15] L. DE BROGLIE, *Research on Quantum Theory*, Ann. Phys., 1924.

[16] M. BORN and R. OPPENHEIMER, *Annalen Der Physik* **84**, 457 (1927).

[17] W. PAULI, *Zeitschrift Fur Physik* **31**, 765 (1925).

[18] J. SLATER, *Phys. Rev.* **32**, 339 (1928).

[19] J. SLATER, *Phys. Rev.* **35**, 210 (1928).

[20] D. HARTREE, *Proc. Cambridge Phil. Soc.* **24**, 89 (1928).

[21] D. HARTREE, *Proc. Cambridge Phil. Soc.* **24**, 111 (1928).

[22] D. HARTREE, *Proc. Cambridge Phil. Soc.* **24**, 426 (1928).

[23] V. FOCK, *Comp. Rend. de l'Ac. Sci. de l'URSS* **8**, 295 (1935).

[24] A. SZABO and N. S. OSTLUND, *Modern Quantum Chemistry: Introduction to Advanced Electronic Structure Theory*, Dover Publications, Inc., 1996.

[25] I. LEVINE, *Quantum Chemistry, Fifth Edition*, Prentice Hall, 2000.

[26] C. ROOTHAAN, *Rev. Mod. Phys.* **23**, 69 (1951).

[27] J. POPLE and R. NESBET, *J. Chem. Phys.* **22**, 571 (1954).

[28] M. HEAD-GORDON and J. A. POPLE, *J. Phys. Chem.* **92**, 3063 (1988).

[29] W. PRESS, S. TEUKOLSKY, and W. VETTERLING, *Numerical Recipes: The Art of Scientific Computing, Third Edition*, Cambridge University Press, 2007.

[30] T. VAN VOORHIS and M. HEAD-GORDON, *Mol. Phys.* **100**, 1713 (2002).

[31] H. FUKUTOME, *Progress of Theoretical Physics* **53**, 1320 (1975).

[32] K. PEI and H. LI, *THEOCHEM* **676**, 105 (2004).

[33] K. HOUK, P. LEE, and M. NENDEL, *J. Org. Chem.* **66**, 5517 (2001).

[34] Z. QU, D. ZHANG, C. LIU, and Y. JIANG, *J. Phys. Chem. A* **113**, 7909 (2009).

[35] P. HOHENBERG and W. KOHN, *Phys. Rev. B* **136**, B864 (1964).

[36] W. KOCH and M. HOLTHAUSEN, *A Chemist's Guide to Density Functional Theory*, Wiley-VCH, 2001.

[37] W. KOHN and L. J. SHAM, *Phys. Rev.* **140**, 1133 (1965).

[38] S. KURTH, J. PERDEW, and P. BLAHA, *Int. J. Quantum Chem.* **75**, 889 (1999).

[39] M. ERNZERHOF and G. SCUSERIA, *J. Chem. Phys.* **110**, 5029 (1999).

[40] J. PERDEW and W. YUE, *Phys. Rev. B* **33**, 8800 (1986).

[41] J. PERDEW, J. CHEVARY, S. VOSKO, K. JACKSON, M. PEDERSON, D. SINGH, and C. FIOLHAIS, *Phys. Rev. B* **46**, 6671 (1992).

[42] A. BECKE, *J. Chem. Phys.* **98**, 5648 (1993).

[43] C. BAUSCHLICHER, *Chem. Phys. Lett.* **246**, 40 (1995).

[44] B. G. JOHNSON, C. A. GONZALES, P. M. W. GILL, and J. A. POPLE, *Chem. Phys. Lett.* **221**, 100 (1994).

[45] S. KUMMEL and J. P. PERDEW, *Mol. Phys.* **101**, 1363 (2003).

[46] T. KORZDORFER, S. KUMMEL, and M. MUNDT, *J. Chem. Phys.* **129**, 014110 (2008).

[47] J. D. CHAI and M. HEAD-GORDON, *J. Chem. Phys.* **128**, 084106 (2008).

[48] P. LÖWDIN, *Adv.Chem. Phys.* **2**, 207 (1959).

[49] B. ROOS and P. SIEGBAHN, *Methods of Electronic Structure Theory, 3rd Ed.*, Plenum, 1977.

[50] C. Bauschlicher and P. Taylor, *J. Chem. Phys.* **85**, 2779 (1986).

[51] P. Knowles and N. Handy, *Chem. Phys. Lett.* **111**, 315 (1984).

[52] C. Møller and M. S. Plesset, *Phys. Rev.* **46**, 618 (1934).

[53] S. Grimme, *J. Chem. Phys.* **118**, 9095 (2003).

[54] Y. Jung, R. Lochan, A. Dutoi, and M. Head-Gordon, *J. Chem. Phys.* **121**, 9793 (2004).

[55] A. Gorling and M. Levy, *Phys. Rev. A* **50**, 196 (1994).

[56] S. Grimme, *J. Chem. Phys.* **124** (2006).

[57] T. Benighaus, R. A. DiStasio, Jr., R. C. Lochan, J.-D. Chai, and M. Head-Gordon, *J. Phys. Chem. A* **112**, 2702 (2008).

[58] J. Čížek, *J. Chem. Phys.* **45**, 4256 (1966).

[59] J. Čížek, *Adv. Chem. Phys.* **14**, 35 (1969).

[60] J. Čížek and J. Paldus, *Int. J. Quantum Chem.* **5**, 359 (1971).

[61] A. C. Hurley, *Electron Correlation in Small Molecules*, Academic Press, London, 1976.

[62] H. J. Monkhorst, *Int. J. Quantum Chem. Symp.* **11**, 421 (1977).

[63] J. A. Pople, R. Krishnan, H. B. Schlegel, and J. S. Binkley, *Int. J. Quantum Chem. Symp.* **14**, 545 (1978).

[64] R. J. Bartlett and G. D. Purvis, *Int. J. Quantum Chem.* **14**, 561 (1978).

[65] G. D. Purvis and R. J. Bartlett, *J. Chem. Phys.* **76**, 1910 (1982).

[66] J. F. Stanton, J. Gauss, J. D. Watts, and R. J. Bartlett, *J. Chem. Phys.* **94**, 4334 (1991).

[67] T. D. Crawford and H. F. Shaefer, *Rev. Comp. Chem.* **14**, 33 (2000).

[68] R. Bartlett, *Annu. Rev. Phys. Chem.* **32**, 359 (1981).

[69] K. Raghavachari, G. Trucks, J. Pople, and M. Head-Gordon, *Chem. Phys. Lett.* **157**, 479 (1989).

[70] Y. Lee, S. Kucharski, and R. Bartlett, *J. Chem. Phys.* **81**, 5906 (1984).

[71] D. Woon and T. Dunning, *J. Chem. Phys.* **100**, 2975 (1994).

[72] K. Brueckner, *Phys. Rev.* **96**, 508 (1954).

[73] R. Nesbet, *Phys. Rev.* **109**, 1632 (1958).

[74] N. Handy, J. Pople, M. Head-Gordon, K. Raghavachari, and G. Trucks, *Chem. Phys. Lett.* **164**, 185 (1989).

[75] W. Allen, D. Horner, R. Dekock, R. Remington, and H. Schaefer, *Chem. Phys.* **133**, 11 (1989).

[76] E. Davidson and W. Borden, *J. Phys. Chem.* **87**, 4783 (1983).

[77] P. Atkins and J. de Paula, *Physical Chemistry*, W. H. Freeman, 2001.

[78] R. Cave and M. Newton, *Chem. Phys. Lett.* **249**, 15 (1996).

[79] T. Yanai, D. Tew, and N. Handy, *Chem. Phys. Lett.* **393**, 51 (2004).

[80] R. Z. Khaliullin, A. T. Bell, and M. Head-Gordon, *J. Chem. Phys.* **128**, 184112 (2008).

[81] M. Head-Gordon, P. Maslen, and C. White, *J. Chem. Phys.* **108**, 616 (1998).

[82] W. Kurlancheek, Y. Jung, and M. Head-Gordon, *Dalton Trans.* , 4428 (2008).

[83] W. Kurlancheek and M. Head-Gordon, *Mol. Phys.* **107**, 1223 (2009).

Chapter 2

Effects of ligands and spin-polarization on the preferred conformation of distannynes

2.1   Introduction

Over the past 9 years, heavier group 14 homologs of alkynes have been experimentally synthesized and characterized, as fully summarized in recent reviews. [1, 2, 3] The first such compound was a lead analog [4], $Ar^*PbPbAr^*$, where $Ar^* = C_6H_3$-2,6(C_6H_2-2,4,6-$(Pr^i)_3)_2$, and Pr^i is an isopropyl group. Its Pb-Pb bondlength, 3.19 Å is actually slightly *longer* than the 2.9 Å or so usually associated with R_3PbPbR_3 compounds. $Ar^*PbPbAr^*$is strongly trans-bent, with a C-Pb-Pb bond angle of 94.3°. Subsequently, a corresponding distannyne, Ar'SnSnAr', (Ar' = C_6H_3-2,6(C_6H_2-2,6-$(Pr^i)_2)_2$ was synthesized and isolated [5] with an SnSn bondlength of 2.67 Å (shorter than the typical 2.8 Å SnSn single bond), and a substantially larger bending angle of 125°. A corresponding digermyne, Ar'GeGeAr', has been structurally characterized [6], which has a GeGe bondlength of 2.29 Å (cf. 2.44 Å for a single bond) with a trans-bending angle of 129°. An analogous disilyne [7] shows a very short SiSi bondlength of 2.06 Å (vs 2.34 Å for a single bond) and a yet larger trans-bending angle of 137°. All isolated compounds have been found to be diamagnetic.

The structural trends going up and down group 14 can be qualitatively rationalized on the basis of a changing balance between the contributing resonance structures shown in Scheme I, which vary between single and triple bonds. For RPbPbR, it appears that resonance form V dominates, while the doubly bonded forms appear to predominate for Si, Ge, and possibly for Sn as well. However, other distannynes have been synthesized which suggest behavior closer to the singly-bonded lead case. The crystal structure of Me₃Me3Si-4-Ar'SnSnAr'-4-SiMe₃ has been solved [8], and shows a significantly longer SnSn bondlength (3.07 Å), and stronger trans-bending effect (angle of 99°). Spectroscopic (^{119}Sn NMR and Mössbauer) studies of $Ar^*SnSnAr^*$suggest that it also adopts the longer bondlength and smaller trans-bending angle [9], although the crystal structure could not be obtained due to poor diffraction. Additionally the solution reactivity of the distannynes (and the corresponding lead species) appears to be lower than the digermynes, based on a comparative

study using the Ar' substituent.[10] This could be consistent with lower contributions from the diradical resonance structure (IV in Scheme 1) for Sn and Pb.
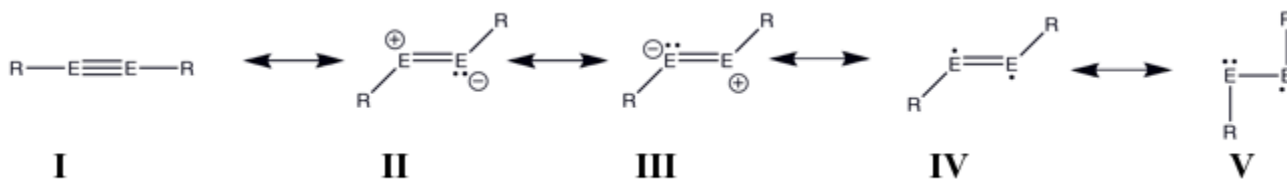
Scheme 2.1: The possible resonance structures for multiply bonded group 14 compounds

The fact that the structural properties of the tin species are sensitive to substituents suggests that electronic and steric effects can play a crucial role in determining such properties. Electronic structure calculations that predate the experiments support this possibility.[11, 12, 13] Bulky substituents can protect a reactive core, and provide electronic stabilization as well, but may impose steric requirements. They can also probe what happens in the absence of such substituents. For example, calculations (e.g. [14])have shown that unsubstituted HEEH compounds display strikingly different structures to the experimentally isolated compounds, including structures with bridged hydrogens. However, for experimentally isolated molecules, it is only for the tin case that two distinct isomeric forms have been isolated to date.

Recent calculations on the tin system support the possibility that Ar'SnSnAr' may in fact exhibit *two* local minima corresponding to singly (**S**) and multiply (**M**) bonded structures.[15] The lower energy of the two isomers is the **M** form, suggesting it should be favored. This would then suggest that crystal packing forces must account for the **S**geometry adopted by Me_3Me3Si-4-Ar'SnSnAr'-4-$SiMe_3$ and implied for $Ar^*SnSnAr^*$. Intriguingly, recent calcualtions on $Ar^*PbPbAr^*$have found that two distinct local minima (both an **S**and a twisted **M** isomer) likewise exist for this compound [16]. In contradiction to the crystal structure [4], the **M**-type isomer is found to be slightly (~ 1 kcal/mol) more stable[16]. It is clear the potential surfaces of these systems are both rich and delicate, and are fertile ground for further study.

Calculations on model systems for the heavier alkyne congeners [17], principally MeEEMe, indicate that the potential surface for MeSnSnMe is very flat with respect to bond-length and angle distortions away from the local minimum corresponding to an **S**-type structure towards an **M**-type geometry. However, the **M** structure does not exist as a local minimum, and indeed the global minimum is a gauche-type structure with a dihedral angle of about 90° (though this will be sterically destabilized with larger substituents). Interestingly, the **S**-type structure is found to have little diradicaloid character, consistent with low reactivity, while calculations at geometries optimized with the bond-length and trans-bending angle constrained to the experimental **M** values, yield significantly higher diradicaloid character, suggesting higher reactivity. This suggests that the reactivity differences seen experimentally between Ar'SnSnAr' and Ar'GeGeAr' could be explained if the tin-compound adopted a **S**-type solution geometry and an **M** geometry for germanium in solution. However, a contradictory set of calculations on MeSnSnMe were reported using apparently similar computational methods [15], where the **M** structure was found to be lower in energy, than the

Sstructure, which was a saddle point. Further effort to clarify the nature of the potential energy surface for both model and synthesized RSnSnR compounds thus appears desirable.

Accordingly, in this paper we discuss several aspects of electronic structure calculations on the distannynes, and report a variety of new calculations on the model system, PhSnSnPh, which should capture the principal through-bond electronic effects of the more complex and bulky Ar*and Ar' substituents. First, we clarify the origin of differences between the two sets of calculations on the MeSnSnMe model [15, 17]. This requires consideration of the role of spin polarization in density functional theory calculations, as in fact one set of calculations allowed for spin-polarization and the other did not. Spin polarization is briefly reviewed in the following section to summarize the key considerations. Second, taking careful account of spin polarization, we then explore the PhSnSnPh model in detail to fully characterize its potential surface, and therefore the main through-bond interactions that are operative in the experimentally synthesized distannynes. Finally we consider the effect of additional changes to the electron-withdrawing and electron donating character of the terminal groups, and compare the results obtained with our models against experimentally characterized molecules.

2.2 Orbital stability and spin polarization in density functional theory calculations

Density functional theory (DFT) in the Kohn-Sham (KS) formalism is the most popular electronic structure method today as it generally yields very good accuracy while requiring little or no more computational effort than mean-field theory [18, 19]. [18, 19]. It represents the density of the real system, $\rho(\{\phi_i\})$, using a single determinant wavefunction $\Phi_0(\{\phi_i\})$ corresponding to a reference system of non-interacting electrons described by the orbitals ϕ_i with the same density. This may be problematical when molecules undergo reactions, breaking bonds and forming new ones, or when they may possess some singlet diradicaloid character. In such electronically near-degenerate cases, present-day exchange correlation functionals are not powerful enough to correctly describe *multi*configurational correlation effects in terms of the orbitals of only a *single* closed shell KS determinant. For example in the simple case of single bond dissociation, the bonding (HOMO) and antibonding (LUMO) orbitals approach degeneracy and so do the two corresponding configurations which have one or the other doubly occupied.

The *only* way in which standard KS-DFT can reasonably describe bond-breaking is to allow spin-polarization of the orbitals. The resulting *unrestricted* KS wavefunction has different spatial orbitals for α and β spin electrons, which correctly describes most separated products ($^3O_2$ is an interesting example). For instance a separated single bond has an α electron on one fragment and a β electron on the other. This avoids the difficult problem of multiple degenerate electronic configurations that arises with restricted orbitals. It introduces spin-contamination in the reference system, but unlike wavefunction theory, this does not necessarily correspond to real spin-contamination. While the benefits of unrestricted orbitals are obvious at the dissociation limit, it is less obvious for partly broken chemical bonds, such as for diradicaloid molecules. Should they be described by orbitals which are

spin-restricted or spin-unrestricted? We advocate *always* allowing the orbitals to unrestrict (spin-polarize) when this yields a lower energy solution, consistent with the variational principle for Kohn-Sham theory [20].

The testing of whether or not energy lowering is possible through spin-polarization is called stability analysis [21, 22, 23]. In practice, the KS orbitals ϕ_i are obtained by solving the self-consistent field (SCF) equations iteratively until the first variation of the energy with respect to orbital mixings is numerically zero. There is no guarantee, however, that the calculated SCF energy is a true local minimum in the orbital space. The converged energy can be a saddle point, and the KS wave function is then said to be unstable. We will focus on the possible instability of the spin-restricted KS orbitals with respect to release of this constraint (unrestriction) since this is directly relevant for singlet diradicaloid molecules such as models of the distannynes. It is denoted as an $R \rightarrow U$ instability and is also called a triplet instability.

Orbital instabilities can be studied by considering response of the energy up to second order, starting from a stationary point, so linear terms vanish:

$$\Delta E = \frac{1}{2}(\mathbf{D}^* \ \mathbf{D}) \begin{pmatrix} \mathbf{A} & \mathbf{B} \\ \mathbf{B}^* & \mathbf{A}^* \end{pmatrix} \begin{pmatrix} \mathbf{D} \\ \mathbf{D}^* \end{pmatrix} \tag{2.1}$$

Here $\mathbf{D}$ is a column vector that describes small mixings of each occupied orbital (i) with each virtual orbital (a), so that:

$$\Phi \cong \Phi_0 + \sum_{ia} D_{ia}\Phi_i^a + \dots \tag{2.2}$$

Φ_i^a denotes the replacement of orbital ϕ_i by ϕ_a. The precise form of the matrices $\mathbf{A}$ and $\mathbf{B}$ is already available in the literature [21, 22, 23] and is not important for our present purposes.

A necessary and sufficient condition for stability (i.e. for ΔE in Eq. 2.1 to be positive for all infinitesimal variations, $\mathbf{D}$) is for the square matrix in eq. 2.1 denoted as Λ, to be positive definite. For real orbitals (and thus real $\mathbf{A}$ and $\mathbf{B}$), the eigenvalues of Λ consist of the union of eigenvalues of the two matrices $\mathbf{A} + \mathbf{B}$ and $\mathbf{A}$ - $\mathbf{B}$. Hence if either of those two matrices is not positive definite, the solution found will be unstable. In particular, the SCF orbitals are unstable to unrestricted spin-polarization if $\mathbf{A} + \mathbf{B}$ has a negative eigenvalue (an $R \rightarrow U$ instability). A negative eigenvalue of $\mathbf{A}$ - $\mathbf{B}$ indicates the (real) SCF orbitals are unstable to variations that introduce a complex component.

In practice, after an SCF calculation is converged, a test for stability is performed by iteratively finding the smallest (least positive) eigenvalue of the matrices $\mathbf{A} + \mathbf{B}$ and $\mathbf{A}$ - $\mathbf{B}$. Each iteration consists of operations basically similar to a step of the SCF cycle itself (forming a Fock-like matrix), and thus the cost of a stability test typically involves a cost that is not greater than the SCF calculation itself. We think it is advisable to routinely perform such a test. If the result indicates an instability, most computational chemistry programs have the ability to distort the SCF solution along the direction of the instability, and then restart the SCF procedure leading to a lower energy solution. This will then give the lowest DFT energy attainable with the given functional, and for this reason should be preferred. While clearly needed for dissociation, there are also some cases where it is known that significantly different stable structures can be obtained in DFT when spin-polarization is allowed [24].

2.3   Computational Methods

All calculations were performed with a development version of the Q-Chem program [25]. In this study, all structures were optimized using DFT with the B3LYP functional [26, 27]. Qualitative differences between DFT and highly correlated wavefunctions have not been observed in previous studies [15], so the decision was made to mostly use DFT for this study. Some additional calculations were performed with the B3PW91 functional [26] to compare with previous work [15]. As discussed in detail above, all DFT calculations at the restricted level were tested for orbital instabilities, and, if detected were re-optimized using unrestricted DFT. Numerical integration was performed with the standard grid 1 (SG1) [28], and test calculations were also performed with larger grids to establish that no significant differences occur for delicate energy differences such as the torsional potential energy scans discussed later.

The 6-31G* basis set was used for all atoms that are not tin in this investigation, which is of medium size. For the tin atoms the CRENBL effective core potential with the CRENBL* basis was used [29]. This removes a krypton core from explicit consideration, while leaving the 3d, 4s, 4p electrons described by (3s3p4d) basis. Some test calculations were also performed using the Huzinaga [433111/433111/43] (spd) all-electron basis set [30] for comparison. An all-electron calculation neglects relativistic effects on the core electrons, which can have a noticeable effect on calculated properties of systems containing heavier elements. On the other hand ECPs themselves contain some intrinsic errors.

The diradicaloid character of several structures is determined by using the perfect pairing method [31, 32]. In this method, we look at the occupation number of the lowest unoccupied molecular orbital in order to determine the percentage of diradical character [33, 34, 35]. If the species is fully diradical, then the LUMO will have an occupation number of 1. Therefore the percentage diradical character is simply the LUMO occupation number multiplied by 100; this procedure has proven useful in comparative studies of diradical character [36]. All perfect pairing calculations were performed taking all valence electrons to define the active space (e.g. 43 pairs for PhSnSnPh).

Localized orbitals are also determined for several structures. The Kohn-Sham energy is invariant to mixing of the occupied amongst themselves, and such mixings may be determined to extremize a measure of orbital locality. We employ the Edmiston-Ruedenberg criterion [37], which maximizes the Coulomb repulsion of all orbitals with themselves (and thereby minimizes the non-classical exchange). Efficient algorithms for this problem are now available [38, 39]. We shall use these orbitals to discuss the chemical bonding that is implied by the KS-DFT calculations.

2.4   Results and Discussion

2.4.1   MeSnSnMe model system

As discussed in the Introduction, we want to investigate the quite surprising difference in DFT results between two theoretical studies on MeSnSnMe [15, 17], which in turn has some implications for the behavior of distannynes with more complex substituents. In the

work of Jung et al [17], the singly bonded isomer, **S**, with an SnSn bond-length of 3.06 Å, and CSnSn angle of 100° is the only minimum that has a planar geometry. No shorter bond-length multiply bonded isomer (**M**) was located as a stationary point. By contrast, in Takagi and Nagase [15], an **S**-like structure is a first-order saddle point while **M** is the planar minimum (with bondlength 2.61 Å, CSnSn angle 126°), where **S** is 6 kcal/mol less stable than **M**.

It turns out that in one case [17], a stable unrestricted DFT solution was used, while in the other case [15], an unstable restricted DFT solution was used. We find that the structure M used by Takagi and Nagase [15] shows a triplet ($R \rightarrow U$) instability using the same method used in their study. However, the two studies also used different density functionals, and different basis sets (one is all-electron and the other also uses an effective core potential (ECP) basis). The effect of each of these differences needs to be established. Therefore, we performed the systematic calculations summarized in Table 2.1.

n(core)	basis	R/U	$\langle \hat{S}^2 \rangle$	stable	ΔE (kcal/mol)	d(Å)	$\angle$(°)	ϕ(°)	Imag. Freq
36	CRENBL^a	U	0.94	$\checkmark$	-7.7	3.06	100	180	0
		R^e	0.00	$\times$	0	2.65^e	125	180	2^{e,f}
28	Def2-SVP^b	U	0.96	$\checkmark$	-4.9	2.93	102	170	0
		R	0.00	$\times$	0	2.65	124	180	1^g
0	Huzinaga^c	U	1.01	$\checkmark$	-1.9	2.85	107	180	0
		R	0.00	$\times$	0	2.63	126	180	0
0	TZVPP^d	R	0.00	$\times$		2.64	126	180	0

Table 2.1: Summary of B3LYP stability analyses for MeSnSnMe with relevant energetic and geometric parameters. See text for references to basis sets.
a. Sn = [3s3p4d] with 36 core electrons. Augmented by a d polarization function for carbon.
b. Sn = [4s4p2d] with 28 core electrons, and 6-31G(d) for carbon.
c. Sn = [7s6p4d], all electron.
d. Sn = [6s5p3d2f], all electron. Only the restricted result is reported.
e. Geometry for the planar **M** structure at RB3LYP/CRENBL was obtained by imposing a geometric constraint d(Sn-Sn) = 2.65 Å and optimizing it, since the fully optimized RB3LYP/CRENBL structure is gauche with d = 2.88 Å, $\angle$ = 68°, and ϕ = 92°.
f. (51i, 52i)
g. (33i)

The B3PW91 functional used by Takagi and Nagase and B3LYP used in Jung et al yield almost the same results for the Huzinaga all-electron basis used by Takagi and Nagase. RB3PW91 and RB3LYP yield d = 2.61 and 2.63 Å, respectively, and UB3PW91 and UB3LYP yield d = 2.82 and 2.85 Å, respectively. Therefore, the remaining results are obtained using just B3LYP, as shown in Table 2.1. Differences between the density functionals are not significant, and can be ruled out as a cause of the difference in results.

The next effect we find is that using an all-electron basis, which does not have relativistic effects for Sn, can tend to shorten the SnSn bond length, relative to an effective core potential, which implicitly includes relativistic effects. The RB3LYP tin-tin distance (2.6 Å), is independent of the basis set used, all-electron or ECP. However, the UB3LYP distance changes from 2.85 Å to 3.06 Å on going from the Huzinaga (all-electron) [30] to CRENBL

(36 effective core electrons) basis [29]. Although 2.85 Å is midway between typical **M** and **S** values in terms of distance, the calculated bending angle suggests that it is closer to the structure **S**. This effect, therefore, while noticeable, does not account for the striking difference in results. We note that in Table 2.1 we also test the effect of making the effective core potential describe fewer core electrons through use of the Def2-SVP ECP and basis [40]. We find this ECP gives qualitatively the same results, although it shows slightly shorter bondlengths. Finally we also examined the effect of using a larger all-electron basis, by using the TZVPP basis [41]. This does not alter the results obtained with the Huzinaga basis significantly.

The most important point is that the short bond isomer **M**, which is located as a minimum in RB3LYP, shows a triplet $(R \rightarrow U)$ instability in all cases, and upon lifting the spin restriction, optimizes to a long bond structure **S**. The structure **S** is more stable than **M** by 2-5 kcal/mol. This is the principal reason that Takagi and Nagase, who used the (unstable) RDFT solutions obtained **M** as more stable than **S** by 6 kcal/mol (their **S** structure was also unstable). It must be emphasized that while this explains the main source of the seemingly dramatic difference reported in refs. [15, 17] it does not establish which (if either) is actually quantitatively correct for this system. Takagi and Nagase tried to address this issue using high-level wavefunction calculations (CASPT2(6,6)), and reported that **S** was 17 kcal/mol less stable than **M**, which appears to support their RDFT results. However such calculations are more difficult to converge with respect to basis set than DFT, which is one possible source of error, and additionally neglected relativistic effects. For the remainder of the paper we shall always permit the DFT calculations to unrestrict whenever this lowers the energy, unless otherwise specified.

2.4.2   PhSnSnPh model system

The global minimum of the MeSnSnMe model is a gauche-like structure rather than either trans-bent species. To probe further, we attempt to separate steric from electronic effects due to the substituents. While the bulky Ar' ligands may be needed to crystallize this compound, and may play a key role in steric interactions, it is likely that the groups immediately next to the tin atoms should provide the most important electronic effects. Other bulky ligands used in previous experimental studies (e.g. Ar*, Ar'-4-SiMe3) have also contained aromatic carbon rings directly attached to the tin core. Therefore, PhSnSnPh may be the simplest appropriate model system to capture the role of through-bond electronic effects.

An optimization was then performed on the PhSnSnPh system in order to find the lowest energy structure. It was discovered that there are several distinct minima corresponding to four different structures. Three of these structures are on the spin-restricted orbital surface while the global minimum is on the spin-unrestricted surface. Only the gauche-like structure, structure **II** in Figure 2.1, is stable to spin-polarization, all of the other structures decrease in energy if the orbitals are allowed to unrestrict. If these calculations had been done without lifting spin symmetry, then the global minimum would have never been uncovered. The global minimum is a planar singly bonded structure shown in Figure 2.1 (structure **I**). This structure has a relatively long Sn-Sn bond distance of 3.134 Å and is quite planar around the central Sn-Sn bond with a dihedral angle of $\omega = 180.0°$. Furthermore, this structure is very trans-bent with a Sn-Sn-C bond angle of $\theta = 98.1°$. These results agree reasonably well with

the results found by Jung et al. for MeSnSnMe, except that the phenyl rings have made a planar structure the global minimum instead of a gauche structure. This is a clear indication of the importance of electronic effects on the preferred conformations of distannynes.

By using a localized orbital procedure, it is possible to explore the character of the bonding and non-bonding orbitals of the central tin atoms. The Edmiston-Ruedenberg localized orbitals (Figure 2.2) show one Sn-Sn σ bonding orbital and two lone pair orbitals, one on each tin atom. These orbitals, therefore, confirm the singly bonded nature of this molecule. Based on this global minimum structure, it appears that these distannynes should act more like diplumbynes, which adopt a singly bonded structure, rather than digermynes, which adopt a multiply bonded structure. However, given the sensitivity to electronic effects, one should also bear in mind that this character can be quite readily altered by chemical substitution.

If spin-symmetry is maintained (rather than broken as above) than the optimization yields a gauche like structure seen in Figure 2.1 (structure **II**). This structure is very twisted and breaks the symmetry about the central Sn bond seen in the singly bonded structure. With an Sn-Sn bond length of 3.127 Å, the gauche structure would still be classified as a singly bonded structure, since a multiply bonded structure at this geometry would necessarily break the π-like bonds. This gauche structure has a dihedral angle $\omega = 73.6°$ and a Sn-Sn-C angle of both 103.1° and 91.6°. With a drastically different geometry, it is surprising that the gauche structure is only 0.3 kcal/mol less stable than the planar structure. This result implies that the potential energy surface for this compound is very flat, as was indeed already reported for the MeSnSnMe model.

A cross-section of the PhSnSnPh potential energy surface scanned with respect to dihedral angle is mapped out in Figure 2.3. Several features of this surface are of particular interest. First, as already discussed is that the global minimum occurs at the planar geometry when spin symmetry is lifted. The next lowest point on the surface is the gauche structure which is only 0.3 kcal/mol higher in energy. Since there is only a very small energetic barrier, interconversion between these two structures should be facile. Finally, it should be noted that this surface is very shallow and bumpy, creating several local minima and a delicate global minimum, which could readily be perturbed by changes in substituents.

The model system can also adopt a geometry classified as a multiply bonded distannyne if we force the orbitals to be spin-restricted (in other words this is an unstable solution). The multiply bonded structure is not located on the surface pictured in Figure 2.3 and is, in fact, 7.6 kcal/mol less stable than the planar singly bonded structure. This multiply bonded structure is planar with a Sn-Sn bond distance of 2.770 Å and a $\theta = 122.3°$. These results along with the other structures are summarized in Table 2.2. The most interesting aspect of this structure is that the plane of the phenyl rings is perpendicular to the plane of the Sn-Sn bond (Figure 2.1 structure **III**). This result is somewhat surprising since this is not the same multiply bonded structure that is seen in the Ar'SnSnAr' calculations or experimental structure. By looking at the Edmiston-Ruedenberg localized orbitals (figure 2.4), there are three orbitals that have bonding character, thereby confirming the Sn-Sn multiple bond of this species (though only one is a true bonding orbital).

If the starting geometry of an optimization resembles a planar multiply bonded structure and the symmetry of the molecule is constrained to C_{2h}, and if the orbitals are constrained to be spin-restricted, then (finally) it is possible to obtain an optimized planar structure
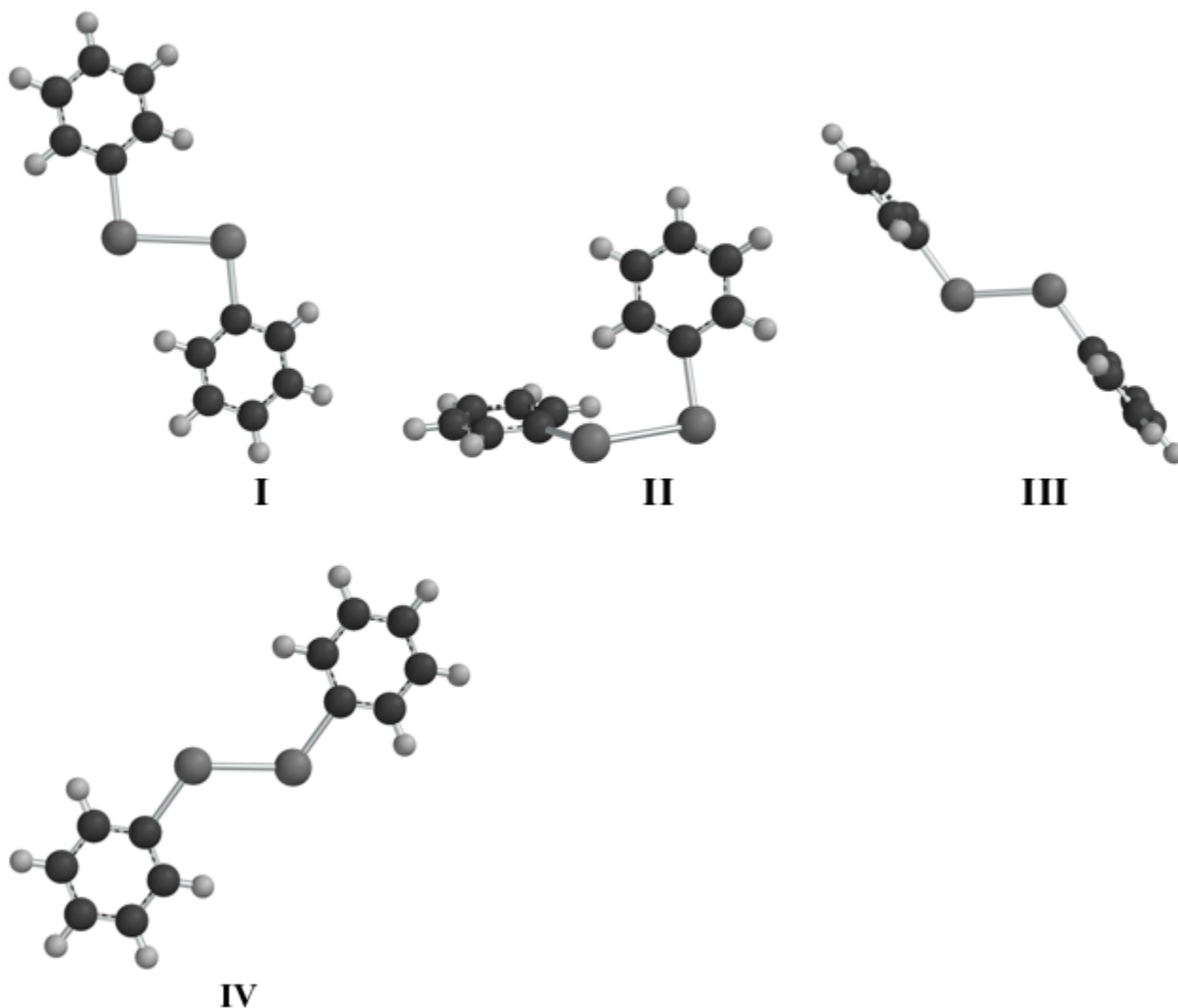
Figure 2.1: Optimized PhSnSnPh Structures. Structure I is the planar singly bonded structure. Structure II is the gauche structure. Structure III is the multiply bonded structure, obtained with restricted orbitals (unstable to spin polarization, but a local minimum on the spin-restricted PES). Structure IV is a multiply bonded structure with the Ph rings in the CSnSnC plane (unstable to spin polarization, and also not a local minimum on the spin-restricted PES).

Structures	Sn-Sn (Å)	θ (°)	ω (°)	ΔE(kcal/mol)
I	3.134	98.1	180	–
II	3.127	103.1/91.6	73.6	0.3
III	2.77	122.3	179.9	7.6
IV	2.758	125.0	180	12.5

Table 2.2: Structural details and energetics for each of the four structures shown in Figure 2.1

σ-bond　　　　　**Lone Pair 1**　　　　　**Lone Pair 2**
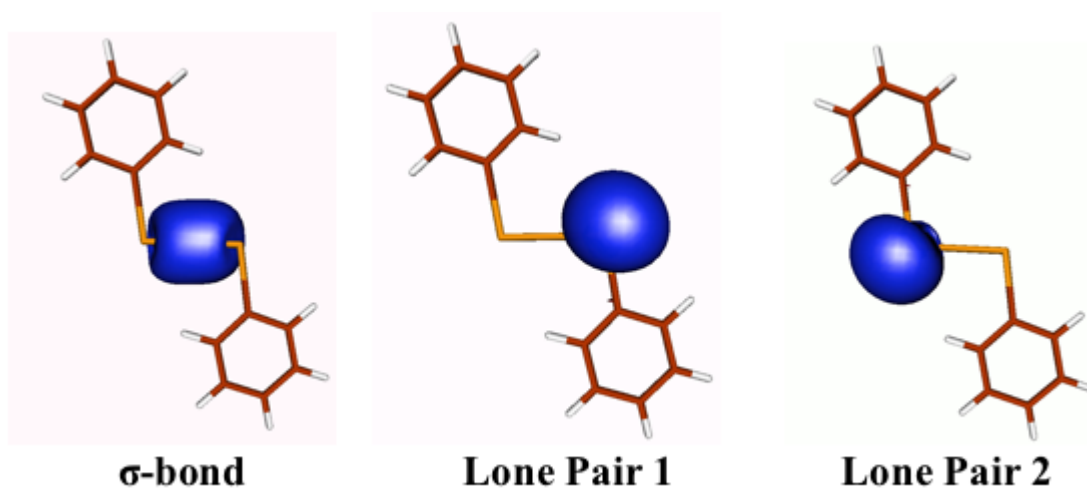
Figure 2.2: Localized Edminston-Ruedenberg orbitals for the planar singly bonded structure (structure I of Fig. 2.1).
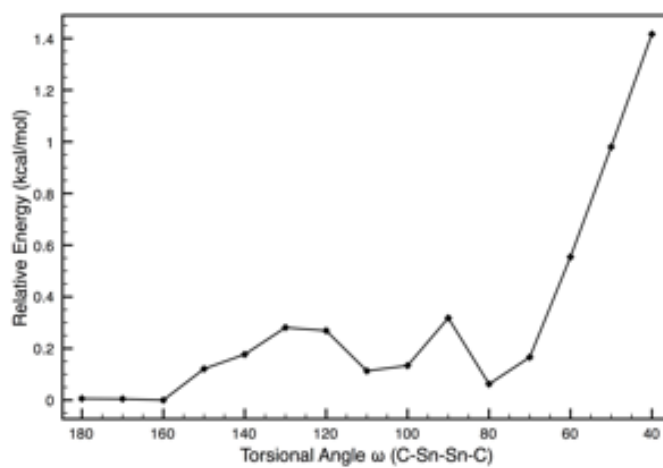
Figure 2.3: Potential energy surface for PhSnSnPh with respect to dihedral angle changes
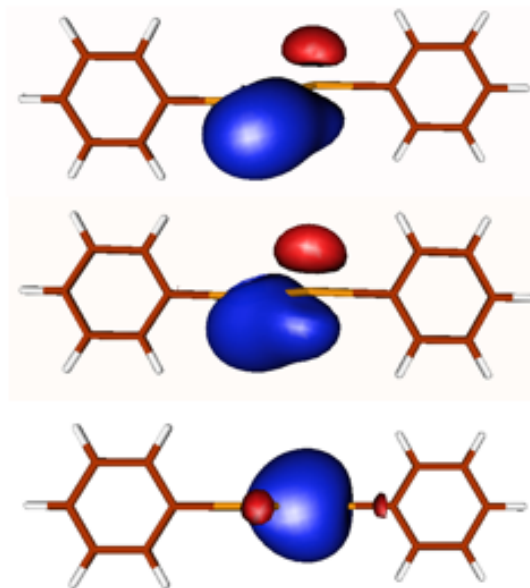
Figure 2.4: The three Edmiston-Ruedenberg bonding orbitals between the two tin atoms in structure III of Fig. 2.1

that is multiply bonded with the phenyl rings in the plane of the Sn-Sn bond instead of perpendicular. This structure is planar with a Sn-Sn bond distance of 2.758 Å and $\theta = 125.0°$(Figure 2.1 structure **IV**). The Edmiston-Ruedenberg localized orbitals of this species are almost identical to those belonging to structure **III** (Figure 2.5). This confirms that both structure **III** and **IV** are similarly bonded and can be classified as multiply bonded. It should be noted that this structure is the highest energy PhSnSnPh structure being 12.5 kcal/mol less stable than the global minimum. This result is surprising since the full crystal Ar'SnSnAr' structure adopts a ground state geometry very similar to this one. The notably large energetic differences between the full crystal structure and this model suggests that further inquiry into the stability and energetics of the full molecule is necessary (see final section).
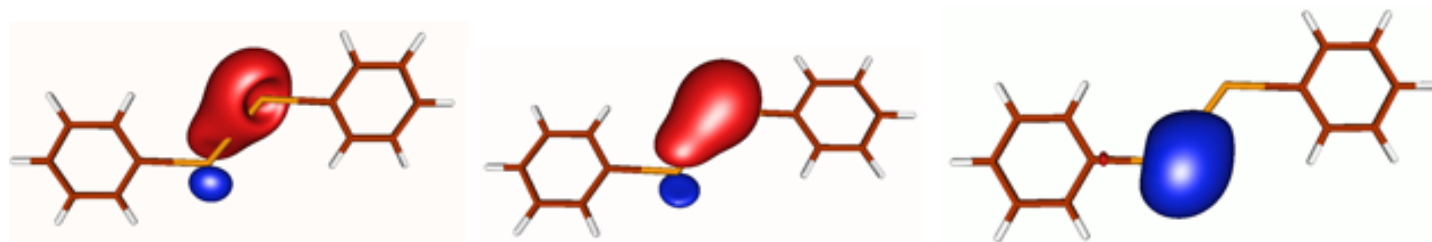
Figure 2.5: The three Edmiston-Ruedenberg bonding orbitals between the two tin atoms in structure IV of Fig. 2.1.

It must be emphasized that these last two structures are only obtained if spin symmetry is enforced. If spin symmetry is lifted and these structures are re-optimized, they will collapse down to the planar global minimum (structure **I**). In other words, both structures

are obtained with KS orbitals that are saddle-points in the space of wavefunctions, rather than minima. Stability analysis on this structure confirms that these solutions display a triplet instabilities and a lower energy solution available when spin symmetry is lifted. Of course this does not mean that the multiply bonded solution is always a saddle-point – this can be influenced by further changes in substituents as we explore later.

Perfect pairing calculations were run on the four structures shown in Figure 2.1 in order to determine the LUMO occupation numbers and therefore the amount of diradical character for each structure. Structures **I** & **II** both have similar diradical character with total LUMO occupations being about 0.05 for both structures. These numbers are in line with previous results that stated that a singly bonded structure should have a LUMO occupation of 0.04. Having a low LUMO occupation number is also consistent with the fact that these structures have the singly bonded characteristics of the diplumbynes. The multiply bonded structures **III** and **IV** have LUMO occupation numbers that are quite a bit larger at 0.16 and 0.12, respectively, signifying between 2 and 3 times more diradical character. The higher diradical character for the multiply bonded structure (**III**) is also consistent with the earlier results for multiply bonded digermynes that showed a LUMO occupation number of about 0.13 electrons.

2.5 Effect of electron-withdrawal and electron-donation

Other structures were investigated for the purpose of further exploring electronic effects on distannynes. In order to investigate different charges, the model system was oxidized or reduced, and the structure fully reoptimized. In this series, the cation has the longest Sn-Sn bond distance at 3.29 Å, followed by the neutral species with 3.13 Å, and the anion has the smallest Sn-Sn bond distance at 3.02 Å. Both the anionic and neutral species have planar structures where the cation has a slightly puckered structure with the dihedral $\omega = 160°$. As the model system becomes more reduced, the system becomes more trans-bent with the angle of the cation being $\theta = 103°$ and the anion being $\theta = 97°$. All of these results are summarized in Table 2.3. By comparing the neutral species to the anion and the cation, it is fairly clear from a structural point of view that the neutral species resembles the anionic species more than the cationic species. It has been previously reported that reduced distannyne crystal salts take a singly bonded structure. Therefore, it should be no surprise that the planar singly bonded neutral species resembles the anionic species known to take a singly bonded geometry. The contraction in Sn-Sn distance is also consistent with the behavior of triplet MeSnSnMe relative to singlet which as reported previously also showed a bond-length contraction. These results indicate that the LUMO of the neutral singlet species has partial bonding character. All of these species have fairly similar geometry, and would be classified as singly bonded species. The multiply bonded structure of this model system cannot be found as a global energy minimum by altering the oxidation state of the model system.

We performed additional calculations that further probe electronic effects using reasonably strong electron withdrawing (nitro) and electron donating (amino) groups as substituents instead of fully reducing or oxidizing the species. Both substituents create tin nitrogen bonds, and therefore differences in these two structures cannot be ascribed to dif-

Species	Sn-Sn (Å)	θ (°)	ω (°)
PhSnSnPh$^-$	3.022	96.7	180
PhSnSnPh	3.134	98.1	180
PhSnSnPh$^+$	3.293	103.2	160.1

Table 2.3: Structural details concerning the anion, neutral, and cation of PhSnSnPh

ferences in their bonding to the central tin atoms. The amine structure is planar with a central angle of $\theta = 92°$, and an Sn-Sn bond distance of 3.20 Å, which would classify this species as a singly bonded structure, similar to the global minimum of PhSnSnPh discussed earlier. The nitro structure adopts a gauche geometry with the dihedral $\omega = $ -112° and a Sn-Sn bond distance of 3.12 Å. Similar to the PhSnSnPh gauche structure, the nitro structure breaks symmetry with the central bond angles measuring $\theta = 104°$ and 71°. These results are summarized in Table 2.4. Evidently electron withdrawing groups preferentially stabilize a gauche structure, whereas electron donating groups tend to stabilize a planar singly bonded structure. Similarly the contrasting global minima for MeSnSnMe (gauche) and PhSnSnPh (trans singly bonded) suggest that the phenyl rings are more electron-donating towards the SnSn moity than methyl groups. We note in passing that the effects of phenyl substitution to the lead system (PhPbPbPh) have been studied previously [13]. There, both the steric and electronic effects of 2,6-$Ph_2C_6H_3$ substituents were seen to play a role in stabilizing and making the singly bonded lead isomer a true energy minimum as in experiments.

R	Sn-Sn (Å)	θ (°)	ω (°)
Ph	3.134	98.1	180
NH_3	3.197	92.3	180
NO_2	3.12	104/71	-112.3

Table 2.4: Structural details concerning RSnSnR with R = Ph, NH3, NO2

2.6 Comparison with experimentally synthesized molecules and discussion

Preliminary calculations were done on the large Ar'SnSnAr' (Ar' = C_6H_3-2,6(C_6H_2-2,6-$(Pr^i)_2)_2$) system in order to compare with experimental structural data and earlier calculations. These calculations using spin-restricted DFT confirmed the earlier findings [15] that this structure does indeed take a multiply bonded structure, consistent with experiment. In particular, the optimized bond-length is 2.832 Å and the C-Sn-Sn bond angles are 128.2° and 130.7°. Even though the bond length is long enough to classify it as a single bond, the C-Sn-Sn angle is highly suggestive of a multiple bond. The key question raised by our model studies is whether or not this spin-restricted solution is stable or unstable to spin-polarization. Therefore we performed stability analysis at the optimized geometry, and, in striking contrast to the PhSnSnPh model, it was found that the spin-restricted orbitals are stable and no triplet instabilities occur.

Earlier computational results [11] suggest that even bulky ligands can take the planar singly bonded structure as a global minimum. Both TbtSnSnTbt (Tbt = C_6H_2-2,4,6-

[CH-(SiMe$_3$)$_2$]$_3$) and Ar*SnSnAr*(Ar*= C$_6$H$_3$-2,6(C$_6$H$_2$-2,4,6-(Pr^i)$_3$)$_2$) were found to adopt a slightly puckered ($\omega \approx$ 170°) singly bonded structure with Sn-Sn bond lengths over 3.00 Å (albeit at a relatively low level of theory). Experimental evidence also suggests that the Ar*SnSnAr*and Me$_3$Si-4-Ar'SnSnAr'-4-SiMe$_3$ structures both adopt a singly bonded structure in the solid state. All of these structures contain a central core that have the central tin atoms bonded to aromatic carbon rings, so it is perhaps quite reasonable that PhSnSnPh also takes a singly bonded structure. On this basis, we suggest it is a reasonable model compound for understanding electronic effects in Ar*SnSnAr*and Me$_3$Si-4-Ar'SnSnAr'-4-SiMe$_3$.

However, Ar'SnSnAr' does display the multiply bonded structure to be a local minimum within DFT, which is stable both with respect to spin-polarization, and with respect to nuclear displacements. This is in contrast to the PhSnSnPh model treated earlier at the same level of theory, where the **M** structure was unstable both with respect to nuclear displacements (the phenyl rings twisted perpendicular) and with respect to spin-polarization. The question of why the **M** structure arises with Ar' substituents is therefore of considerable interest. We had previously speculated that a preferred **S** structure was distorted to the **M** form due to crystal packing effects, but since isolated molecule optimizations yield an optimized **M**-type geometry that is in good agreement with the crystal structure, this cannot be the case. We must therefore conclude that there are additional intramolecular interactions associated with the Ar' ligands used in the experimentally synthesized molecule that are not present in the PhSnSnPh model. It is an intriguing issue for the future to better characterize what these interactions are, and how they exert such a substantial differential effect on the relative stability of the singly and multiply bonded motifs. Separately, there remain some possible uncertainties and errors associated with the approximate DFT electronic structure methods used by all workers in this field, but they may not yet be limiting us in terms of understanding these systems.

2.7   Conclusions

In this report we have briefly reviewed a sometimes-neglected aspect of density functional theory (DFT) electronic structure calculations that are relevant to characterizing potentially reactive heavy element congeners of the alkynes specifically the role of spin-polarization and its detection by stability analysis. This proved to be the basis for a resolution of the striking discrepancy seen between two apparently similar sets of DFT calculations [15, 17] on the MeSnSnMe model of distannynes.

Seeking a better, yet still simple model for electronic interactions of experimental terphenyl substituents with the SnSn system, we then reported a detailed characterization of PhSnSnPh. From this investigation we conclude that the singly bonded (**S**) structure is the global minimum of PhSnSnPh. This global minimum can only be reached when spin-polarization is lifted. Other structures for distannynes exist as local minima on both the spin-polarized and the (sometimes unstable) spin-symmetric potential energy surface. These structures are all very close in energy so that any one of these structures can become the global minimum based on the electron donating and steric effects of the ligands attached directly to the tin atoms. Some of these possibilities were illustrated with different substitutions and oxidation states.

Finally, a comparison of the PhSnSnPh results with various experimentally isolated systems indicates that there are significant additional electronic effects associated with the terphenyl ligands. Some experimentally isolated species, such as Ar*SnSnAr* and Me$_3$Si-4-Ar'SnSnAr'-4-SiMe$_3$, exhibit **S**-type structures that are reasonably consistent with PhSnSnPh (and indeed with MeSnSnMe as well). However, we find that, in contrast to PhSnSnPh, no spin-polarization occurs for the multiply-bonded (**M**) structure of Ar'SnSnAr' (Ar' = C$_6$H$_3$-2,6(C$_6$H$_2$-2,6-(Pr^i)$_2$)$_2$) which becomes a stable local minimum, consistent with the experimental geometry. Since loss of spin-polarization should be considered a consequence of electronic stabilization, and as through-bond interactions associated with Ar' should not be substantially different to Ph itself, it appears that, intriguingly, we still have more to learn about the specific intramolecular interactions in this species.

Bibliography

[1] P. POWER, *Appl. Organomet. Chem.* **19**, 488 (2005).

[2] A. SEKIGUCHI, M. ICHINOHE, and R. KINJO, *Bull. Chem. Soc. Jpn.* **79**, 825 (2006).

[3] P. P. POWER, *Organometallics* **26**, 4362 (2007).

[4] L. PU, B. TWAMLEY, and P. POWER, *J. Am. Chem. Soc.* **122**, 3524 (2000).

[5] A. PHILLIPS, R. WRIGHT, M. OLMSTEAD, and P. POWER, *J. Am. Chem. Soc.* **124**, 5930 (2002).

[6] M. STENDER, A. PHILLIPS, R. WRIGHT, and P. POWER, *Angew. Chem.-Int. Edit.* **41**, 1785+ (2002).

[7] A. SEKIGUCHI, R. KINJO, and M. ICHINOHE, *Science* **305**, 1755 (2004).

[8] R. C. FISCHER, L. PU, J. C. FETTINGER, M. A. BRYNDA, and P. P. POWER, *J. Am. Chem. Soc.* **128**, 11366 (2006).

[9] G. H. SPIKES, J. R. GIULIANI, M. P. AUGUSTINE, I. NOWIK, R. H. HERBER, and P. P. POWER, *Inorg. Chem.* **45**, 9132 (2006).

[10] C. CUI, M. OLMSTEAD, J. FETTINGER, G. SPIKES, and P. POWER, *J. Am. Chem. Soc.* **127**, 17530 (2005).

[11] N. TAKAGI and S. NAGASE, *Organometallics* **20**, 5498 (2001).

[12] K. KOBAYASHI, N. TAKAGI, and S. NAGASE, *Organometallics* **20**, 234 (2001).

[13] Y. CHEN, M. HARTMANN, M. DIEDENHOFEN, and G. FRENKING, *Angew. Chem.-Int. Edit.* **40**, 2052 (2001).

[14] M. LEIN, A. KRAPP, and G. FRENKING, *J. Am. Chem. Soc.* **127**, 6290 (2005).

[15] N. TAKAGI and S. NAGASE, *Organometallics* **26**, 469 (2007).

[16] N. TAKAGI and S. NAGASE, *Organometallics* **26**, 3627 (2007).

[17] Y. JUNG, M. BRYNDA, P. POWER, and M. HEAD-GORDON, *J. Am. Chem. Soc.* **128**, 7185 (2006).

[18] R. G. PARR, *Density-functional theory of atoms and molecules*, Oxford University Press, Clarendon Press, New York, Oxford [England], 1989.

[19] W. KOHN, A. BECKE, and R. PARR, *J. Phys. Chem.* **100**, 12974 (1996).

[20] J. POPLE, P. GILL, and N. HANDY, *Int. J. Quantum Chem.* **56**, 303 (1995).

[21] J. CIZEK and J. PALDUS, *J. Chem. Phys.* **47**, 3976 (1967).

[22] R. SEEGER and J. POPLE, *J. Chem. Phys.* **66**, 3045 (1977).

[23] R. BAUERNSCHMITT and R. AHLRICHS, *J. Chem. Phys.* **104**, 9047 (1996).

[24] Y. JUNG, Y. SHAO, M. GORDON, D. DOREN, and M. HEAD-GORDON, *J. Chem. Phys.* **119**, 10917 (2003).

[25] Y. SHAO, L. F. MOLNAR, Y. JUNG, J. KUSSMANN, C. OCHSENFELD, S. T. BROWN, A. T. B. GILBERT, L. V. SLIPCHENKO, S. V. LEVCHENKO, D. P. O'NEILL, R. A. DISTASIO, JR., R. C. LOCHAN, T. WANG, G. J. O. BERAN, N. A. BESLEY, J. M. HERBERT, C. Y. LIN, T. VAN VOORHIS, S. H. CHIEN, A. SODT, R. P. STEELE, V. A. RASSOLOV, P. E. MASLEN, P. P. KORAMBATH, R. D. ADAMSON, B. AUSTIN, J. BAKER, E. F. C. BYRD, H. DACHSEL, R. J. DOERKSEN, A. DREUW, B. D. DUNIETZ, A. D. DUTOI, T. R. FURLANI, S. R. GWALTNEY, A. HEYDEN, S. HIRATA, C.-P. HSU, G. KEDZIORA, R. Z. KHALLIULIN, P. KLUNZINGER, A. M. LEE, M. S. LEE, W. LIANG, I. LOTAN, N. NAIR, B. PETERS, E. I. PROYNOV, P. A. PIENIAZEK, Y. M. RHEE, J. RITCHIE, E. ROSTA, C. D. SHERRILL, A. C. SIMMONETT, J. E. SUBOTNIK, H. L. WOODCOCK, III, W. ZHANG, A. T. BELL, A. K. CHAKRABORTY, D. M. CHIPMAN, F. J. KEIL, A. WARSHEL, W. J. HEHRE, H. F. SCHAEFER, III, J. KONG, A. I. KRYLOV, P. M. W. GILL, and M. HEAD-GORDON, *Phys. Chem. Chem. Phys.* **8**, 3172 (2006).

[26] A. BECKE, *J. Chem. Phys.* **98**, 5648 (1993).

[27] R. HERTWIG and W. KOCH, *Chem. Phys. Lett.* **268**, 345 (1997).

[28] P. GILL, B. JOHNSON, and J. POPLE, *Chem. Phys. Lett.* **209**, 506 (1993).

[29] C. NASH, B. BURSTEN, and W. ERMLER, *J. Chem. Phys.* **106**, 5133 (1997).

[30] S. HUZINAGA, *Gaussian basis sets for molecular calculations*, Elsevier, Distributors for the United States and Canada Elsevier Science Pub. Co., Amsterdam; New York, New York, 1984.

[31] J. CULLEN, *Chem. Phys.* **202**, 217 (1996).

[32] A. Sodt, G. Beran, Y. Jung, B. Austin, and M. Head-Gordon, *J. Chem. Theory Comput.* **2**, 300 (2006).

[33] L. Salem and C. Rowland, *Angew. Chem.-Int. Edit.* **11**, 92 (1972).

[34] D. Dohnert and J. Koutecky, *J. Am. Chem. Soc.* **102**, 1789 (1980).

[35] M. Gordon, M. Schmidt, G. Chaban, K. Glaesemann, W. Stevens, and C. Gonzalez, *J. Chem. Phys.* **110**, 4199 (1999).

[36] Y. Jung and M. Head-Gordon, *J. Phys. Chem. A* **107**, 7475 (2003).

[37] C. Edmiston and K. Ruedenberg, *Rev. Mod. Phys.* **35**, 457 (1963).

[38] J. Subotnik, Y. Shao, W. Liang, and M. Head-Gordon, *J. Chem. Phys.* **121**, 9220 (2004).

[39] J. E. Subotnik, A. Sodt, and M. Head-Gordon, *Phys. Chem. Chem. Phys.* **9**, 5522 (2007).

[40] F. Weigend and R. Ahlrichs, *Phys. Chem. Chem. Phys.* **7**, 3297 (2005).

[41] F. Weigend, M. Haser, H. Patzelt, and R. Ahlrichs, *Chem. Phys. Lett.* **294**, 143 (1998).

Chapter 3

Violations of N-representability from Spin-Unrestricted Orbitals in Møller-Plesset Perturbation Theory and Related Double-Hybrid Density Functional Theory

3.1   Introduction

Orbitals generated from an electronic wavefunction have allowed the quantum chemist to obtain a simple qualitative picture from a very complicated quantitative expression. In the infancy of quantum chemistry, these orbitals were the canonical orbitals, generated by diagonalizing the Fock matrix. However, these orbitals only reflect the results of a Hartree-Fock calculation and therefore do not include any static or dynamic correlation effects. In 1954, P-O. Löwdin discovered a different set of orbitals that he called the natural orbitals, defined as the set of vectors that diagonalize the one particle density matrix or the relaxed one density matrix.[1, 2] For a calculation done only at the Hartree-Fock level, the canonical orbitals and the natural orbitals can be taken as equivalent. In the natural scheme the focus is on the density matrix instead of the Fock matrix, which is needed if any correlation effects are to be included in the orbital picture.[1] Since the density matrix is used to calculate physical properties,[3] it seems instinctive to use orbitals generated from this matrix to reflect trends seen in these properties. The natural orbitals are not only used for qualitative purposes, [4, 5] but they are also currently being used as a starting guess for multiconfigurational methods.[6]

Recently, there has a been renewed interest in using solely the density matrix to obtain energies and physical properties and completely bypassing the wavefunction-based HF theory.[7, 8, 9, 10] In order to ensure that the resulting energy is variational, several restrictions have to be imposed upon the n-particle density matrices. One of the major constraints is that all of the n-particle density matrices have to be positive semidefinite, a feature commonly abbreviated as p-positivity.[11, 12, 13] Also, the one-particle density matrix can-

not have eigenvalues greater than two.[2] These eigenvalues are frequently referred to as the natural orbital occupation numbers (NOON),[2] since they correspond to the eigenvectors that form the natural orbitals. Therefore, this restriction on the one-particle density matrix can be thought of as a reformulation of the Pauli exclusion principle. Satisfying these restrictions along with several other constraints is commonly referred to as ensuring N-representability.[11, 12]

Ensuring N-representability is very desirable, and is the explicit focus in development of reduced density matrix methods. By contrast, little research has focused on when this tenet is broken in conventional quantum chemistry, perhaps because it is generally assumed to be satisfied. On the other hand, Gordon *et al.*[14] demonstrated the appearance of negative NOONs for non-variational methods using *spin-restricted* orbitals and on this basis suggested to use their appearence as a diagnostic in order to determine when to use multi-reference methods. Of course the alternative is to allow the orbitals to unrestrict. Therefore, in this paper, we will focus on *unrestricted* second-order Møller-Plesset perturbation theory (MP2) because it is one of the simplest ways of incorporating electron correlation in a wavefunction-based method and still dissociates correctly. By contrast, the restricted MP2 energy becomes strongly non-variational towards dissociation as the gap between filled and empty orbitals becomes small.

There has been a resurgence in usage and interest in MP2-like methods due to two factors: very large reductions in computational cost,[15, 16, 17, 18, 19] and improvements in accuracy.[20, 21] These developments began with decomposing the four-center integrals into three-center integrals via the Resolution-of-the-Identity (RI) approximation[15] or more recently with a Cholesky decomposition.[16] The RI approximation is now very widely used, and often reduces the cost of large basis set MP2 calculations by more than a factor of 10. It is possible to obtain improvements in accuracy based on the fact that the MP2 energy expression can be split into same-spin and opposite-spin portions and rescaled separately.[20] By using the opposite-spin portion along with an empirically determined parameter to compensate for the missing same-spin portion[18, 19], the scaling of MP2 is reduced to N^4, while maintaining the advantages of the RI approach, and the accuracy improvements of spin-component scaling. Further reductions in computational cost can be obtained by local correlation methods.[22, 23, 24] These methods employ localized occupied and virtual orbitals, and a truncated definition (using either a distance metric[22] or an atom-based metric[24]) of which correlations to include, so as to cut down the total number of integrals that need to be calculated. As a result, often MP2 calculations are dominated by the cost of the pre-requisite Hartree-Fock calculation, which can be reduced using dual basis methods which only attain full self-consistency in a small basis[25, 26]

With the computational cost reductions described above, it has become more feasible to combine MP2-like correlation expressions with density functional theory,[27, 28, 29, 30] to create a new class of non-local functionals often referred to as 'double hybrids.' These methods work by using the orbitals from a DFT calculation for a second-order perturbation theory correction for correlation. This correction involves is MP2-like, where the Kohn-Sham orbitals and eigenvalues replace the Hartree-Fock reference.[28, 30] These methods have tremendous promise because they appear to yield significant improvements in accuracy relative to generalized gradient approximation and hybrid functionals, while fixing one of their major deficiencies,[31] which is the inability to accurately describe dispersion-bound

complexes.[32, 33] Since the defining equations work similarly to conventional MP2 theory using the HF reference, all of the conclusions and equations shown in this paper will also apply to these 'double-hybrid' functionals.

With regard to the MP2 one-particle density matrix, we observe that because the MP2 energy is non-variational, the Hellmann-Feynman theorem does not hold.[34] This makes the definition of the density matrix ambiguous, since it can be formulated as either to be consistent with an energy derivative or as the second order expansion of an expectation value.[34] The energy derivative approach is consistent with MP2 responses to applied fields, and is therefore generally preferred.[34, 35, 36] In the energy derivative formalism, the one-particle density matrix is defined by contractions of pair correlation amplitudes with integrals, and the solving of the coupled-perturbed self consistent field (CPSCF) equations to account for the response of the energy to changes in orbitals.[34, 35, 37, 38, 39, 36, 40] As will be made explicit later, the solving of the CPSCF equations can lead to a singularity (or near-singularity) which results in non-physical NOONs, thereby violating N-representability, *even when the MP2 energy is not behaving non-variationally.* This work will first look at how violating N-representability is theoretically possible followed by several examples including bond breaking, effects on first order physical properties, and occurrence at both neutral and ionic equilibrium.

3.2   Theory

Consider first a brief review of the definition of the one-particle density matrix (1-PDM) based on the derivative of the MP2 energy.[35, 34, 36]. The 1-PDM can be partitioned into two matrices; one resulting from the reference wave function and one resulting from the perturbative correction to that reference:

$$P_{tot} = P_{HF} + P^{[2]} \tag{3.1}$$

In (**1**), what is labeled P_{tot} is commonly referred to as the *relaxed one-particle density matrix* or simply the *one-matrix*. Since HF theory is completely variational, there cannot be any N-representability problems emanating from P_{HF}. Logically, all of the problems must come from the MP2 correction to the HF density matrix. In the molecular orbital basis, the $P^{[2]}$ matrix can be divided into 4 blocks: the occupied-occupied block (OO), the occupied-virtual block (OV), the virtual-occupied block (VO), and the virtual-virtual block (VV). Taking into account the fact that the density matrix is Hermitian, the off-diagonal OV and VO blocks are necessarily equivalent. In order to get the explicit forms for each of these blocks the MP2 gradient is needed.

The MP2 gradient can be written in a form where it is split between the contributions from the molecular orbitals and atomic orbitals. Contributions from the atomic orbitals will yield skeleton derivatives which will not affect the density, so they will be omitted in order to avoid confusion. In this form the MP2 gradient can be written in terms of the OO and VV blocks of $P^{[2]}$ and the MP2 Lagrangian.[35, 34, 36]

$$\left.\frac{\partial E_{MP2}}{\partial x}\right|_{x=0} = \sum_{ij} P^{[2]}_{ij} B^x_{ij} + \sum_{ab} P^{[2]}_{ab} B^x_{ab} + 2\sum_{ia} L_{ia} U^x_{ia} + \cdots \tag{3.2}$$

$$B_{ij}^x = F_{ij}^{(x)} - S_{ij}^{(x)}\epsilon_j - \sum_{kl} S_{kl}^{(x)}[2(ij|kl) - (ik|jl)] \tag{3.3}$$

Throughout this work $i, j, k...$ refer to occupied molecular orbitals while $a, b, c...$ refer to the virtual molecular orbitals. In equations (**2**) and (**3**) the superscript x refers to a derivative with respect to x while a superscript x with parenthesis refers to a skeleton derivative. Although equation (**2**) could be recast in terms of the density matrix with a perturbation on each block, this form is preferred because it emphasizes the fact that the density matrix is not derived from a corresponding wavefunction but rather from the MP2 energy expression. The explicit expressions for the OO and VV blocks of $P^{[2]}$ are calculated by taking the derivative of the MP2 energy expression with respect to the nuclear coordinate x and matching the form of equation (**2**). The explicit form of these blocks are formed by contracting pair correlation amplitudes that have already been calculated in order to get the MP2 energy correction.[35, 34, 36]

$$P_{ij}^{[2]} = -\frac{1}{2}\sum_{kab} t_{ik}^{ab}t_{jk}^{ab} \tag{3.4}$$

$$P_{ab}^{[2]} = \frac{1}{2}\sum_{ijc} t_{ij}^{ac}t_{ij}^{bc} \tag{3.5}$$

$$t_{ik}^{ab} = \frac{(ia||jb)}{\epsilon_i + \epsilon_k - \epsilon_a - \epsilon_b} \tag{3.6}$$

Since these amplitudes only incur problems when the denominator of a t-amplitude approaches zero, these blocks rarely contribute to N-representability problems. Also, if there are no problems with the MP2 energy, then it will be a safe assumption to make that the OO and VV blocks are not contributing to the violation of N-representability in contrast to the study by Gordon *et al.*[14] which solely focuses on problems in these blocks. The OV block is calculated through the third term in equation (**2**), which includes the MP2 Lagrangian (L_{ia}) and the orbital response matrix (U_{ia}^x), by using the coupled-perturbed Hartree-Fock (CPHF) equations. Solving the Z-vector equations based on CPHF will give the explicit forms of the OV and the VO blocks for the $P^{[2]}$ matrix.[36, 35, 34, 37]

$$A_{ia,jb}' = (\epsilon_a - \epsilon_i)\delta_{ij}\delta_{ab} + (ia||jb) - (ib||ja) \tag{3.7}$$

$$\sum_{ia} A_{ia,jb}'U_{ia}^x = B_{bj}^x \implies U_{ia}^x = (A_{ia,jb}')^{-1}B_{bj}^x \tag{3.8}$$

$$L_{ia}U_{ia}^x = L_{ia}(A_{ia,jb}')^{-1}B_{bj}^x \tag{3.9}$$

$$Z_{bj} = L_{ia}(A_{ia,jb}')^{-1} \tag{3.10}$$

$$\sum_{ia} L_{ia}U_{ia}^x = \sum_{ia} P_{ia}^{[2]}B_{ia}^x \implies Z_{bj} = P_{ia}^{[2]} = L_{ia}(A_{ia,jb}')^{-1} \tag{3.11}$$

When solving the Z-vector equations, problems can arise when the A' matrix becomes non-invertible. In this equation, the A' matrix is the part of the orbital Hessian that determines whether a restricted solution is a minimum or a saddle point.[41] If allowing for spin-polarization does not lower the SCF energy, then the eigenvalues of the A' matrix are

positive definite. When including spin-polarization lowers the SCF energy, then at least one eigenvalue of the A' matrix is negative when restricted orbitals are employed. At the point of unrestriction, one eigenvalue will be zero, making the inverse of A' ill-defined.[41] It is at this point, and slightly after it (when the A' matrix is still near-singular), where the $P^{[2]}$ matrix can potentially cause a violation of N-representability in the 1-PDM. Since the 1-PDM is used to calculate physical properties, if this matrix is non-N-representable, unphysical expectation values may result.

In the proceeding section, it was analytically shown how problems in the MP2 density matrix can arise from a singularity in the z-vector equations. It should be noted that these problems may appear in a large variety of theories, and therefore there is a need to generalize the above result. This will be accomplished through the use of derivatives with respect to orbital rotations (θ) and the generalized coordinate(x). [42] These derivatives will then be connected back to the z-vector equations seen in the MP2 derivation. The condition for convergence of an SCF calculation is that the SCF energy with respect to occupied-virtual orbital rotations is zero. This quantity is also the occupied-virtual block of the Fock matrix.

$$\frac{\partial E_{SCF}}{\partial \theta_{ai}} = 0 = F_{ai} \tag{3.12}$$

Since this derivative is zero, then any subsequent derivatives must also be zero.

$$\frac{\partial}{\partial x}\left[\frac{\partial E_{SCF}}{\partial \theta_{ai}}\right] = 0 \tag{3.13}$$

$$\frac{\partial}{\partial x}\left[\frac{\partial E_{SCF}}{\partial \theta_{ai}}\right] = \frac{\partial^2 E_{SCF}}{\partial \theta_{ai}\partial \theta_{bj}}\frac{\partial \theta_{bj}}{\partial x} + \frac{\partial^2 E_{SCF}}{\partial \theta_{ai}\partial x} = 0 \tag{3.14}$$

Based on eq. 3.14, a general equation can be written for the derivative of an orbital rotation with respect to x.

$$\frac{\partial \theta_{bj}}{\partial x} = -\left(\frac{\partial^2 E_{SCF}}{\partial \theta_{ai}\partial \theta_{bj}}\right)^{-1}\frac{\partial^2 E_{SCF}}{\partial \theta_{ai}\partial x} \tag{3.15}$$

For any given correlation energy not satisfying the Hellman-Feynman theorem, ϵ_c, the first derivative includes contributions from orbital derivatives:

$$\frac{\partial \epsilon_c}{\partial x} = \frac{\partial \epsilon_c}{\partial \theta_{ai}}\frac{\partial \theta_{ai}}{\partial x} \tag{3.16}$$

Based on eq. 3.15, the correlation energy derivative can be expanded further by substituting in for the derivative of the orbital rotation.

$$\frac{\partial \epsilon_c}{\partial x} = -\left[\frac{\partial \epsilon_c}{\partial \theta_{ai}}\left(\frac{\partial^2 E_{SCF}}{\partial \theta_{ai}\partial \theta_{bj}}\right)^{-1}\right]\frac{\partial^2 E_{SCF}}{\partial \theta_{ai}\partial x} \tag{3.17}$$

Based on this equation, one can see that the gradient of any correlation energy will be dependent on the orbital hessian of the SCF energy. The two terms in the square brackets in eq. 3.17 are the z-vector equation seen in eq.10.

$$Z_{bj} = L_{ia}(A'_{ia,jb})^{-1} = \frac{\partial \epsilon_c}{\partial \theta_{ai}}\left(\frac{\partial^2 E_{SCF}}{\partial \theta_{ai}\partial \theta_{bj}}\right)^{-1} \tag{3.18}$$

When the orbital hessian is zero, the inverse will be undefined and the correlation energy gradient will also be undefined causing potential problems in the density matrix. This problem can affect all methods unless the derivative of the correlation energy with respect to occupied-virtual orbital rotations is zero. Therefore, this problem is averted in orbital optimized methods because the first term is necessarily zero. The implication of this equation is that this problem can occur in coupled-cluster singles and doubles theory (CCSD) when applied to a system that requires more than doubles excitations. However, there has been no evidence of CCSD giving erroneous results near the unrestriction. This can be attributed to the notion that CCSD is fairly orbital invariant and therefore yield a nearly zero Lagrangian.

The rest of this study will outline several examples of this N-representability problem. All calculations were performed with the Q-Chem electronic structure program package.[43]

3.3   Results

3.3.1   LiH Bond Breaking

The most typical example of a transition from a determinant with restricted orbitals to one that is unrestricted is by stretching a bond from equilibrium to dissociation. This example is ideal since the distance between the two atoms can be tuned exactly to the point of unrestriction. LiH was chosen because it is a simple diatomic with less symmetry than H_2 (necessary for a non-zero dipole moment). In order to approach the complete basis set limit, a fairly large cc-pVQZ basis set was chosen. Also a basis set of this size would not show artifacts that are occasionally seen in a minimal basis set.

For the LiH test system, the unrestriction point occurs at about 2.27943 Å(Fig. 3.1). At this point, with orbitals very slightly spin-polarized, 2 out of the total 85 eigenvalues of the 1-PDM violate N-representability rules with the largest being 2.845664 and the lowest being -0.788560. Another interesting aspect of Fig. 3.1 is that the deviation from N-representability occurs over a small neighborhood and not just at the restriction point. Since the inverse of the very small eigenvalues of A' will give large numbers that result in the unphysical eigenvalues then the fact that the violation of N-representability occurs over a neighborhood is justified. The fact that at the unrestriction point the eigenvalues stay finite and do not approach negative and positive infinity is another interesting aspect seen in Fig. 3.1.

Another way to measure the degree of unrestriction is to calculate the overlap between the occupied alpha and beta orbitals. When the molecule is restricted, then by definition, the overlap between alpha and beta orbitals has to be one. At complete dissociation there should be no overlap between the valence alpha and beta orbital in this LiH example because the orbitals are located on separate atomic centers. Conventional thinking will lead us to think that this transition from 1 to 0 should happen smoothly as the molecule is dissociated. Furthermore, the angle of unrestriction, θ, can be defined as $1/2$ multiplied by the arc-cosine of the minimum alpha-beta overlap which will be the valence alpha-beta overlap. This equation can be worked out by examining a simple system in 2-d space. Two orbitals α and β will be defined by the amount of bonding and antibonding character denoted by the symbols A and B.

$$|\phi_\alpha\rangle = \cos\theta|B\rangle + \sin\theta|A\rangle$$
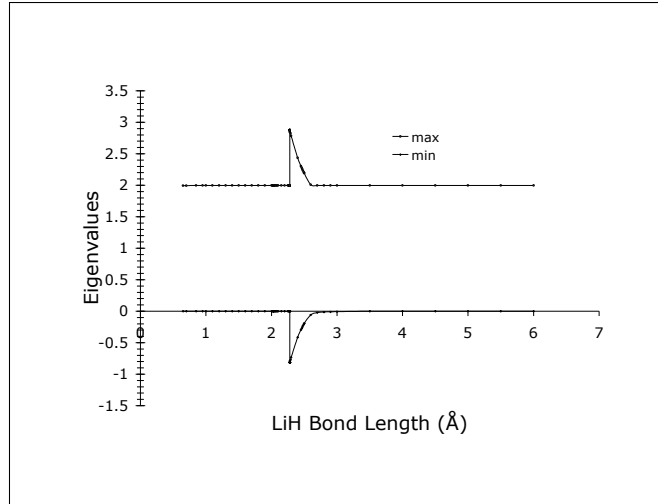
Figure 3.1: Maximum and minimum eigenvalues of the 1-PDM for LiH dissociation

$$|\phi_\beta\rangle = \cos\theta|B\rangle - \sin\theta|A\rangle \tag{3.19}$$

From the scalar product of α and β an expression defining θ can be written.

$$\begin{aligned} \langle\phi_\alpha|\phi_\beta\rangle &= \cos^2\theta - \sin^2\theta \\ &= \cos 2\theta \\ \therefore \theta &= \frac{1}{2}\arccos(\langle\phi_\alpha|\phi_\beta\rangle) \end{aligned} \tag{3.20}$$

Looking carefully at eq. 3.15, it suggests that the derivative of orbital rotations with respect to nuclear position should be undefined at the unrestriction point. When LiH is dissociated the derivative of orbital rotations with respect to the nuclear coordinate x becomes undefined at the unrestriction point (Fig. 3.3).
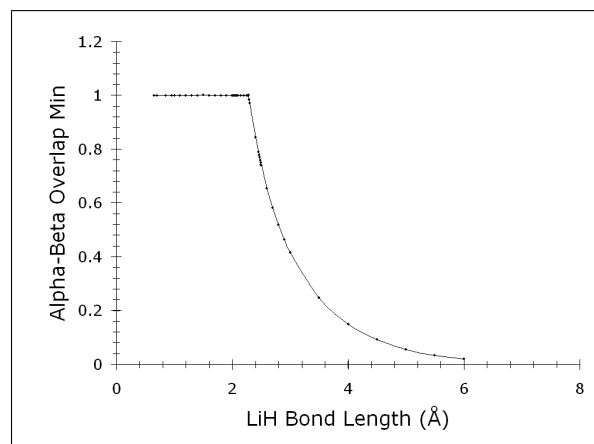
Figure 3.2: Minimum singular value of $S_{\alpha\beta}$ encounters a discontinuity at the unrestriction point

The most pressing issue is what are the physical implications of violating N-representability in MP2 theory. In computing physical properties, the relaxed density matrix is needed to
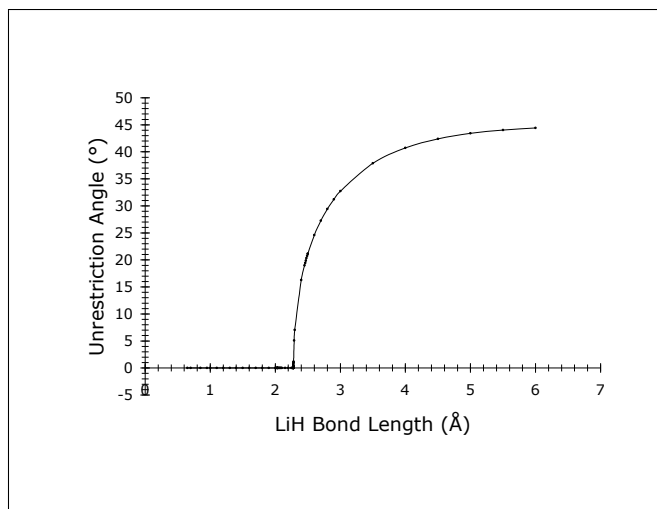
Figure 3.3: The unrestriction angle θ is not smooth clearly exhibiting a discontinuity at the unrestriction point making $\frac{\partial \theta}{\partial x}$ undefined at this point

calculate expectation values. Since LiH has a dipole moment, this will be an instructive physical property to track through bond dissociation (Fig. 3.4). When the bond length is near equilibrium ($\sim$1.6 Å) and the reference orbitals are restricted, the dipole moment is 5.92 Debyes. This value is very close to the experimental value of 5.828 Debyes, as would be expected from an accurate basis set. As the bond is lengthened away from equilibrium toward the unrestriction, the dipole moment increases from 5.920 D to 7.542 D. The increase can be attributed to the fact that separating restricted orbitals is essentially separating two point charges, resulting in a significant shift in the dipole moment. It should be noted that Fig. 3.4 also displays the correct behavior at dissociation. Two infinitely separated neutral atoms should have no dipole moment and that fact is seen when the unrestricted MP2 method is used to calculate the dipole moment. The most striking facet of this figure is the large spike at the unrestriction point. At 2.27943 Å the dipole moment jumps from 7.542 Debyes to 15.342 Debyes, a jump of almost 8 Debyes.
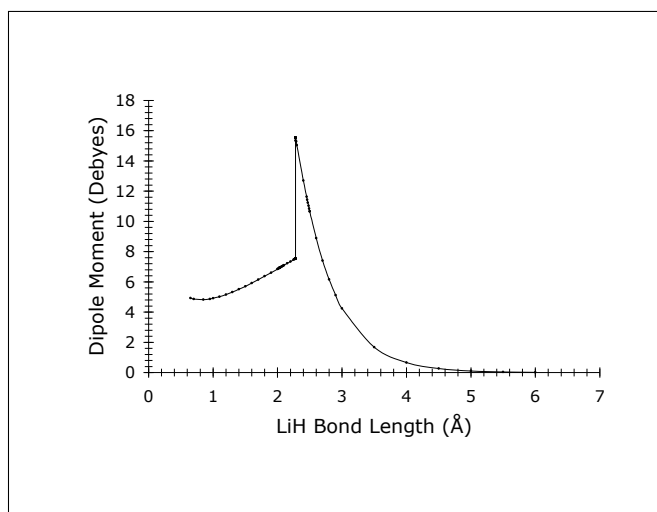
Figure 3.4: MP2 Dipole moment as a function of bond length

Physically, there is no reason for such a sudden and sharp increase in dipole moment. When the region of unphysicality is plotted along with the region that violates N-representability, it becomes clear that these two regions completely overlap (see figure 3.5). The only conclusion to make is that violating N-representablility can lead to unphysical results. Since these results are not limited to the test system, anytime there is an elongated bond near the unrestriction point there is a danger of obtaining unphysical results. Other examples, which will follow, include radical species and species with some singlet diradicaloid character. It should be noted that just because violating N-representability can lead to unphysical results, does not necessarily mean that the converse is true.
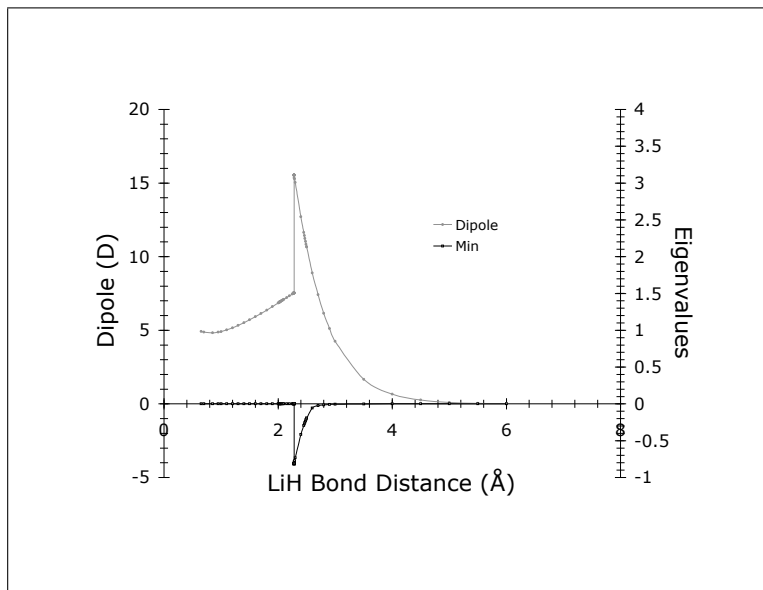
Figure 3.5: Overlay of the minimum eigenvalue from the 1-PDM and the dipole moment in order to show that the unphysical dipole region perfectly coincides with the region of non-N-representability for the MP2 method

The dipole moment represents the first derivative of the energy with respect to electric field. What is evident in Figs. 3.4 and 3.5 is that the MP2 dipole moment is *discontinuous* as the orbitals change from restricted to unrestricted. Thus while the MP2 energy changes continuously as orbitals unrestrict, there is a discontinuity in the first derivative. Other properties such as the nuclear force also exhibit a discontinuity at the unrestriction point.

This process was repeated for the B2PLYP double hybrid functional[44, 28] where perturbation theory is using Kohn-Sham orbitals is performed as a correlation correction after self-consistent evaluation of the Kohn-Sham orbitals. Since Kohn-Sham density functional theory also has an unrestriction point, there will be a point where the A' matrix will have a zero eigenvalue. This singularity will cause problems in the Z-vector equations in a completely analogous fashion to traditional MP2 theory. Therefore, when LiH is dissociated, similar behavior to MP2 theory is expected and is indeed what happens (Fig. 3.6). The violation of N-representability is less severe in this case and the discontinuity in the dipole moment is lessened, as a result of scaling the perturbation correction by a factor of 0.27, thereby lessening the contribution of $P^{[2]}$ on the 1-PDM. But fundamentally, doing perturbation theory on the Kohn-Sham reference yields the same N-representability problems as

doing perturbation theory on the Hartree-Fock reference.
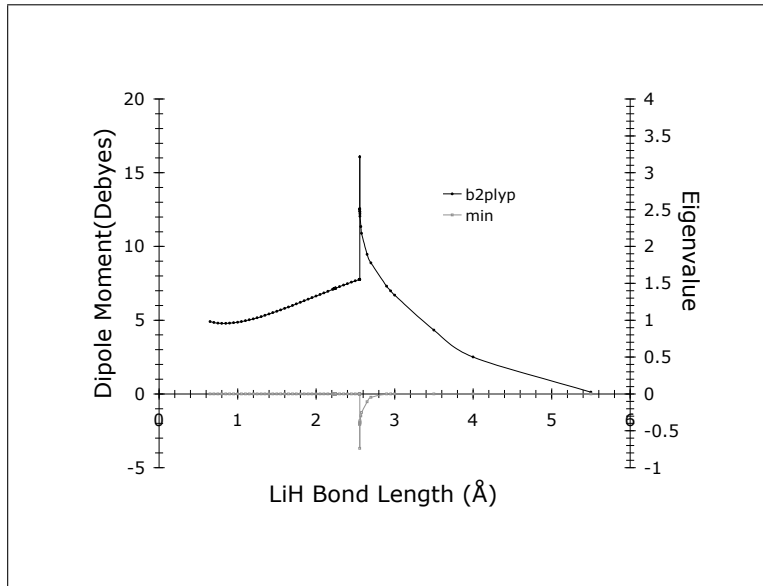
Figure 3.6: Overlay of the minimum eigenvalue from the 1-PDM and the dipole moment in order to show that the unphysical dipole region perfectly coincides with the region of non-N-representability for the B2PLYP functional

3.3.2   Hydrogen Molecule

In some situations, N-representability can be violated without any negative bearing on physical properties. One such example is tracking the dipole moment during the dissociation of the H_2 molecule. Since this bond breaking is done in a minimal STO-3G basis, the 1-PDM only has two eigenvalues. As the H-H bond length becomes larger, the NOONs should smoothly transition from having one bonding and one antibonding orbital to two singly occupied orbitals. Instead, there is an abrupt rise in the NOONs at the point of unrestriction, at 1.154 Å, which is elongated from the equilibrium bond length of 0.76 Å. At the point of unrestriction, the maximum eigenvalue of the 1-PDM is 2.254592 while the minimum eigenvalue is -0.254592. Since there are only 2 orbitals in this case, at complete dissociation, both orbitals should be singly occupied, which is indeed seen in Fig. 3.7.

Based on the previous results, one should expect to get poor physical properties at, and just past, the point of unrestriction. However, because the total charge density does not break symmetry, the dipole moment is always zero, even though the 1-PDM is not always N-representable. On the other hand, a property like the gradient with respect to the nuclear coordinates still exhibits a discontinuity at the point of unrestriction. It is clearly advisable to avoid calculating physical properties when the relaxed 1-PDM violates N-representability, even if there are some situations where the physical property matrix (such as dipole integrals) does not couple to the unphysically large values in the OV block of the 1-PDM.
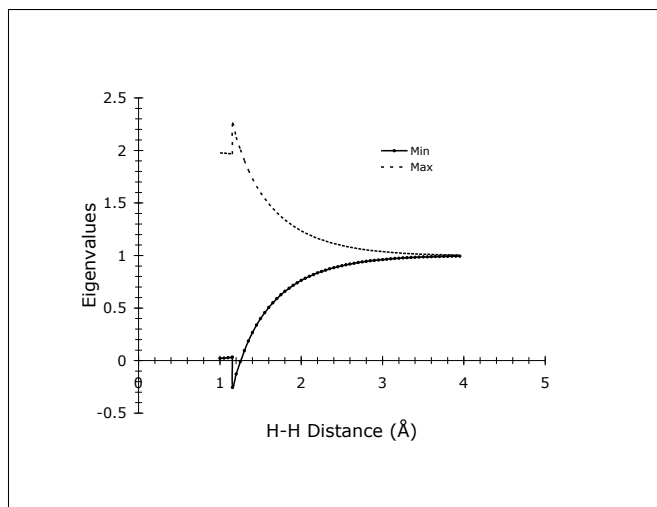
Figure 3.7: Eigenvalues of the 1-PDM for the unrestricted dissociation of H_2

3.3.3 Radical Frequencies

When employing relatively low-level quantum chemical techniques such as MP2 theory, there are several molecules that are difficult for single determinant methods to get correct. One class of especially difficult molecules are small radical species. These molecules generally have several low-lying excited states, which makes it easy for the wavefunction to become spin-contaminated. Some years ago, a paper by Byrd *et al.*[45] did a survey of frequencies for these small molecules and ions using a variety of methods and basis sets of differing quality.

One of the most peculiar findings of this paper was that MP2 theory could fail dramatically in the prediction of vibrational frequencies for several radical species including NO, O_2^+, and CO_2^+. When MP2 frequencies were calculated for these species, the vibrational levels were in error by over 400 cm^{-1}. However, MP2's performance for the other radical species was comparatively satisfactory. In light of the discussion in this paper, it seems possible that the effective density matrix in the species yielding unphysical frequencies may not be N-representable. A closer look at the eigenvalues of the 1-PDM therefore seems warranted as a possible explanation for these unphysical frequencies. These results are summarized in Table 3.1, where it is evident that two of the three most problematic molecules do indeed have N-representability issues when the geometry is optimized using MP2.

One interesting feature about these three molecules is that O_2^+ does not have any unphysical NOONs. Upon closer inspection, the NO and CO_2^+ molecules have frequencies that are in error by over 1000 cm^{-1} whereas O_2^+ is only in error by about 400 cm^{-1}. In this example, it is clear that having a non-N-representable wavefunction can result in catastrophic errors in predicted vibrational frequencies. However, not all large failures in frequencies result from a violation of N-representability; errors can also result from having a spin-contaminated reference, or spatial symmetry breaking. Finally, it may not always be the case that MP2 frequencies will be unacceptably poor when an MP2 1-PDM results in unphysical eigenvalues in the 1-PDM.

Molecule[a]	Basis	NOON > 2	NOON < 0	calc. freq. (cm^{-1})	exp. freq. (cm^{-1})
CO_2^+	cc-pVDZ	2.061308	-0.061872	2759.78	1423
			-0.000612		
CO_2^+	cc-pVTZ	2.048468	-0.053591	2793.15	1423
			-0.000460		
O_2^+	cc-pVDZ	N/A	N/A	1443.73	1905
O_2^+	cc-pVTZ	N/A	N/A	1522.40	1905
NO	cc-pVDZ	2.043760	-0.051375	3643.76	1904
NO	cc-pVTZ	2.006234	-0.019550	3229.35	1904

[a] Geometries optimized using MP2 within the given basis

Table 3.1: Unphysical NOONs and calculated frequencies for several radical species

3.3.4   1,3-Butadiene and Longer Polyenes

Previously, it was discussed how N-representability problems could occur at non-equilibrium geometries (i.e. bond breaking). This does not mean that this problem only occurs away from equilibrium as is seen for the radical species of the previous section. All that is needed is a molecule with a large amount of radical character in the ground state. As opposed to the radicals seen in the previous section, an example of a closed-shell molecule with potentially large radicaloid character is 1,3-butadiene and the larger polyenes.[46, 47] For instance, butadiene is a superposition of the traditional bonding motif and one with a central double bond and a radical on each terminal carbon (Scheme 3.1). Since this molecule will have di-
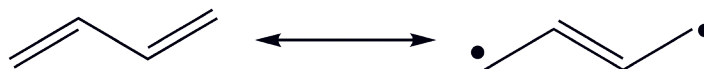
Scheme 3.1: Resonance structures of 1,3-butadiene

radicaloid character even in the ground state, it is possible to be at or near the unrestriction point for this molecule even at the equilibrium geometry.

Using the experimental geometry,[48] the ground state of 1,3-butadiene was calculated using MP2 theory with a cc-pVDZ basis set. The diradical structure in Scheme 1 will lead to a mixing in of the triplet state even in the ground state which will necessarily lead to a non-zero $\langle S^2 \rangle$ value. The resulting wavefunction is fairly spin-contaminated with an $\langle S^2 \rangle$ value of 0.4115. Even though the restricted MP2 wavefunction results in a lower energy, the restricted reference wavefunction does not reflect the biradicaloid character shown in Scheme 3.1. Therefore the unrestricted MP2 wavefunction is used even though it is not the lowest energy MP2 solution available. When the resulting relaxed density matrix from the unrestricted MP2 wavefunction is diagonalized, there are 4 eigenvalues which violate the N-representability rules. Two values are greater than 2 and two values are less than 0 (2.281511, 2.062887, -0.082335, and -0.299645, respectively).

It should be noted that the unphysical NOONs are not limited to 1,3-butadiene, but will most likely occur for the whole polyene series. In Table 3.2, the unphysical NOONs associated with several of the longer polyenes are shown. Also, this problem does not go away when the basis set is improved. For instance in the butadiene case, larger basis set results are poorer because the double-ζ basis set is not that close to the unrestriction point. As the basis

set is enlarged, the spin-polarization decreases slightly, bringing the wavefunction closer to the unrestriction point, which increases the deviation in the NOONs. In the polyene series, as the number of double bonds grow, so does the number of unphysical NOONs, except for decapentaene (where the geometry is not taken from experiment but from CASSCF calculations). As the number of unphysical NOONs increases, the largest deviation from 0 and 2 decreases.

Molecule[a]	Basis	NOON > 2	NOON < 0
1,3-butadiene	cc-pVDZ	2.062884	-0.082332
		2.281495	-0.299628
1,3-butadiene	cc-pVTZ	2.066291	-0.091037
		2.310525	-0.333645
1,3-butadiene	cc-pVQZ	2.068523	-0.094721
		2.324101	-0.348511
1,3,5-hexatriene	cc-pVDZ	2.015680	-0.036444
		2.064412	-0.082945
		2.130776	-0.148059
1,3,5,7-octatetraene	cc-pVDZ	2.010327	-0.030853
		2.031388	-0.051848
		2.101808	-0.119498
		2.143870	-0.161121
1,3,5,7,9-decapentaene	cc-pVDZ	2.000688	-0.021180
		2.011111	-0.031426
		2.051396	-0.068697
		2.082166	-0.099492

Table 3.2: Unphysical NOONs for the first polyenes. [a] Geometries from Ref. [48]

We note that we cannot in fact compute UMP2 frequencies for the polyenes. In order to obtain UMP2 vibrational frequencies, an unrestricted MP2 minimum is necessary. However, since the restricted MP2 energy is lower, the molecule does not have a local minimum on the unrestricted MP2 surface.

3.4   Discussion

The main focus of this study is to show how MP2 can fail in certain situations by yielding 1-PDMs that violate the rules of N-representability. However we have not yet addressed the question of which method to use in these situations when UMP2 becomes an unusable option. If one wishes to continue to use a simple MP2-like method, which thus continues to require unrestricted orbitals, then we need to remove the large orbital response terms. Since they are the response of the orbitals to changes in the reference wavefunction, the natural solution would be to use a method which employs orbital optimization. Orbital-Optimized opposite spin MP2 (O2)[19] is therefore one suitable choice since this method is simply opposite spin MP2 with orbital optimization so as to keep computational cost scaling manageable, while orbital optimization means that the orbital response is always zero, mitigating the

N-representability problem. Applying the O2 method to the LiH problem discussed above confirms that the results are greatly improved (see Fig. 3.8). Some limitations of low-order perturbation theory linger, however, in the form of an unphysical kink in the dipole moment at the point of unrestriction, suggesting a jump from the restricted to the unrestricted surface. Evidently we have pushed the discontinuity in the energy function from the first derivative to the second derivative. In this respect O2 behaves similarly to SCF methods themselves, which also will have discontinuities in the second derivative properties, because they depend on orbital first derivatives, which are discontinuous (via eq. 3.14).
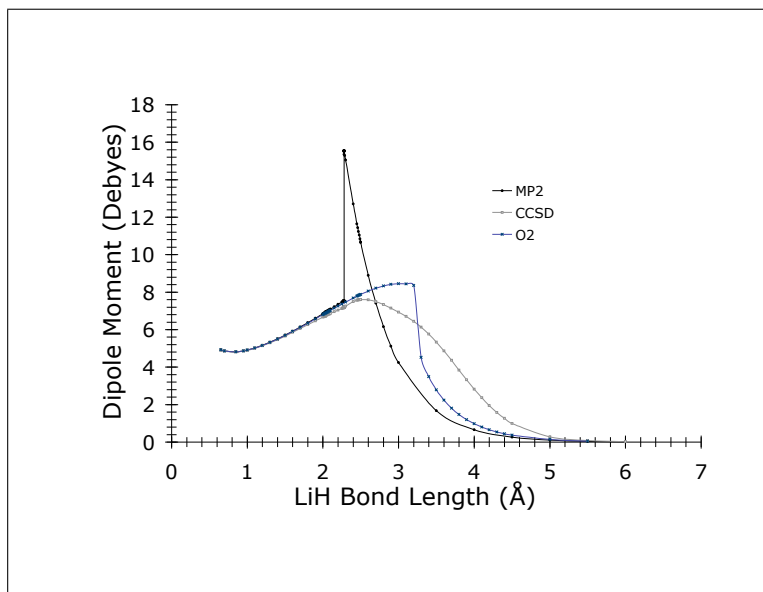
Figure 3.1: Unphysical jumps in the dipole moment of LiH at the unrestriction point as calculated by MP2 and O2-MP2. The dipole moment as calculated by the UCCSD method is also included in order to emphasize the unphysical jump seen in the O2 method.

If MP2 fails to maintain N-representability and the system of interest is relatively small, then it would be advisable to use a more computationally sophisticated and expensive coupled-cluster method. The system size has to be relatively small because the scaling of even singles and doubles coupled cluster theory (CCSD) is N^6 instead of the fourth order scaling of O2 or opposite spin MP2. Yet, if a perturbative triples correction is added to the CCSD energy, as in *e.g.* CCSD(T), then one can still have N-representability problems when orbitals unrestrict. This occurs because the only term that changes in eq. 3.11 is the Lagrangian, which will be non-zero for methods with perturbative corrections.

Another way to maintain N-representability is to employ several configurations using multi-configurational SCF. However, this method requires the user to pick the configurations and is therefore not a black box method. For the LiH problem, this method is relatively simple to employ, but for some of the more complex problems shown in this study, like the polyene series, the number of configurations required becomes very large making this method an undesirable choice.

3.5 Conclusions

From this study, it should evident that researchers should be wary of MP2 results emanating from near the unrestriction point. This is because the orbital response (Z-vector) equations which form the off-diagonal blocks of the one particle density matrix have a potential singularity at the unrestriction point. This singularity leads to abnormally large and small eigenvalues of the 1-PDM, which is a violation of N-representability. These large values can lead to physical properties that are unphysical, like vibrational frequencies or dipole moments. Orbital optimized MP2 will solve the N-representability problem by eliminating orbital response, yet this method still has issues at the unrestriction point. Even though we have shown that unrestricted MP2 is unreliable near the unrestriction point, in the large majority of cases, MP2 is a perfectly fine method to use in order to capture the leading part of the correlation energy, and the use of unrestricted orbitals to allow correct bond-breaking is preferable to enforcing spin-restricted orbitals.

Bibliography

[1] P. LOWDIN and H. SHULL, *Phys. Rev.* **101**, 1730 (1956).

[2] P. LOWDIN, *Phys. Rev.* **97**, 1474 (1955).

[3] P. PULAY, G. FOGARASI, F. PANG, and J. BOGGS, *J. Am. Chem. Soc.* **101**, 2550 (1979).

[4] V. STAROVEROV and E. DAVIDSON, *Chem. Phys. Lett.* **330**, 161 (2000).

[5] M. HEAD-GORDON, *Chem. Phys. Lett.* **372**, 508 (2003).

[6] H. JENSEN, P. JORGENSEN, H. AGREN, and J. OLSEN, *J. Chem. Phys.* **88**, 3834 (1988).

[7] U. SCHOLLWOCK, *Rev. Mod. Phys.* **77**, 259 (2005).

[8] D. MAZZIOTTI, *Phys. Rev. A* **57**, 4219 (1998).

[9] H. NAKATSUJI and K. YASUDA, *Phys. Rev. Lett.* **76**, 1039 (1996).

[10] F. COLMENERO and C. VALDEMORO, *Int. J. Quantum Chem.* **51**, 369 (1994).

[11] A. COLEMAN, *Rev. Mod. Phys.* **35**, 668 (1963).

[12] A. COLEMAN, *Adv. Chem. Phys.* **134**, 3 (2007).

[13] D. MAZZIOTTI and R. ERDAHL, *Phys. Rev. A* **6304** (2001).

[14] M. GORDON, M. SCHMIDT, G. CHABAN, K. GLAESEMANN, W. STEVENS, and C. GONZALEZ, *J. Chem. Phys.* **110**, 4199 (1999).

[15] F. Weigend, M. Haser, H. Patzelt, and R. Ahlrichs, *Chem. Phys. Lett.* **294**, 143 (1998).

[16] F. Aquilante and T. B. Pedersen, *Chem. Phys. Lett.* **449**, 354 (2007).

[17] Y. Jung, R. Lochan, A. Dutoi, and M. Head-Gordon, *J. Chem. Phys.* **121**, 9793 (2004).

[18] R. Lochan, Y. Jung, and M. Head-Gordon, *J. Phys. Chem. A* **109**, 7598 (2005).

[19] R. C. Lochan and M. Head-Gordon, *J. Chem. Phys.* **126** (2007).

[20] S. Grimme, *J. Chem. Phys.* **118**, 9095 (2003).

[21] R. A. Distasio, Jr. and M. Head-Gordon, *Mol. Phys.* **105**, 1073 (2007).

[22] M. Schutz, G. Hetzer, and H. Werner, *J. Chem. Phys.* **111**, 5691 (1999).

[23] S. Saebo and P. Pulay, *Annu. Rev. Phys. Chem.* **44**, 213 (1993).

[24] M. Lee, P. Maslen, and M. Head-Gordon, *J. Chem. Phys.* **112**, 3592 (2000).

[25] R. P. Steele, R. A. DiStasio, Jr., Y. Shao, J. Kong, and M. Head-Gordon, *J. Chem. Phys.* **125** (2006).

[26] R. A. Distasio, Jr., R. P. Steele, and M. Head-Gordon, *Mol. Phys.* **105**, 2731 (2007).

[27] A. Tarnopolsky, A. Karton, R. Sertchook, D. Vuzman, and J. M. L. Martin, *J. Phys. Chem. A* **112**, 3 (2008).

[28] S. Grimme, *J. Chem. Phys.* **124** (2006).

[29] J. Angyan, I. Gerber, A. Savin, and J. Toulouse, *Phys. Rev. A* **72** (2005).

[30] A. Gorling and M. Levy, *Phys. Rev. A* **50**, 196 (1994).

[31] T. Benighaus, R. A. DiStasio, Jr., R. C. Lochan, J.-D. Chai, and M. Head-Gordon, *J. Phys. Chem. A* **112**, 2702 (2008).

[32] P. Hobza, J. Sponer, and T. Reschel, *J. Comput. Chem.* **16**, 1315 (1995).

[33] S. Kristyan and P. Pulay, *Chem. Phys. Lett.* **229**, 175 (1994).

[34] G. Trucks, E. Salter, C. Sosa, and R. Bartlett, *Chem. Phys. Lett.* **147**, 359 (1988).

[35] E. Salter, G. Trucks, G. Fitzgerald, and R. Bartlett, *Chem. Phys. Lett.* **141**, 61 (1987).

[36] M. Frisch, M. Headgordon, and J. Pople, *Chem. Phys. Lett.* **166**, 275 (1990).

[37] N. Handy and H. Schaefer, *J. Chem. Phys.* **81**, 5031 (1984).

[38] K. Raghavachari, J. Pople, E. Replogle, and M. Headgordon, *J. Phys. Chem.* **94**, 5579 (1990).

[39] P. Jorgensen and T. Helgaker, *J. Chem. Phys.* **89**, 1560 (1988).

[40] R. A. Distasio, Jr., R. P. Steele, Y. M. Rhee, Y. Shao, and M. Head-Gordon, *J. Comput. Chem.* **28**, 839 (2007).

[41] R. Seeger and J. Pople, *J. Chem. Phys.* **66**, 3045 (1977).

[42] T. Crawford, J. Stanton, W. Allen, and H. Schaefer, *J. Chem. Phys.* **107**, 10626 (1997).

[43] Y. Shao, L. F. Molnar, Y. Jung, J. Kussmann, C. Ochsenfeld, S. T. Brown, A. T. B. Gilbert, L. V. Slipchenko, S. V. Levchenko, D. P. O'Neill, R. A. DiStasio, Jr., R. C. Lochan, T. Wang, G. J. O. Beran, N. A. Besley, J. M. Herbert, C. Y. Lin, T. Van Voorhis, S. H. Chien, A. Sodt, R. P. Steele, V. A. Rassolov, P. E. Maslen, P. P. Korambath, R. D. Adamson, B. Austin, J. Baker, E. F. C. Byrd, H. Dachsel, R. J. Doerksen, A. Dreuw, B. D. Dunietz, A. D. Dutoi, T. R. Furlani, S. R. Gwaltney, A. Heyden, S. Hirata, C.-P. Hsu, G. Kedziora, R. Z. Khalliulin, P. Klunzinger, A. M. Lee, M. S. Lee, W. Liang, I. Lotan, N. Nair, B. Peters, E. I. Proynov, P. A. Pieniazek, Y. M. Rhee, J. Ritchie, E. Rosta, C. D. Sherrill, A. C. Simmonett, J. E. Subotnik, H. L. Woodcock, III, W. Zhang, A. T. Bell, A. K. Chakraborty, D. M. Chipman, F. J. Keil, A. Warshel, W. J. Hehre, H. F. Schaefer, III, J. Kong, A. I. Krylov, P. M. W. Gill, and M. Head-Gordon, *Phys. Chem. Chem. Phys.* **8**, 3172 (2006).

[44] F. Neese, T. Schwabe, and S. Grimme, *J. Chem. Phys.* **126** (2007).

[45] E. Byrd, C. Sherrill, and M. Head-Gordon, *J. Phys. Chem. A* **105**, 9736 (2001).

[46] J. H. Starcke, M. Wormit, J. Schirmer, and A. Dreuw, *Chem. Phys.* **329**, 39 (2006).

[47] C. M. Marian and N. Gilka, *J. Chem. Theory Comput.* **4**, 1501 (2008).

[48] K. Nakayama, H. Nakano, and K. Hirao, *Int. J. Quantum Chem.* **66**, 157 (1998).

Chapter 4

Exploring the competition between localization and delocalization of the neutral soliton defect in polyenyl chains with the orbital optimized second order opposite spin method

4.1 Introduction

One of the major accomplishments of quantum chemistry is the ability to accurately predict the geometries of complicated molecular systems using analytical gradient methods [1, 2, 3]. Relatively inexpensive methods such as Kohn-Sham density functional theory (DFT) with functionals such as BLYP [4, 5] or B3LYP [6] are generally very successful for the prediction of molecular geometries, not only for closed shell molecules, but also for many radicals since DFT is generally less susceptible to the symmetry-breaking and spin contamination issues [7] that plague Hartree-Fock theory, the simplest wave function treatment. However, even Hartree-Fock theory, which ignores electron correlation effects, yields generally reliable results for molecular geometries of closed shell organic molecules [8, 9].

Particularly significant challenges in the prediction of molecular geometries using DFT still arise in some classes of systems where there is an odd electron, or hole whose extent of localization (or delocalization) depends on a delicate balance of competing factors. A first class of examples involve effect of ionization in either simple molecules, such as homonuclear diatomic cations [10], or complex systems, such as radiation damage in DNA [11], as illustrated by strong geometric changes in model base pairs upon ionization. Another class of examples involve the effect of electron attachment, where an analogous question arises about the extent of localization of the excess electron, and the associated structural relaxations relative to the neutral. A third class of examples are neutral radicals. These challenges arise because DFT suffers from the well-known self-interaction error [12, 13], which causes common functionals to prefer electronic structure where the odd electron or hole is overly delocalized.

Conversely, the HF model will tend to make the odd electron or hole too localized as a result of neglecting electron correlation effects. Recent functionals such as range-separated hybrids [14, 15] reduce but do not eliminate this problem.

For purposes of this paper, we shall consider a polyenyl chain (i.e. a polyacetylene (PA) chain with an odd number of C atoms, $C_{2n-1}H_{2n+1}$), as illustrative of a system of this type. The question is how localized is the charge distribution associated with the odd electron? Resonance structures can be drawn with the electron localized at any carbon site, but the energy advantage associated with multiple resonance structures must be weighed against the energy penalty associated with at least partial loss of the bond alternation that exists in closed shell PA chains. In other words, we can anticipate that there is a potentially delicate balance between competing effects that will determine the extent of delocalization and therefore the geometric deformation associated with the "defect" represented by the radical electron. These considerations are schematically illustrated in Fig. 4.1 below. From the viewpoint of orbital energies, the polymeric all-trans PA is a semiconductor with a band gap of 1.5 eV [16, 17]. The energy level associated with the radical electron will reside in this gap.
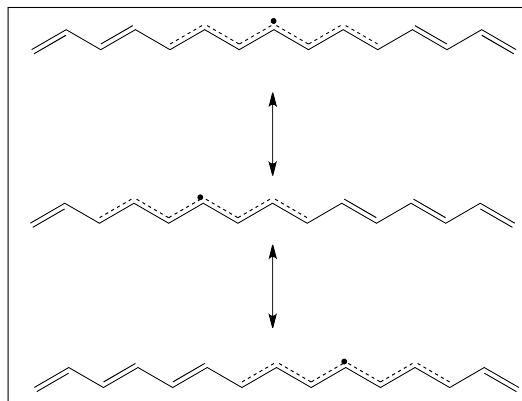
Figure 4.1: Possible resonance structures for a neutral soliton on a polyacetylene chain

The region associated with the radical electron in a $C_{2n-1}H_{2n+1}$ polyenyl chain is a model of a neutral soliton in PA [18]. A soliton may be defined as a solitary wave capable of propagating without either dissipation or changes in shape. In a very long PA chain, the defect associated with a radical electron may move in this way. Solitons occur as electromagnetic waves in a dielectric medium, such as in fiber optic cables, where it has been hoped that they might be used to transmit large amounts of data [19, 20, 21, 22, 23, 24]. In the context of PA, the soliton defect can play a role in the conduction properties of doped PA [25, 26, 27, 28, 29, 30, 31, 32, 33, 34, 35, 36]. The discovery that doped PA chains are good conductors has played an important role in the development of conductive polymers, an area that was recognized with the Nobel Prize in Chemistry in 2000. It is possible that PA chains might be used in organic electronics as molecular wires.[37, 38, 39, 40] These wires could possibly be used in organic light-harvesting devices in order to facilitate electron transfer from the organic chromophore to the traditional electronics.

In light of this interest, there have been numerous previous calculations on the neutral soliton defect [41, 42, 43, 44, 45, 46]. If a single reference method like unrestricted Hartree-Fock is used to solve this problem, the result is a highly spin contaminated wavefunction,

which makes both HF itself and perturbation corrections unreliable [47, 48, 49, 50, 51, 52], even for optimized geometries [53, 54]. This same problem also plagues hybrid DFT methods that rely on Hartree-Fock theory to supply a portion of the exact exchange. In order to reliably determine the electronic structure and geometry of even non-defective chains of double bonds, very expensive quantum chemical methods are believed to be needed [55]. The implications for neutral soliton modeling are well-illustrated by the work of Bally et al [41]. When the CASSCF and CCSD methods are used, the electronic structure and geometry of these PA chains were incorrect, and a perturbative correction, CASPT2 and CCSD(T) respectively, appeared to be required. With such computationally expensive methods (N^7 for CCSD(T) and exponential for CASSCF) treating large systems becomes computationally intractable [56, 57]. Standard DFT methods also perform quite poorly [58], with standard functionals underestimating the degree of bond alternation in small polyenyl chains.

In this paper we introduce the analytical gradient for an economical wave function method for treating electron correlation, which may have the ability to address the challenge of treating the neutral soliton defect in long chains. The approach is the optimized orbital scaled opposite spin 2nd order Møller Plesset perturbation theory, which we abbreviate as O2. O2 is a simplification of MP2 with orbital optimization, which has also been recently explored [59]. Since O2 allows the orbitals to be determined in the presence of electron correlation, the competition between localization and delocalization of a radical electron may be much better described than when MP2 is applied from an unrestricted (or restricted) HF reference. Furthermore, O2 can be evaluated with only N^4 scaling computational effort, unlike MP2 (or OO-MP2) which is N^5. Scaling the spin components of MP2 theory originated with Grimme [60], was later adapted to scale only the opposite spin terms, yielding the N^4 scaling SOS-MP2 method [61]. The O2 method also has the important formal advantage of providing 1-particle density matrices that avoid n-representability problems of MP2 theory [62], and has already been demonstrated to greatly reduce artificial symmetry breaking in radicals [59], and, therefore significantly improve on MP2 predictions for optimized geometries and vibrational frequencies for such radicals. O2 (and indeed also OO-MP2) are essentially very tractable approximations to Brueckner coupled cluster methods that include orbital optimization [59, 63].

The outline of the remainder of the paper is as follows. In the theory section we introduce the analytical gradient theory for the O2 method. This presentation is relatively brief, because both the theory and the implementation can be conveniently developed as extensions of the SOS-MP2 analytical gradient theory, which has already been reported [64], and separately extended to excited states [65]. With this new computational tool in hand, we then turn to its application to the problem of the width of the neutral soliton defect in finite polyenyl chains. The O2 method will be compared against accurate coupled cluster calculations for small chains, and then applied to long chains, and compared against a variety of density functionals, including range-separated hybrids[66] which significantly reduces the self-interaction problem that plagues standard functionals.

4.2 Theory

We begin by summarizing the O2 correlation energy expression, which was introduced previously [59]. We start from the opposite spin MP2 correlation energy, and introduce two approximations that each yield chemically negligible errors when properly employed [61]. First, we employ an auxiliary basis for use in a resolution-of-the-identity approximation [67, 68] to replace 4 center two electron integrals by linear combinations of 2 and 3 center integrals. Second, we use a numerical quadrature evaluation of the Laplace transform of the standard MP2 energy denominators [69]. With these approximations, the opposite spin energy (E_{OS}) can be written as shown in Eqs. (4.1)-(4.3).

$$E_{OS} = -\sum_{\tau}^{N_\tau} \omega_\tau \sum_{PQ} X_{PQ}^\alpha(\tau) X_{PQ}^\beta(\tau) \tag{4.1}$$

$$X_{PQ}^\alpha = \sum_{ia}^{\alpha} B_{ia}^P(\tau) B_{ia}^Q(\tau) \tag{4.2}$$

$$B_{ia}^P = \sum_R (ia|R)(R|P)^{-1/2} exp[(\epsilon_i - \epsilon_a)t_\tau] \tag{4.3}$$

In the aforementioned equations we adopt the conventions of $i,j,...$ referring to occupied orbitals and $a,b,...$ referring to virtual orbitals. $P,Q,...$ indicate auxiliary basis functions and $\tau, N_\tau, \omega_\tau, t_\tau$ refer to the quadrature point, total number of quadrature points, and weight and root corresponding to each quadrature point, respectively. The O2 total energy will then simply be the scaled-opposite spin correlation energy added to a reference energy.

$$E_{O2} = E_{ref} + \omega_{OS} E_{OS} \tag{4.4}$$

$$E_{ref} = \sum_i F_{ii} - \frac{1}{2} \sum_{ij} \langle ij||ij\rangle \tag{4.5}$$

Here we define the scaling parameter ω_{OS} to be 1.2, this value was empirically determined previously [59]. Orbitals are optimized using the following condition.

$$\frac{dE_{O2}}{d\theta} = L_{O2}\frac{dU}{d\theta} = 0 \tag{4.6}$$

The O2 Lagrangian is the same as the standard SOS-MP2 occupied-virtual Lagrangian except for an extra term to account for the fact that when the orbitals are optimized, they will not satisfy Brilloun's condition ($F_{ov} \neq 0$). Therefore the ov Lagrangian has four terms

instead of the usual three.

$$\overline{L}_{ck} = (\overline{L1})_{ck} + (\overline{L2})_{ck} + (\overline{L3})_{ck} + (\overline{L4})_{ck} \tag{4.7}$$

$$^\tau\Gamma_{ia}^{M,\beta} = \sum_{KL}(M|K)^{-1/2}\,{}^\tau X_{KL}^\beta B_{ia}^L \tag{4.8}$$

$$(\overline{L1})_{ck} = \sum_\tau^{N_\tau}\omega_\tau\sum_a^\alpha exp(t_\tau(\epsilon_c - \epsilon_a))\sum_M {}^\tau\Gamma_{ka}^{M,\beta}(ca|M) \tag{4.9}$$

$$(\overline{L2})_{ck} = \sum_\tau^{N_\tau}\omega_\tau\sum_i^\alpha exp(t_\tau(\epsilon_i - \epsilon_c))\sum_M {}^\tau\Gamma_{ic}^{M,\beta}(ik|M) \tag{4.10}$$

$$(\overline{L3})_{ck} = \sum_{ij}A_{ijck}\overline{P}_{ij} + \sum_{ab}A_{abck}\overline{P}_{ab} \tag{4.11}$$

$$A_{pqrs} = (pq||rs) - (ps||qr) \tag{4.12}$$

$$(\overline{L4})_{ck} = \sum_i F_{ci}\overline{P}_{ik}^{(2)} + \sum_a F_{ka}\overline{P}_{ac}^{(2)} \tag{4.13}$$

In the above equations, the overbar refers to quantities that are independent of Laplace quadrature.

Much like the energy formulation of O2, the corresponding analytic gradient is extremely similar to the SOS-MP2 analytic gradient for obvious reasons. [64] Essentially the form of the SOS-MP2 gradient will be seen here as well with a slight modification to the energy-weighted density (W). The general form of the closed-shell gradient using the RI approximation is shown below

$$E_{RI}^x = \sum_{\mu\nu} P_{\mu\nu}H_{\mu\nu}^x + \sum_{\mu\nu} W_{\mu\nu}S_{\mu\nu}^x + \sum_{\mu\nu\lambda\sigma}\Gamma_{\mu\nu\lambda\sigma}^S(\mu\nu|\lambda\sigma)^x + \sum_{\mu\nu}\sum_K\Gamma_{\mu\nu}^K(\mu\nu|K)^x + \sum_{KL}\gamma_{KL}(K|L)^x \tag{4.14}$$

where $\Gamma_{\mu\nu\lambda\sigma}^S$, $\Gamma_{\mu\nu}^K$, and γ_{KL} are the separable 2-PDM and the RI-specific 2-PDM contracted with three- and two-centered electron integral derivatives, respectively.[65] Explicit definitions for all these terms can be found elsewhere, but we will focus on the terms unique to the O2 gradient. The energy-weighted density (W) can be expressed in the mixed Lagrangian formalism where parts density are formed from the Lagrangian. Since the occupied-occupied (oo) and virtual-virtual (vv) blocks of the W matrix are the same formally as the SOS-MP2 gradient, only the ov block will be examined.

$$\overline{W}_{ai}^{(2)} = -(\overline{L2})_{ai} - \overline{P}_{ai}^{(2)}\epsilon_i - (\overline{L4})_{ai} \tag{4.15}$$

In the update to the energy-weighted density the first two terms are from the normal formulation of the SOS-MP2 gradient, whereas the third term is another consequence of having orbitals that do not satisfy the Brillouin condition. Another result of orbital optimization is that the ov block of the relaxed one particle density matrix (1-PDM) is zero. This occurs because the ov block of the 1-PDM is equivalent to the Z-vector equation, which is based on the ov Lagrangian, which since the orbitals are optimized to be formally zero. Therefore the update to the ov block of the W matrix, in practice, only has two terms that are based on parts of the ov Lagrangian. So the only update needed to the nuclear gradient from the result

of orbital optimization is the extra term seen in the update of the energy-weighted-matrix and the ov terms of the one particle density matrix are now zero. This simple addition makes the scaling of the gradient the same as the scaling for calculating the energy.

4.3   Results

All calculations were done with the Q-Chem electronic structure software package using the Pople style 6-31G(d) basis set unless otherwise stated [70]. Although this basis set is only double zeta quality, more computationally demanding methods like CASSCF and UCCSD(T) limit the size of the basis set significantly and fair comparison will necessitate the use of the same basis set for all methods. Unless otherwise stated, all calculations are performed with spin-polarized (unrestricted) orbitals.

One of the best ways to objectively validate a method is to compare results directly to experiment. However, experimental geometries are only available for the small allyl radical, yet a valid comparison will still warrant insight. In a paper published in 2000, Bally et al. investigated smaller polyenyl radicals using a range of methods.[41] For the allyl radical, the computationally expensive CASSCF and UCCSD(T) methods both compare favorably to experiment with UCCSD(T) slightly outperforming CASSCF.[41] It is therefore reasonable to use both of these methods as a benchmark for testing the O2 method with bigger polyenyl radical systems. Starting with the small system so as to compare O2 to experiment is a worthwhile endeavor in order to contrast with the other accurate methods. For the smallest allyl radical there are four geometrical parameters: two carbon-hydrogen bond distances, one carbon-carbon bond distance, and one bond angle. Comparing the bond distances in table 4.1, UCCSD(T) has a maximal error of 0.005 Å from experiment and this would be considered chemical accuracy. The O2 method has similar accuracy with a maximum error of 0.006 Å, outperforming CASSCF which has a maximal error of 0.013 Å. All three methods faithfully reproduce the central bond angle. It is of note that the magnitude of the maximum error become larger as the basis set increases for the O2 method. Evidently, there is some fortuitous cancellation of errors with the smaller basis set. The geometrical results of O2 for the allyl radical are comparable to CASSCF and UCCSD(T), albeit slight larger in error than UCCSD(T). Henceforth, the CCSD(T) results will be considered the benchmark and the basis of comparison for slightly larger polyenyl radicals.

	Exp.[a]	CASSCF[a]	UCCSD(T)[a]	O2	O2[b]
r_{C-C}	1.387	1.390	1.392	1.388	1.380
r_{C-H1}	1.091	1.078	1.093	1.086	1.077
r_{C-H2}	1.084	1.074	1.089	1.090	1.078
α	124.7	124.7	124.3	124.4	124.4

[a]Geometries from Bally[41]
[b]Calculation done at the triple-ζ level to show results closer to the complete basis set limit

Table 4.1: Comparison of geometries for the allyl radical

Another geometrical measure of accuracy in polyenyl radicals is the bond alternation at the end of the molecule.[41] If the soliton is localized toward the center of the molecule (as

will be seen later), the first and last carbon-carbon bonds will have double bond character with the next carbon-carbon bond toward the center of the molecule having significant single bond character. As the polyenyl chain becomes longer, this bond length difference should eventually level off to the value matching the experimental polyacetylene terminal bond length alternation value of 0.09 Å± 0.01 Å. [71]

Figure 4.2 shows the bond length difference between the first and second carbon-carbon bonds for a variety of methods in several small and large PA chains. Highly accurate CCSD(T) and CASSCF methods are not computationally feasible for $C_{41}H_{43}$ chain because of the large size of the molecule coupled with the steep size scaling of the computational cost of these methods. Therefore the only methods that are practical to run on a molecule of this size are DFT, Hartree-Fock (HF), and MP2-based methods. The two features in figure 4.2 that have physical importance is that the bond-length difference for the two largest chains should be similar and that the largest polyenyl chain should have a terminal bond length difference of 0.09 Å. The justification for the first feature is that the soliton is experimentally known to be less than 20 carbons long while the second feature is based on the experimental long-chain limit. [71, 72]
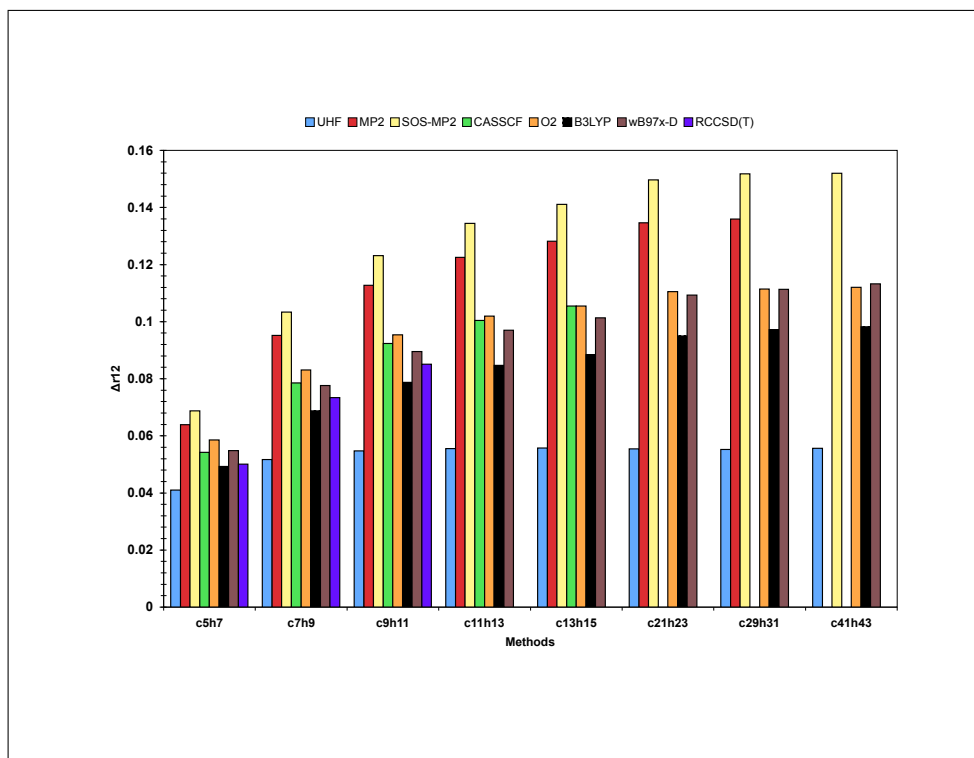
Figure 4.2: Comparison of the difference of first two carbon-carbon bond lengths in polyenyl chains for various methods

The MP2 and SOS-MP2 bond difference keeps increasing as the polyenyl chain becomes longer, suggesting that the soliton is affecting the end carbons even in the largest chain. Both of these methods culminate in a terminal bond difference that is significantly larger than the experimental value. The results for the UHF method imply that there is a soliton always influencing the terminal bond difference causing the terminal bond difference to be

too small. Comparing at the final two columns, it appears that the O2 method, ωB97x-D, and B3LYP produce the most satisfactory results and capture the correct physicality for the terminal bond length difference.

Another way to measure the accuracy of a given method on PA solitons is to look at the expectation value of the spin squared operator ($\langle S^2 \rangle$). For these polyenyl radical chains containing an odd-numbered of carbon atoms, there should be one unpaired electron resulting in a $\langle S^2 \rangle = 0.75$, i.e. a doublet. However, UHF-based methods applied to the underlying PA chain are known to have problems with spin-contamination because of the various resonance structures that can be formed by homolytically cleaving double bonds into a single bond and two radicals as seen in figure 4.3.[58, 42] Since the number of double bonds grows with chain length, it follows that UHF spin-contamination problems get worse as the number of possible biradical resonance structures increases. In turn, this issue can lead to N-representablility problems for UMP2 methods, especially in larger chain lengths, which can lead to unphysical results and is in general undesirable.[62] We might expect the methods that incorrectly describe the PA chain would also be physically incorrect for the polyenyl radical. This fact can be seen by looking at the $\langle S^2 \rangle$ value for a variety of polyenyl chains with a variety of methods in table 4.2.
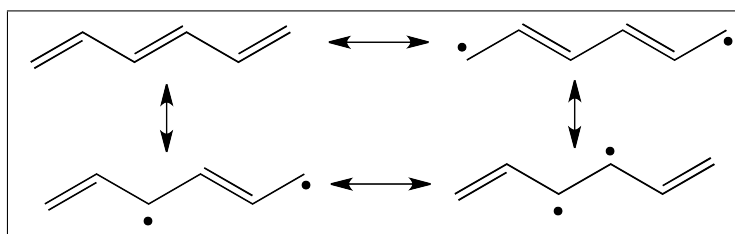
Figure 4.3: Possible biradical resonance structures for a small polyacetylene chain

Method	C_5H_7	C_7H_9	C_9H_{11}	$C_{11}H_{13}$	$C_{13}H_{15}$	$C_{41}H_{43}$
RCCSD(T)^a	0.747	0.746	0.746	—	—	—
UHF	1.218	1.513	1.838	2.177	2.521	7.384
MP2	1.164	1.392	1.643	1.913	2.200	6.752
SOS-MP2	1.167	1.393	1.641	1.906	2.188	6.760
B3LYP	0.798	0.814	0.830	0.846	0.864	1.234
ωB97x-D	0.822	0.857	0.898	0.943	0.993	2.049
O2	0.777	0.781	0.784	0.786	0.787	0.788

^{a}Expectation values from Bally et al.[41]

Table 4.2: Values for $\langle S^2 \rangle$. Deviations from 0.75 can be thought of as a measure of spin-contamination

With UHF and UMP2, spin-contamination is an issue even at the smaller polyenyl chain lengths. For UHF, UMP2, and USOS-MP2, applied to $C_{13}H_{15}$ the spin expectation value is around the value for a triplet ($\langle S^2 \rangle = 2.0$) instead of the expectation value for a doublet. This large expectation value is the result of the UHF reference over-localizing radicals on each carbon. Instead of having just one radical, there are now effecively additional radicals leading to a high amount of spin-contamination. This problem only becomes worse as the

polyenyl chain lengthens to $C_{41}H_{43}$, with the spin expectation value closer to an absurd sextet ($\langle S^2 \rangle = 7.5$). Quite obviously, these methods cannot give an accurate electronic description of these molecules.

At first glance, ωB97X-D[66] appears to be a decent method to describe these polyenyl chains, because $\langle S^2 \rangle$ is just slightly above 0.75 and does not seem to grow all that much from C_5H_7 to $C_{13}H_{15}$. However, for $C_{41}H_{43}$, the value becomes closer to value of a triplet which suggests that this method may not be satisfactory for larger chains because the amount of spin-polarization increases as the chain length increases. In this way it is similar to the HF method, but the error is much less severe. However, it is a great deal better than MP2 method which is more computationally demanding.

The O2 method does quite well, particularly given the poor performance of the other methods. It is known that the O2 method does well for spin-contaminated cases,[59] but its success for this difficult system is perhaps surprising. The correct physicality seems to stem from the fact that there is orbital optimization in the presence of electron correlation in the O2 method, thereby bypassing the need to correct for a severely spin-polarized reference as is the case for UMP2 and USOS-MP2. The surprising aspect is that the correlation treatment in O2 is only at the SOS-MP2 level, while the soliton defect might be considered a static correlation problem. These results also suggest that the O2 method could be used for even larger systems, while still maintaining a physical amount of spin-polarization since the $\langle S^2 \rangle$ value is barely larger than the doublet value even in the $C_{41}H_{43}$ chain.

Another measure to compare against is the Mulliken spin population for the small polyenyl chain, C_9H_{11}, for the direct comparison to RCCSD(T) and CASSCF. As seen in table 4.3, several patterns emerge even in this small example. Looking at the UHF results, the physical picture is that there is essentially an unpaired electron on every carbon. This description explains why the bond alternation is so low, essentially all the bonds are quite similar. When comparing the two DFT methods to the RCCSD(T) method, the striking feature is that the soliton is not as localized to the central carbons. Basically the soliton delocalizes to the outer carbons and the soliton wave is much larger. Taking this trend to the limit, the soliton essentially will delocalize over the entire molecule at larger chain lengths, instead of the experimental value of a half-width of 18 carbons. CASSCF also tends to delocalize the soliton, but not to the same extent that is seen in the DFT functionals. From the CASSCF results it can be inferred that either some of the σ-space needs to be included, or that dynamic correlation is crucial. By contrast, the fairly good agreement between O2 and RCCSD(T) is fairly striking in this comparison. It seems that O2 slightly overlocalizes the soliton to the central carbons, which will lead to the soliton wave being too short.

In the previous paragraphs we have justified the use of O2 to describe the properies of solitons. For the smaller polyenyl chains, the O2 method does a very good job of reproducing the results of RCCSD(T) and also seemed promising for the longer chain based on the stability of the $\langle S^2 \rangle$ value. Ideally, the method would be able to reproduce the experimental half-width of 18 carbon atoms as seen using ENDOR spectroscopy.[72] Since this technique is based on electron spin, the Mulliken spin population of the longer $C_{41}H_{43}$ polyenyl chain will serve as a good theoretical equivalent to the experimental results. Another way to estimate the width of the soliton is by looking at the bond length differences along the entire polyenyl chain. The bond length difference between neighboring carbon-carbon bonds should be close to zero where the soliton resides and should be similar to polyacetylene elsewhere.

Carbon #	UHF	B3LYP	ωB97x-D	O2	CASSCF [a]	RCCSD(T) [a]
1	0.904	0.334	0.340	0.228	0.201	0.280
2	-0.782	-0.166	-0.199	-0.132	-0.097	-0.161
3	0.910	0.391	0.452	0.419	0.346	0.437
4	-0.866	-0.223	-0.301	-0.241	-0.163	-0.255
5	0.921	0.459	0.502	0.551	0.426	0.505

[a]Values from Bally et al.[41]

Table 4.3: Mulliken spin population in a.u. of C_9H_{11} for various methods. Carbons are numbered from outside to the center and the rest are omitted because of symmetry.

The positive to negative spin peak ratio is another experimental value that can be used for comparison to theory. The experimental value for this ratio is 0.44. [72]

In order to compare to experiment, we will use the Mulliken spin partitioning scheme instead of other schemes like Løwdin scheme. Also since these values oscillate between positive and negative values, with the negative values being much less in magnitude than the positive values, we will also implement a stabilization scheme as well. First, the total spin density for each position is calculated by adding the spin values of the carbon and the connected hydrogens together. Next, all of the oscillating negative values are converted to positive values in order to properly calculate full width at half maximum (FWHM) values. Finally, each value is averaged by the neighboring values through the following formula,

$$st(n) = \frac{1}{2}s(n) + \frac{1}{4}[s(n+1) + s(n-1)] \tag{4.16}$$

where s(n) is the total spin in a given position and st(n) is then the stabilized spin. For the terminal carbon positions, the stabilized spin value is exactly the same as the total spin value. This stabilization procedure results in a very distinct soliton wave for the three methods that have been studied: O2 method, B3LYP functional, and UHF method.

In looking at the stabilized spin for the longer $C_{41}H_{43}$ polyenyl chain, one will notice features for each of the methods studied. For the B3LYP method, the soliton is delocalized over the entire molecule leading to a half-width of 36 carbon atoms as can be seen in figure 4.4. While this might seem to be close to the experimental half-width of 18 carbon atoms, it also essentially occupies the entire model chain, and may therefore reflect confinement effects rather than being the limiting B3LYP value. This assertion is can be tested by examining the larger $C_{61}H_{63}$ chain with the B3LYP method. The stabilized spin picture for this larger chain is qualitatively the same as the shorter chain. This point can be visualized by inserting the stabilized spin picture for the $C_{41}H_{43}$ inside the stabilized spin picture for $C_{61}H_{63}$ seen in figure 4.4. Therefore it is clear that the intrinsic B3LYP width of the soliton is still larger than 61 carbons - perhaps significantly larger. Therefore this functional is inappropriate for soliton modeling.

The stabilized spin picture could also be examined for the density functional ωB97X-D. When examining the terminal carbon diagnostic, it seemed as though this method would adequately describe the soliton although the $\langle S^2 \rangle$ value is a little high for $C_{41}H_{43}$. Unfortunately the stabilized spin numbers are qualitatively the same as B3LYP with the peaks being slightly higher due to the larger $\langle S^2 \rangle$ value. The ωB97X-D functional can be grouped with
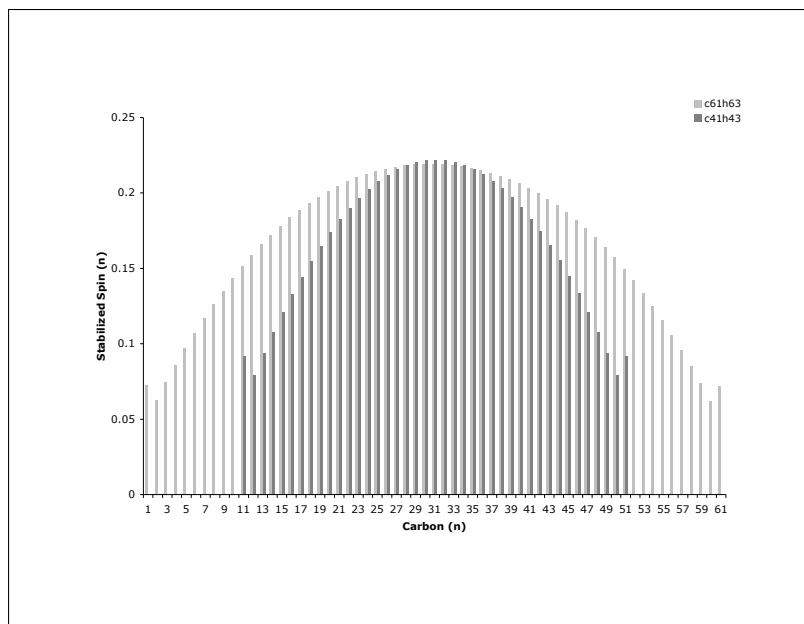
Figure 4.4: Visualization of the soliton wave solved by the B3LYP method using stabilized total atomistic Mulliken spin populations for $C_{41}H_{43}$ together with the stabilized spin for the $C_{61}H_{63}$

the other range-separated functionals derivied from the B97 functional,[73] namely ωB97 and ωB97X. These three functionals are interesting because each of them has a different value of ω, the parameter that determines the cutoff for short-range and Hartree-Fock (long-range) exchange. The ωB97, ωB97X, and ωB97 have ω values of 0.4, 0.3, and 0.2 bohr^{-1}, respectively.[66] However, each of these functionals performs qualitatively the same as the B3LYP functional with the only notable difference being the peak heights as seen in figure 4.5. As the value of ω decreases the overall peak height also decreases, meaning that the featured ωB97X-D functional will have the smallest amount of spin-polarization. In a similar analysis to the B3LYP functional, we plotted the $C_{41}H_{43}$ stabilized spin results together with the $C_{61}H_{63}$ to examine the amount of delocalization with chain length. As is seen in the B3LYP functional, the ωB97X-D functional delocalizes the soliton over the entire molecule as seen in figure 4.6. Therefore the ωB97X-D soliton width is larger than the largest chain studied here, making the prediction with this functional qualitatively incorrect.

The UHF method also performs quite poorly when one examines the stabilized spin in figure 4.7. This fact was already known given the poor $\langle S^2 \rangle$ value for the long chain. The figure does confirm the physical picture that we suggested earlier for the UHF method. In figure 4.7, one can see that the largest stabilized spin value would be 0.83 and the smallest would be 0.77, meaning that the soliton is over the entire molecule. Since the stabilized values are so large, it is equally correct to say that there are radicals on each carbon as to say that the soliton is spread out over the entire molecule. Figure 4.7 also solidifies the view that UHF creates radicals on most carbon leading to a spin-contaminated $\langle S^2 \rangle$ value.

The soliton wave seen in figure 4.8 for the O2 method is the only scalable method that properly localizes the soliton. The half-width of the soliton in this figure is 9 carbon atoms, smaller than the experimental value but still a valuable result. We note that the half-width

Figure 4.5: Visualization of the soliton wave solved by the ωB97 series using stabilized total atomistic Mulliken spin populations for $C_{41}H_{43}$

Figure 4.6: Visualization of the soliton wave solved by the ωB97X-D method using stabilized total atomistic Mulliken spin populations for $C_{41}H_{43}$ together with the stabilized spin for the $C_{61}H_{63}$

Figure 4.7: Visualization of the soliton wave solved by the UHF method using stabilized total atomistic Mulliken spin populations for $C_{41}H_{43}$

of the soliton wave for the smaller $C_{29}H_{31}$ polyenyl chain is 7 carbons. Therefore it is possible that the O2 value for the soliton width would increase a little beyond 9 if a longer chain calculation was performed. One can see that the O2 soliton wave has a much sharper peak than the B3LYP peak which leads to a smaller area under the curve and therefore a lower $\langle S^2 \rangle$ value. The SOMO orbital of the O2 method is included in figure 4.9. It is evident that the orbital is centered on the molecule with large values in the center that lessen towards the ends. From the stabilized spin figures, it becomes clear that only the O2 method gives the correct physical picture of the soliton.
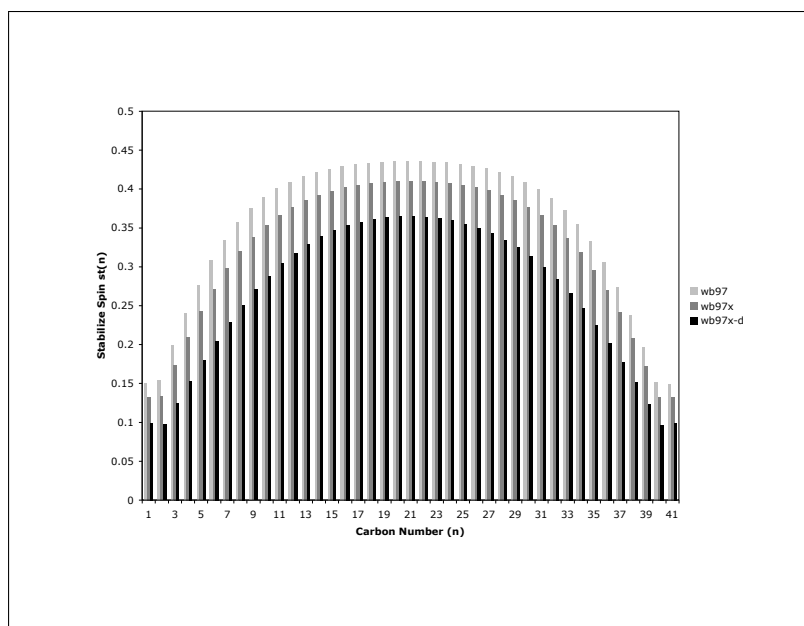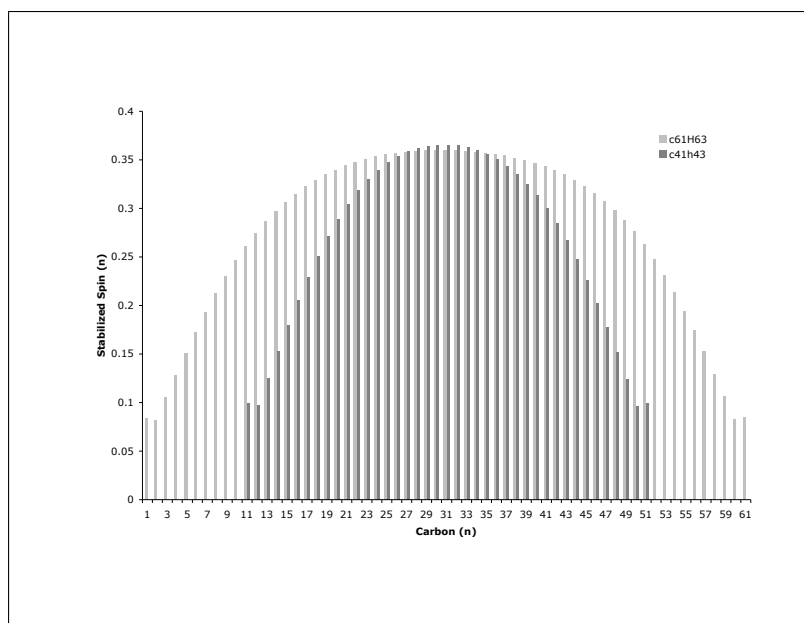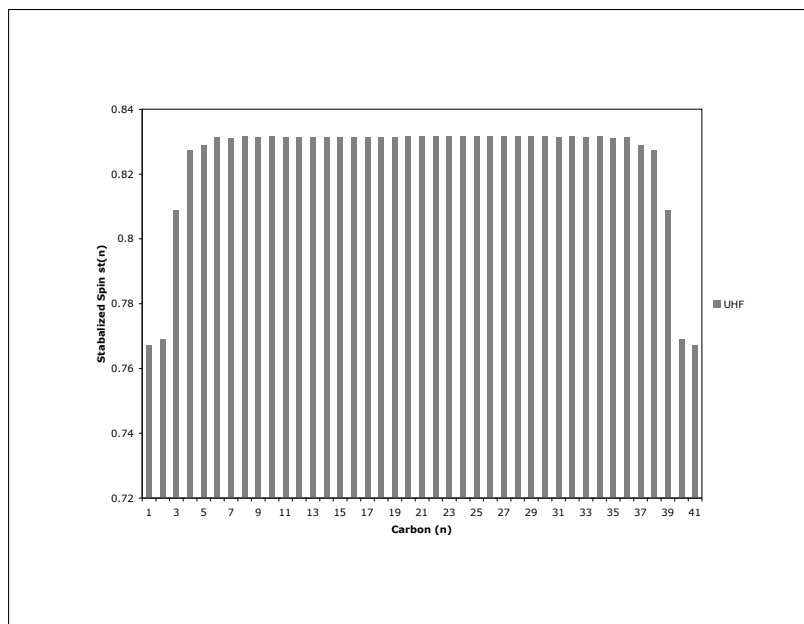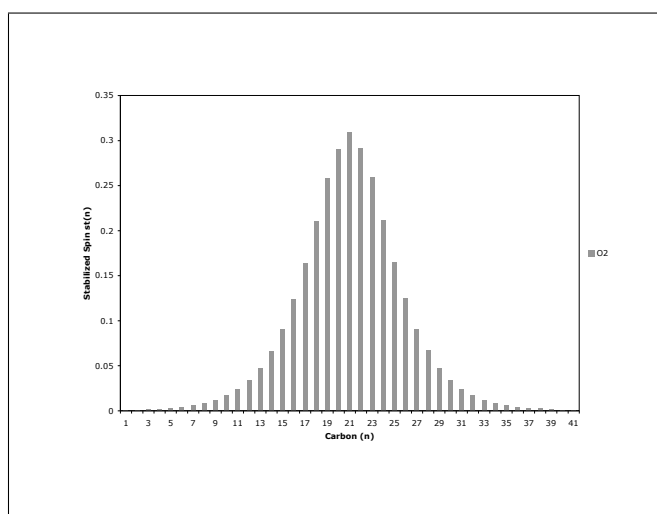

Figure 4.8: Visualization of the soliton wave solved by the O2 method using stabilized total atomistic Mulliken spin populations for $C_{41}H_{43}$
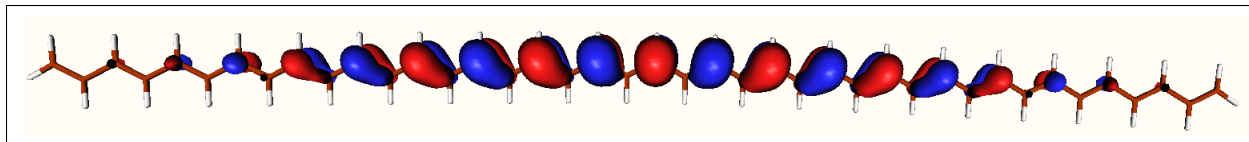
Figure 4.9: The SOMO orbital containing the soliton in the O2 method for $C_{41}H_{43}$. Contour value is set to 0.02 $\text{Å}^{-\frac{3}{2}}$.

The other comparisons to experiment are the geometrical measure of the soliton and the ratio of positive and negative spin peaks. The geometrical measure of the soliton is virtually the same as the stabilized spin picture. As shown in figure 4.10 where the deviation of every neighboring pair of C-C bonds from maximum bond alternation is plotted, both B3LYP and UHF predict a large soliton half-width for the same reasons given in the previous paragraph. The O2 method performs quite well with the soliton length being a little small though of course comparison to the experimental width is not an absolutely direct one. The main point that should be taken away from the geometrical description is that the localization of the soliton has geometric consequences. Therefore calculating the electronic structure with one theory and the geometry with another theory is an invalid procedure for this problem. The molecular geometry of the polyenyl chain will bias the electronic wavefunction. If we take the O2 optimized geometry for $C_{41}H_{43}$ and then compute the electronic wavefunction with the B3LYP functional, we obtain a localized soliton with a half-width of 18 carbon atoms and $\langle S^2 \rangle = 0.945$ as seen in figure 4.11 . However, this convenient cancellation of errors does not imply that the B3LYP method correctly describes the physicality of the system. Since the localization of the soliton is intrinsically related to the geometry of the polyenyl chain, any study that does not include geometric degrees of freedom should be questioned.

Figure 4.10: Visualization of the soliton wave from geometric distortions for $C_{41}H_{43}$. This graph is created by subtracting the C-C bond length alternation from the maximal C-C bond length difference.
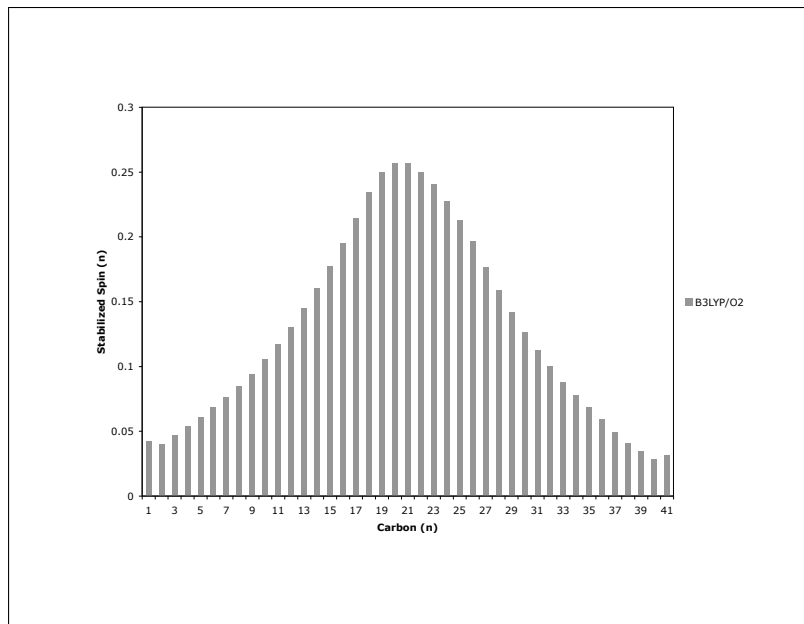
Figure 4.11: Visualization of the soliton wave by the O2 geometry and B3LYP electronic wavefunction using stabilized total atomistic Mulliken spin populations for $C_{41}H_{43}$
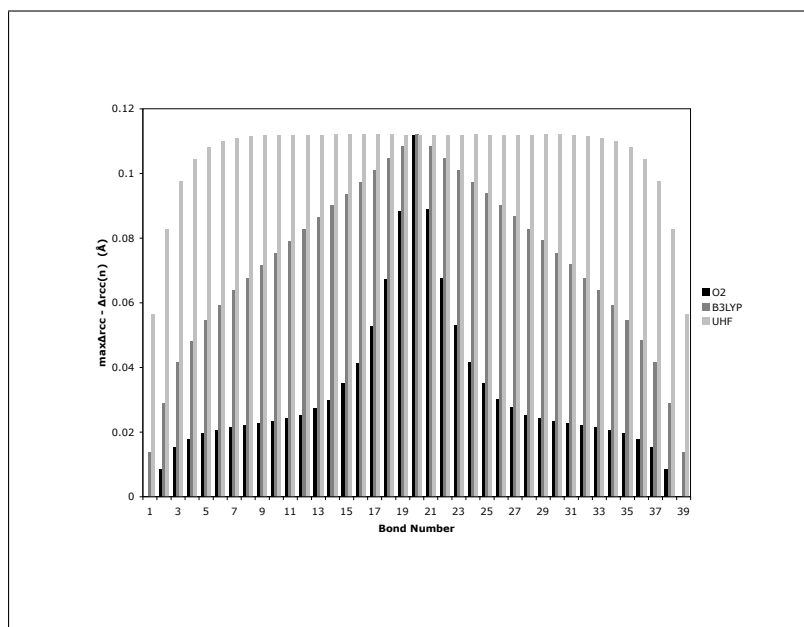
The final comparison to experiment will be the ratio of peak heights of negative and positive peaks with the experimental value being 0.44. In order to compare to this experimental value, we took the most positive and most negative Mulliken spin population on the carbon atoms to create this ratio and can be seen in the final column of table 4.4. If the ratio is greater than the experimental value, then it would imply that the given theory is not a sharp enough peak. A ratio that is too low implies that the given theory creates a peak that is too steep. From looking at the spin and geometry pictures of the soliton, one can guess that both UHF and B3LYP will be too high because of the delocalized nature of the soliton in both methods. This assumption holds true with both ratios being around twice the experimental value, which should be expected as the widths of these solitons are about twice the experimental values as well. The result for O2 closely matches experiment only being 0.04 too high, which suggests that the shape of the soliton is correct just the width needs to increase. Finally, the cancellation of errors method of O2/B3LYP corrects the error of B3LYP but this method would still have a fundamentally incorrect shape and that fact manifests with ratio that is too large. In fact the ratio for this method is just slightly less than the average of the two methods used in this procedure. Although this point was made quite forcefully in the previous paragraph it is worth repeating; the quality of results are greatly influenced by the geometry of the molecule. A decent but fundamentally wrong method can produce good results when given a clever geometry as is seen with B3LYP when given an O2 geometry.

As a side note there should be a significant amount of self-interaction error in this system because of the delocalized charge present in the soliton. The delocalized nature of the soliton will result in the need for non-local exchange, a situation in which DFT hybrid methods are known to yield an amount of self-interaction error. Self-interaction error is caused by the fact that in these hybrid functionals, the exchange functional does not cancel with

Method	width (spin)	width (geom)	ρ_-/ρ_+
O2	9	7	0.48
B3LYP	33	31	0.83
UHF	41	41	0.98
ωB97x-D	31	24	0.91
O2/B3LYP	18	N/A	0.61
Experiment[a]	18	???	0.44

[a] Ref [72]

Table 4.4: Comparison of the soliton FWHM widths and the spin ratio for $C_{41}H_{43}$ for a variety of methods and experiment

the Coulomb term with the difference defined as the self-interaction error. The canonical example of the self-interaction error is the dissociation of H_2^+. In this case the popular B3LYP functional dissociates to the incorrect limit, resulting in a self-interaction error of 55 kcal/mol. Physically, in this system B3LYP dissociates the radical with an artificial splitting of the electron into a final system of $H^{0.5+}$ + $H^{0.5+}$. The single electron will interact with itself, henceforth the name self-interaction error (SIE). However, in the context of this research, if the problem was as simple as H_2^+ dissociation, then there would have been a significant improvement in the ωB97X-D versus the B3LYP results due to the range-separation. Yet, both of these functionals perform equally poorly for this problem, which we can attribute to the fact that there is a fractional electron on multiple carbons. This situation leads to a many-electron self-interaction error which has been shown to occur when there are fractional numbers of electrons on carbon atoms.[74, 75] When this type of self-interaction error is present, both hybrid functionals and range-separated hybrids tend to yield errors in overall energy and in the amount of spin-polarization.[74, 75] Therefore, unless the functional is specifically created to reduce this type of error, it will not successfully describe the locality of the neutral soliton.

4.4 Conclusions

An analytic nuclear gradient for the O2 method has been presented with almost no additional cost to the original method. This method could then be used for geometry optimizations of difficult molecules like polyenyl chains, where long chain lengths are necessary to capture physical effects seen in the infinite chain length limit. The O2 method estimates that the half-width of the soliton to be 9 carbon atoms for $C_{41}H_{43}$, slightly shorter than the experimental value of 18 carbon atoms. Therefore, O2 is one of the few methods that can be used to calculate the geometry of long polyenyl chains, and give a correct electronic and physical description of the molecular system.

For the problem of localizing an electron on a polyene backbone, large amounts of static correlations do not seem to be necessary. O2 is a method that does not have large amounts of static correlation like CCSD(T) or CASSCF, but it still correctly captures the physicality of the soliton. Also the recently developed UAP method has been shown to localize orbitals as well without a significant amount of static correlation.[76] Therefore based on the results

of this study and the results of the UAP method, we conclude that the soliton problem does not inherently contain large amounts of static correlation, rather the problem is a competition between localization and delocalization. While methods with a large amount of static correlation do perform well for this problem, the underlying reason is not simply that these methods include static correlation.

In general, O2 should be used when correlation and electron localization/delocalization effects are important and lead to geometric relaxation effects. Other uses would be when spin contamination leads to unphysical results.

Bibliography

[1] P. PULAY, *Mol. Phys.* **17**, 197 (1969).

[2] Y. YAMAGUCHI, Y. OSAMURA, J. D. GODDARD, and H. F. SCHAEFER III, *A New Dimension to Quantum Chemistry: Analytical Derivative Methods in ab Initio Molecular Structure Theory*, Oxford University Press, New York, 1994.

[3] R. BARTLETT, *J. Phys. Chem.* **93**, 1697 (1989).

[4] A. BECKE, *Phys. Rev. A* **38**, 3098 (1988).

[5] C. LEE, W. YANG, and R. PARR, *Phys. Rev. B* **37**, 785 (1988).

[6] A. BECKE, *J. Chem. Phys.* **98**, 1372 (1993).

[7] P. KOZLOWSKI, G. RAUHUT, and P. PULAY, *J. Chem. Phys.* **103**, 5650 (1995).

[8] T. HELGAKER, P. JØRGENSEN, and J. OLSEN, *Molecular electronic-structure theory*, Wiley, 2000.

[9] A. SZABÓ and N. OSTLUND, *Modern quantum chemistry: introduction to advanced electronic structure theory*, Dover Publications, 1996.

[10] C. SHERRILL, M. LEE, and M. HEAD-GORDON, *Chem. Phys. Lett.* **302**, 425 (1999).

[11] X. LI, Z. CAI, and M. SEVILLA, *J. Phys. Chem. A* **106**, 1596 (2002).

[12] Y. ZHANG and W. YANG, *J. Chem. Phys.* **109**, 2604 (1998).

[13] V. POLO, E. KRAKA, and D. CREMER, *Mol. Phys.* **100**, 1771 (2002).

[14] J. ANGYAN, I. GERBER, A. SAVIN, and J. TOULOUSE, *Phys. Rev. A* **72**, 012510 (2005).

[15] O. A. VYDROV, J. HEYD, A. V. KRUKAU, and G. E. SCUSERIA, *J. Chem. Phys.* **125**, 074106 (2006).

[16] J. FALK and R. FLEMING, *J. Phys. C.* **8**, 627 (1975).

[17] J. MINTMIRE, C. WHITE, and M. ELERT, *Synth. Met.* **16**, 235 (1986).

[18] H. THOMANN, L. DALTON, M. GRABOWSKI, and T. CLARKE, *Phys. Rev. B* **31**, 3141 (1985).

[19] M. ABLOWITZ and G. BIONDINI, *Opt. Lett.* **23**, 1668 (1998).

[20] S. SCHMITT, J. FICKER, M. WOLFF, F. KONIG, A. SIZMANN, and G. LEUCHS, *Phys. Rev. Lett.* **81**, 2446 (1998).

[21] H. SUNNERUD, M. KARLSSON, C. XIE, and P. ANDREKSON, *J. Lightwave Technol.* **20**, 2204 (2002).

[22] S. TURITSYN, V. MEZENTSEV, and E. SHAPIRO, *Opt. Fiber Technol.* **4**, 384 (1998).

[23] J. JACOB, E. GOLOVCHENKO, A. PILIPETSKII, G. CARTER, and C. MENYUK, *IEEE Photonics Technol. Lett.* **9**, 130 (1997).

[24] R. LI, P. KUMAR, and W. KATH, *J. Lightwave Technol.* **12**, 541 (1994).

[25] W. SU, J. SCHRIEFFER, and A. HEEGER, *Phys. Rev. Lett.* **42**, 1698 (1979).

[26] H. TAKAYAMA, Y. LINLIU, and K. MAKI, *Phys. Rev. B* **21**, 2388 (1980).

[27] D. CAMPBELL and A. BISHOP, *Phys. Rev. B* **24**, 4859 (1981).

[28] B. WEINBERGER, E. EHRENFREUND, A. PRON, A. HEEGER, and A. MACDIARMID, *J. Chem. Phys.* **72**, 4749 (1980).

[29] S. KIVELSON, *Phys. Rev. Lett.* **46**, 1344 (1981).

[30] S. IKEHATA, J. KAUFER, T. WOERNER, A. PRON, M. DRUY, A. SIVAK, A. HEEGER, and A. MACDIARMID, *Phys. Rev. Lett.* **45**, 1123 (1980).

[31] E. MELE and M. RICE, *Phys. Rev. Lett.* **45**, 926 (1980).

[32] D. BOUDREAUX, R. CHANCE, J. BREDAS, and R. SILBEY, *Phys. Rev. B* **28**, 6927 (1983).

[33] S. ROTH and H. BLEIER, *Adv. Phys.* **36**, 385 (1987).

[34] K. SUBBASWAMY and M. GRABOWSKI, *Phys. Rev. B* **24**, 2168 (1981).

[35] J. HIRSCH and M. GRABOWSKI, *Phys. Rev. Lett.* **52**, 1713 (1984).

[36] A. HEEGER and J. SCHRIEFFER, *Solid State Commun.* **48**, 207 (1983).

[37] M. OLSON, Y. MAO, T. WINDUS, M. KEMP, M. RATNER, N. LEON, and V. MUJICA, *J. Phys. Chem. B* **102**, 941 (1998).

[38] J. REIMERS and N. HUSH, *Chem. Phys.* **176**, 407 (1993).

[39] A. ONIPKO, *Phys. Rev. B* **59**, 9995 (1999).

[40] J. REIMERS, J. CRAW, A. WONG, G. BACSKAY, and N. HUSH, *Mol. Cryst. Liq. Cryst. Sci. Technol. Sect. A-Mol. Cryst. Liq. Cryst.* **234**, 51 (1993).

[41] T. BALLY, D. HROVAT, and W. BORDEN, *Phys. Chem. Chem. Phys.* **2**, 3363 (2000).

[42] U. SALZNER, *J. Chem. Theory Comput.* **3**, 219 (2007).

[43] J. GU, Y. LIN, B. MA, W. WU, and S. SHAIK, *J. Chem. Theory Comput.* **4**, 2101 (2008).

[44] H. MA, F. CAI, C. LIU, and Y. JIANG, *J. Chem. Phys.* **122**, 104909 (2005).

[45] J. H. STARCKE, M. WORMIT, and A. DREUW, *J. Chem. Phys.* **131**, 144311 (2009).

[46] Y. LUO, L. SONG, W. WU, D. DANOVICH, and S. SHAIK, *ChemPhysChem* **5**, 515 (2004).

[47] E. RUIZ, Theoretical study of the exchange coupling in large polynuclear transition metal complexes using DFT methods, in *Principles and Applications of Density in Inorganic Chemistry II*, volume 113 of *Structure and Bonding*, pp. 71–102, Springer-Verlag Berlin, Heidelberger Platz 3, D-14197 Berlin, Germany, 2004.

[48] K. V. LAWLER, G. J. O. BERAN, and M. HEAD-GORDON, *J. Chem. Phys.* **128**, 024107 (2008).

[49] P. LOWDIN, *Rev. Mod. Phys.* **36**, 966 (1964).

[50] K. YAMAGUCHI, Y. TAKAHARA, T. FUENO, and K. HOUK, *Theor. Chim. Acta* **73**, 337 (1988).

[51] K. YAMAGUCHI, M. OKUMURA, W. MORI, J. MAKI, K. TAKADA, T. NORO, and K. TANAKA, *Chem. Phys. Lett.* **210**, 201 (1993).

[52] S. YAMANAKA, M. OKUMURA, M. NAKANO, and K. YAMAGUCHI, *Theochem-J. Mol. Struct.* **116**, 205 (1994).

[53] P. MASLEN, J. FAEDER, and R. PARSON, *Chem. Phys. Lett.* **263**, 63 (1996).

[54] J. KROGH and J. OLSEN, *Chem. Phys. Lett.* **344**, 578 (2001).

[55] K. NAKAYAMA, H. NAKANO, and K. HIRAO, *Int. J. Quantum Chem.* **66**, 157 (1998).

[56] Y. LEE, S. KUCHARSKI, and R. BARTLETT, *J. Chem. Phys.* **81**, 5906 (1984).

[57] B. ROOS and P. TAYLOR, *Chem. Phys.* **48**, 157 (1980).

[58] B. CHAMPAGNE, E. PERPETE, S. VAN GISBERGEN, E. BAERENDS, J. SNIJDERS, C. SOUBRA-GHAOUI, K. ROBINS, and B. KIRTMAN, *J. Chem. Phys.* **109**, 10489 (1998).

[59] R. C. LOCHAN and M. HEAD-GORDON, *J. Chem. Phys.* **126**, 164101 (2007).

[60] S. GRIMME, *J. Chem. Phys.* **118**, 9095 (2003).

[61] Y. JUNG, R. LOCHAN, A. DUTOI, and M. HEAD-GORDON, *J. Chem. Phys.* **121**, 9793 (2004).

[62] W. KURLANCHEEK and M. HEAD-GORDON, *Mol. Phys.* **107**, 1223 (2009).

[63] S. KOSSMANN and F. NEESE, *J. Phys. Chem. A* **114**, 11768 (2010).

[64] R. C. LOCHAN, Y. SHAO, and M. HEAD-GORDON, *J. Chem. Theory Comput.* **3**, 988 (2007).

[65] Y. M. RHEE, R. A. DISTASIO, JR., R. C. LOCHAN, and M. HEAD-GORDON, *Chem. Phys. Lett.* **426**, 197 (2006).

[66] J.-D. CHAI and M. HEAD-GORDON, *Phys. Chem. Chem. Phys.* **10**, 6615 (2008).

[67] B. DUNLAP, *Theochem-J. Mol. Struct.* **529**, 37 (2000).

[68] Y. JUNG, A. SODT, P. GILL, and M. HEAD-GORDON, *Proc. Natl. Acad. Sci. U. S. A.* **102**, 6692 (2005).

[69] J. ALMLOF, *Chem. Phys. Lett.* **181**, 319 (1991).

[70] Y. SHAO, L. F. MOLNAR, Y. JUNG, J. KUSSMANN, C. OCHSENFELD, S. T. BROWN, A. T. B. GILBERT, L. V. SLIPCHENKO, S. V. LEVCHENKO, D. P. O'NEILL, R. A. DISTASIO, JR., R. C. LOCHAN, T. WANG, G. J. O. BERAN, N. A. BESLEY, J. M. HERBERT, C. Y. LIN, T. VAN VOORHIS, S. H. CHIEN, A. SODT, R. P. STEELE, V. A. RASSOLOV, P. E. MASLEN, P. P. KORAMBATH, R. D. ADAMSON, B. AUSTIN, J. BAKER, E. F. C. BYRD, H. DACHSEL, R. J. DOERKSEN, A. DREUW, B. D. DUNIETZ, A. D. DUTOI, T. R. FURLANI, S. R. GWALTNEY, A. HEYDEN, S. HIRATA, C.-P. HSU, G. KEDZIORA, R. Z. KHALLIULIN, P. KLUNZINGER, A. M. LEE, M. S. LEE, W. LIANG, I. LOTAN, N. NAIR, B. PETERS, E. I. PROYNOV, P. A. PIENIAZEK, Y. M. RHEE, J. RITCHIE, E. ROSTA, C. D. SHERRILL, A. C. SIMMONETT, J. E. SUBOTNIK, H. L. WOODCOCK, III, W. ZHANG, A. T. BELL, A. K. CHAKRABORTY, D. M. CHIPMAN, F. J. KEIL, A. WARSHEL, W. J. HEHRE, H. F. SCHAEFER, III, J. KONG, A. I. KRYLOV, P. M. W. GILL, and M. HEAD-GORDON, *Phys. Chem. Chem. Phys.* **8**, 3172 (2006).

[71] M. YU, S. KALVODA, and M. DOLG, *Chem. Phys.* **224**, 121 (1997).

[72] S. KURODA, *Int. J. Mod. Phys. B* **9**, 221 (1995).

[73] A. BECKE, *J. Chem. Phys.* **107**, 8554 (1997).

[74] R. HAUNSCHILD, T. M. HENDERSON, C. A. JIMENEZ-HOYOS, and G. E. SCUSERIA, *J. Chem. Phys.* **133**, 134116 (2010).

[75] P. Mori-Sanchez, A. J. Cohen, and W. Yang, *J. Chem. Phys.* **125**, 201102 (2006).

[76] K. V. Lawler, D. W. Small, and M. Head-Gordon, *J. Phys. Chem. A* **114**, 2930 (2010).

Chapter 5

Second order Møller-Plesset energy decomposition analysis for intermolecular interactions with applications to the ethylene dimer, He-BeO complex, and the water dimer

5.1 Introduction

Reliable calculations of intermolecular interactions are now more or less standard using wave function methods. The most accurate methods are based on high level coupled cluster theory, such as CCSD(T), but computational cost restricts their applicability to small molecule complexes.[1] Second order Møller-Plesset (MP2) theory is applicable to much larger molecules, and is known to yield excellent results for systems such as hydrogen-bonding in water clusters[2, 3] and DNA bases[4, 5], although it tends to overestimate stacking interactions.[6, 7] Spin-component scaling of the MP2 correlation energy offers some advantages.[8] However, regardless of how good or bad the numbers are, *ab initio* calculations of intermolecular binding energies are essentially numerical experiments. To obtain insight beyond the overall binding energy, it is therefore desirable to divide the interaction energy into physically meaningful components, via an energy decomposition analysis (EDA).

5.2 Theory

We confine discussion of existing EDAs (in this section) to the ones relevant to the present work (though many others also exist, all with their own advantages). The Kitaura-Morokuma approach was early and influential, and spawned a variety of follow-on improvements.[9] It divides an interaction energy into a frozen component (permanent electrostatics and Pauli repulsion), and an induced component (polarization, if present, and charge transfer). The

Ziegler-Rauk approach is essentially the same.[10] Going further, it is possible to separate the induced component into polarization effects that are treated by an absolutely localized MO (ALMO) self-consistent field (SCF) calculation in which the MO coefficient matrix is block diagonal in the fragments.[11] Charge transfer effects are the remaining contributions, which can be pair-wise decomposed to a very good approximation. Thus we can summarize the SCF-level ALMO-EDA as:

$$\begin{aligned} \Delta E_{SCF}(AB) &= E_{SCF}(AB) - E_{SCF}(A) - E_{SCF}(B) \\ &= \Delta E_{SCF}^{frzn}(AB) + \Delta E_{SCF}^{pol}(AB) + \Delta E_{SCF}^{CT}(AB) \end{aligned} \qquad (5.1)$$

The primary limitation of these KM-derived approaches is their restriction to SCF models either Hartree-Fock or density functional theory unless the correlation contribution to binding is added on at the end as a fourth contribution. The purpose of this letter is to describe an extension of the SCF-level ALMO-EDA to MP2 theory in which correlation contributions to the frozen interactions, polarization effects, and charge transfer are evaluated separately. In other words, since $E = E_{SCF} + E_{corr}$, we aim to define, in direct analogy to Eq. 5.1:

$$\begin{aligned} \Delta E_{corr}(AB) &= E_{corr}(AB) - E_{corr}(A) - E_{corr}(B) \\ &= \Delta E_{corr}^{frzn}(AB) + \Delta E_{corr}^{pol}(AB) + \Delta E_{corr}^{CT}(AB) \end{aligned} \qquad (5.2)$$

In a qualitative sense, one expects that the frozen interactions (where the fragment orbitals are not allowed to relax) will include correlation contributions that become dispersion-like as the overlap becomes small, in addition to intramolecular correlations. However, correlation effects that involve moving an electron from one fragment to another should clearly be grouped as part of the CT contribution. Thus a partition of correlation effects is necessary if we wish to evaluate correlation contributions to frozen, polarization and charge transfer interactions.

The partition can be made more explicit by recalling that the correlation energy in MP2 theory can be written as the contraction of two-electron integrals with pair correlation amplitudes, t_{ij}^{ab},which describe the promotion of a pair of occupied levels i and j to a pair of empty levels a and b, such that

$$E_{corr} = \frac{1}{2} \sum_{ijab} (ia|jb) t_{ij}^{ab} \qquad (5.3)$$

For an intermolecular interaction, the orbitals can be localized onto the fragments indeed this is the constraint that is imposed in the ALMO-SCF. We can therefore categorize the pair correlation amplitudes for a system of two fragments according to whether they belong to one fragment, or are split between two fragments without charge transfer, or involve overall charge transfer between the fragments. These categories are illustrated in Figure 5.1 below.

In the MP2 ALMO-EDA we evaluate 2 subsets of the MP2 energy in addition to the total MP2 energy. The first subset is based on the intra-fragment correlations only, which is to be added to the SCF energy for the isolated fragment. This contribution can be evaluated with only minor modifications of a standard MP2 code. The second subset contains both the intra-fragment correlations, and the non-CT inter-fragment correlations from category (b) above. We will denote this contribution as E_{corr}^{frzn} when it is evaluated with the frozen

(a) Intra   (b) Inter: no CT   (c) Inter: with CT

Figure 5.1: Classes of correlation amplitudes involving 2 fragments (each corresponding to a pair of levels in the diagram), which are separated to accomplish the EDA. (a) Intra-fragment correlations both occupied and virtual levels belong to a single fragment (the left one in the diagram). These contributions are included in isolated fragment energies (b) Inter-fragment correlations that do not involve charge transfer one correlated electron is associated with each fragment. These effects are included in addition to (a) in frozen and polarized energies (c) Inter-fragment correlations that are accompanied by charge transfer they included in the charge transfer energy in addition to (a) and (b).

orbitals, and combined with the corresponding E_{SCF}^{frzn}. The same terms will be denoted as E_{corr}^{pol} when evaluated with the polarized ALMOs, and combined with the ALMO SCF energy, E_{SCF}^{pol}.

The second subset is non-trivial to evaluate. In detail the occupied orbitals are the occupied ALMOs (frozen or relaxed) of the fragments. The ALMOs on one fragment are non-orthogonal to those of the next. The virtual orbitals are the corresponding ALMO virtuals, projected against the full occupied space. These functions, while localized to fragments, are also non-orthogonal. The problem of solving the MP2 problem with the subset of substitutions (a) and (b) in this representation is isomorphic to the local correlation model called diatomics-in-molecules (DIM),[12] with the atom of the DIM model being re-defined as an individual fragment for our present purposes. Therefore our pilot program, implemented as an extension to the Q-Chem program,[13] simply modified an existing DIM code to define fragments as superatoms. It should be noted that this scheme, while convenient for initial testing as we report here, scales very poorly with size of the fragment (sixth power scaling). We intend to report a fully optimized implementation in due course.

Given the components above, we can now fully specify the following three individual correlation contributions to the total defined in Eq. 5.2. The first contribution, ΔE_{corr}^{frzn} contains the correlations that are clearly dispersion as the fragments become non-overlapping which we can rename as frozen dispersive interactions (FDI):

$$\Delta E_{corr}^{frzn} = E_{corr}^{frzn}(AB) - E_{corr}(A) - E_{corr}(B) \tag{5.4}$$

It may be combined with the SCF-level frozen energy. These effects are modified (the change can be either positive or negative) due to the effects of polarization, so that we define a similar quantity for the polarized level which we can label as dispersive interactions at the ALMO level (ADI):

$$\Delta E_{corr}^{pol} = E_{corr}^{pol}(AB) - E_{corr}^{pol}(A) - E_{corr}^{pol}(B) \tag{5.5}$$

An orbital distortion is present in the change from the frozen monomers to the polarized monomers that will be part of an overall change to be defined later:

$$\Delta E_{corr}^{odist1} = E_{corr}^{pol}(A) + E_{corr}^{pol}(B) - E_{corr}^{frzn}(A) - E_{corr}^{frzn}(B) \tag{5.6}$$

The overall dispersive correlations are then given as $\Delta E_{corr}^{pol} + \Delta E_{corr}^{odist}$, but these will always be split to include the orbital distortion term in an orbital change term. The dispersive interaction can be classified at either the frozen level by Eq. 5.4 (FDI) or at the polarized ALMO level (ADI) by Eq. 5.5. Finally, the correlation contribution to CT is defined by one further subtraction as:

$$\Delta E_{corr}^{CT} = E_{corr_{w/CT}}^{pol}(AB) - E_{corr_{w/oCT}}^{pol}(AB) \tag{5.7}$$

In the above equation, correlation without charge transfer is defined as including excitation of type a and b in Figure 5.1 and correlations with charge transfer includes all types of excitations. As with the dispersive interactions, there is an orbital distortion term associated with charge transfer. This term includes the orbital distortion in going from the polarized orbitals to the full canonical orbitals:

$$\Delta E_{corr}^{odist2} = E_{corr}^{CT}(AB) - E_{corr_{w/CT}}^{pol}(AB) \tag{5.8}$$

This orbital distortion term is combined with the other orbital distortion term to form an overall orbital change term.

$$\Delta E_{corr}^{orb\Delta} = \Delta E_{corr}^{odist1} + \Delta E_{corr}^{odist2} \tag{5.9}$$

Each of these terms can be corrected individually for basis set superposition error (BSSE). These terms can also be combined to form the binding energy.

$$\Delta E_{bind} = \Delta E_{corr}^{orb\Delta} + \Delta E_{corr}^{CT} + \Delta E_{corr}^{pol} + \Delta E_{SCF}^{frzn} + \Delta E_{SCF}^{pol} + \Delta E_{SCF}^{CT} \tag{5.10}$$

As our test systems, we chose the ethylene dimer to examine dispersion interactions, the He-BeO complex to examine charge transfer interactions, and finally the water dimer to examine a system where both types of interactions are significant. While there is no doubt about the magnitude of the binding energy in this scheme, there has been significant controversy associated with the EDA results. While the individual terms should be well-defined in any EDA, there is no unique definition for any contribution: neither the frozen, polarization nor charge transfer terms, in our present context. Therefore one should be very cautious when comparing values obtained from the definitions used in one EDA with those used in another. In general it is much better to use a given EDA for comparative purposes. One exception will be that we can compare the MP2 level ALMO-EDA against the HF-level ALMO-EDA to see the role of electron correlation, and another exception will be that we can compare both of these against the corresponding DFT-level ALMO-EDA with a given approximate functional. Our goal is to make these comparisons, after first assessing the internal stability of the MP2 ALMO-EDA and the ability of MP2 ALMO-EDA to capture the correct physicality.

5.3   Test Cases

In order to examine the validity of this approach, two test cases were chosen to specifically examine the correlated contributions. The first test case is the ethylene dimer, which is

a classic dispersion-bound complex. For the ethylene dimer, the dispersion term should dominate all other intermolecular interactions. The second case is the small charge-transfer complex He $\cdots$ BeO where both the correlated and uncorrelated charge transfer terms should be dominate terms.[14] These cases will illustrate the ability of this scheme to capture these intermolecular interactions in a physical manner and convince the reader that this scheme is appropriate to apply to the water dimer, which has both significant charge transfer and dispersive interactions.

The ethylene dimer is one of the smallest examples of a π orbital stacking complex, which is inherently bound by dispersive forces. In this system there are only 4 heavy atoms, which means that this system can be studied with computationally demanding levels of theory like CCSD(T) and used in benchmark calculations like the S22 test set used to train density functionals.[15] However, in this current implementation of the energy decomposition scheme, the overall binding energy is limited by the MP2 binding energy. It should be noted that this theory does not change the overall binding energy of MP2, but partitions the binding energy into various intermolecular components. The geometry of the ethylene dimer structure was taken from a 2002 study on interactions in the benzene and ethylene dimer.[16] In this geometry, there is a separation of 3.8 Å between the planes of the carbon atoms in the ethene dimer T-like structure. All calculations were run using the Q-Chem software package.[13] with the frozen core approximation. In this example, the dispersive interaction term is responsible for the vast majority of the binding energy, which can be seen in table 5.1. At the SCF level, this complex is unbound because of the repulsive electrostatic interactions. There are also small amounts of charge transfer captured at the SCF level and at the correlated MP2 level (total of -0.28 kcal/mol), but these contributions are an order of magnitude smaller than the dispersive interactions. In fact, the system is unbound if only the dispersive terms are dropped, i.e. including just electrostatics, polarization and charge transfer (both SCF and correlation CT). These findings verify that this method does capture dispersive interactions in a physically reasonable manner.

Basis Set	FE	FDI	ADI	Pol	SCF CT	CCT	Orb Dist
aug-cc-pVDZ	0.685	-1.617	-1.637	-0.045	-0.295	-0.206	-0.065
aug-cc-pVTZ	0.742	-1.880	-1.961	-0.050	-0.167	-0.111	-0.080
aug-cc-pVQZ	0.743	-1.964	-2.011	-0.057	-0.136	-0.123	-0.067

Table 5.1: Convergence as the basis set approaches completeness for each of the intermolecular terms for ethylene dimer reported in kcal/mol

The complex of Helium and Beryllium Oxide is an interesting charge transfer complex. In this system, the BeO molecule will take away electron density from the He atom resulting in an electron transfer. The He$\cdots$ BeO complex is bound with a total binding energy of about 4.8 kcal/mol, about the same binding energy as the water dimer.[17] Based on the results of Natural Bond Orbital analysis, the charge transfer from the He atom to the BeO molecule is a staggering -24 kcal/mol, nearly 5 times the binding energy.[17] While this is certainly an overestimate, this result is not completely an artifact of this method. When a energy decomposition is performed on this molecule, one would expect charge transfer and polarization to be the largest contributors to the binding energy.

The He$\cdots$BeO geometry is optimized with MP2 at the cc-pVTZ level yielding R(HeBe)

= 1.521 Å and R(BeO) = 1.346 Å. This geometry is then used to perform the energy decomposition analysis using the ALMO orbitals as can be seen in table 5.2. In this analysis it is clear that charge transfer and polarization are the two terms that are greatly stabilizing the interaction between the He atom and the BeO molecule. At the SCF level, interestingly, the separation between polarization and charge transfer is not stable to basis set improvements, though the sum is. The dispersive interactions in this system is almost trivial, contributing a positive interaction of about 0.05 kcal/mol. The electrostatic interaction in this system is large, which is expected as noble gases like He rarely bond with other elements or molecules. Although charge transfer contributes more than 3 kcal/mol for binding, the large polarization contribution is somewhat surprising. In the larger basis sets, the attractive charge transfer interaction is not larger enough to overcome the repulsive electrostatic interaction. However, this example proves that this method can effectively capture charge transfer, especially correlated charge transfer, in a system where charge transfer is a significant interaction.

Basis Set	FE	FDI	ADI	Pol	SCF CT	CCT	Orb Dist
cc-pVDZ	4.066	0.265	0.019	-2.332	-5.071	-0.449	0.334
cc-pVTZ	4.261	0.106	-0.045	-4.454	-4.416	-1.417	0.331
cc-pVQZ	4.317	0.190	0.041	-5.993	-2.973	-1.392	0.325
cc-pV5Z	4.281	0.187	0.063	-6.910	-2.000	-1.255	0.345

Table 5.2: Convergence as the basis set approaches completeness for each of the intermolecular terms for He-BeO reported in kcal/mol

5.4   Water Dimer

The water dimer geometry used for these calculations is one that is optimized with MP2 in the aug-cc-pVTZ basis. We will focus on the stability of the energetic contributions and then will consider these results within the context of the current energy decomposition schemes. In terms of stability we will examine the stability with respect to increasing the size of the basis set, with and without the frozen core approximation, and the stability of the energetic terms as the distance between the two water molecules increases. As the distance between the two water molecules increases, the binding energy must asymptote to zero. Therefore, each of the component terms should approach zero as the distance increases, furthermore, each of these terms need to trend to zero smoothly in the physically relevant regions. In fig. 5.2 each of the physical energetic terms is charted as the oxygen-oxygen distance increases. The basis set in this example is the aug-cc-pCVDZ basis which explicitly includes basis functions for the core. Results are qualitatively the same if the frozen core approximation is employed for the aug-cc-pVDZ basis set. One can see that each of the terms smoothly converges to zero at an oxygen-oxygen distance of about 15 Å. Also there are no spurious rises or falls in any of the energetic terms as the distance approaches infinity. From this graph we can conclude that there are no artifacts that manifest from the implementation of correlation contributions.

Another measure of stability is that the individual energy terms should converge to a limiting value as the basis set increases. In tables 5.3 and 5.4 the water dimer is examined
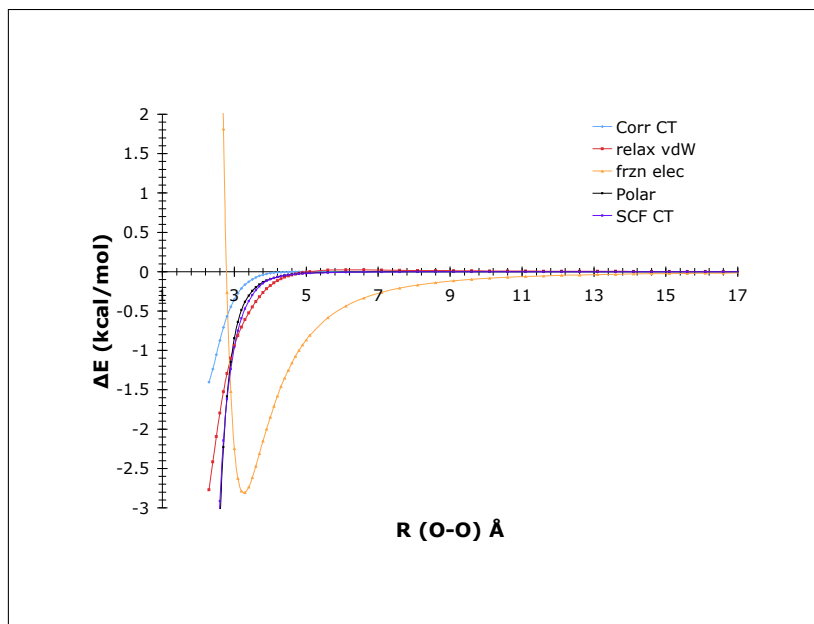
Figure 5.2: The individual energy terms for water dimer separation in the aug-cc-pCVDZ basis as a function of oxygen-oxygen distance. This graph shows that each term converges smoothly to zero.

at a set O-O distance of 3.0 Åwith the basis sets increasing from a double-ζ level to the quadruple-ζ level. In both of these tables there is a relatively big difference (about 40% for both frozen and ALMO dispersive) in the dispersive interaction from the DZ level to the TZ level. However from the TZ to QZ level, all of the correlated components are very stable with the largest change being about 0.1 kcal/mol. There is no reason to suspect that increasing the basis set to the 5Z level will dramatically change the correlated energy terms in this decomposition scheme. From tables 5.3 and 5.4 along with the tables for the He-BeO complex and the ethylene dimer, it should be clear that the correlated quantities reach stable values as the basis set increases for these fundamentally different interactions. Since we have demonstrated that this scheme is stable with respect to decreasing interactions and with respect to basis set size, we will move on to analyzing the results of this scheme and comparing it to the existing literature.

Basis Set	FE	FDI	ADI	Pol	SCF CT	CCT	Orb Dist
aug-cc-pVDZ	-2.238	-0.352	-0.422	-0.846	-0.957	-0.359	0.131
aug-cc-pVTZ	-2.151	-0.629	-0.675	-1.030	-0.688	-0.419	0.162
aug-cc-pVQZ	-2.099	-0.761	-0.771	-1.062	-0.700	-0.414	0.144

Table 5.3: Convergence as the basis set approaches completeness for each of the intermolecular terms reported in kcal/mol in the water dimer

The hydrogen bond interaction in the water dimer complex is one of the most fundamental intermolecular interactions in chemistry. The water dimer is physically relevant to a wide variety of topics ranging from atmospheric absorption of infrared radiation to the structure of water droplet formation.[18, 19, 20, 21] Since this system is quite small and for the previously

Basis Set	FE	FDI	ADI	Pol	SCF CT	CCT	Orb Dist
aug-cc-pCVDZ	-2.249	-0.367	-0.436	-0.846	-0.959	-0.361	0.137
aug-cc-pCVTZ	-2.150	-0.647	-0.694	-1.031	-0.684	-0.435	0.165
aug-cc-pCVQZ	-2.100	-0.786	-0.796	-1.063	-0.697	-0.427	0.149

Table 5.4: Convergence as the basis set with the explicit inclusion of core orbitals approaches completeness for each of the intermolecular terms reported in kcal/mol in the water dimer

stated reasons, the water dimer has been studied extensively by both the theoretical and the experimental communities.[2, 22, 23, 24, 25, 3, 26, 27, 28, 29, 30, 31, 32, 33]

Despite the large amount of both theoretical and experimental evidence, there still exists controversy about which types of intermolecular interactions contribute significantly to the hydrogen bond in the water dimer. There are four main types of intermolecular interactions: electrostatic, polarization, charge transfer and dispersion. Since water has a large dipole moment at 1.85 Debyes, it is expected that the dipole-dipole interaction would be the largest type of intermolecular interaction.[34] Instead of the dipoles being maximally aligned so that the oxygen is in between the two hydrogens, the equilibrium geometry is not in this arrangement, causing the electrostatic interaction to be less than what would be expected from the 1.85 D dipole moment. While the polarization of water is large, it cannot be larger than the energetic contribution from a polarizing bond like Xe-F-, which has a binding energy of -2.43 kcal/mol at the optimized distance of 3.281 Å. The lone pair-lone pair interaction of the water dimer will contribute to some dispersion but much less than the π-stacking interaction seen in the benzene dimer which is -2.78 kcal/mol.[35] The expectation of water is that there should be some charge transfer but not a great amount since the donor and acceptor are both water molecules. Furthermore, in dense bulk water where each water molecule has four hydrogen bonds, every water molecule would be both an electron donor and electron acceptor as opposed to the water dimer where one water molecule is the electron donor and one is the electron acceptor. Therefore, the water dimer is an upper-limit to the amount of charge transfer in each hydrogen bond and would legitimize the use of force-fields for bulk water. Dispersive interactions scale with the size of the molecular system or become large when there are overlapping π-orbitals. However, neither of these situations are present in the water dimer so one would expect the dispersive interaction to be quite small (certainly much less than the ethylene dimer). Therefore, the electrostatic interactions should be the largest and the dispersive interactions the smallest with the other interactions providing significant contributions as well based on these physical justifications.

Attempts have been made to fundamentally understand these interactions. Two recently developed methods give qualitatively different results for the water dimer even though this interaction has been studied since the 1970's. In the Natural Bonding Orbital method, developed by Reed et. al, the main type of stabilization in the water dimer is charge transfer.[36] Using natural energy decomposition analysis (NEDA), which is based on NBOs, also gives a similar result.[37, 38] The NBO method overbinds the dimer by about 2 kcal/mol and both methods calculate the charge transfer contribution to be about -9 kcal/mol, almost double the -5 kcal/mol binding energy of the water dimer. The NEDA method sums to approximately the correct binding energy but includes a fairly large core repulsion term to correct for the large charge term. The NEDA theory was recently extended to density functionals

and applied to the water dimer system in late 2005.[37]

Another recently developed scheme comes from Wu et al. and is a theory that is density-based instead of being based on orbitals.[39] In order to separate the intermolecular terms, this scheme uses the Wu-Yang constrained search algorithm to calculate individual terms via energy subtraction.[40] The advantage of this strategy is that there is less variation in the partitioning based on the type of functional used. Using the PBE functional with a aug-cc-pVQZ basis, the binding energy energy is quite accurate, -4.9 kcal/mol. However, the majority of the binding energy comes from electrostatics at -3.5 kcal/mol with charge transfer being -0.79 kcal/mol and polarization being -0.72 kcal/mol. This method was developed in 2009 and is in direct contradiction to the NEDA method developed in 2005. Even though intermolecular calculations on the water dimer have been occurring for several decades, two recently developed methods arrive at completely different conclusions, showing that this area is still poorly understood. Furthermore, the superposition of fragment densities gives a density that is generally *not* non-interacting V-representable. Therefore the validity of this approach is not yet fully clear.

One of the older schemes, Symmetry Adapted Perturbation Theory (SAPT), is based on treating intermolecular interactions explicitly as a perturbation to the non-interacting Hamiltonian.[41, 42, 43, 44, 45, 46, 47, 48, 49] This theory originally did not separate charge transfer, but recent advances by Stone have alleviated this entanglement.[50, 51, 52] This scheme yields the result that the largest contribution to intermolecular binding is dispersion at -1.91 kcal/mol with all the other intermolecular interactions being around -1 kcal/mol, bringing the total binding energy to -5.23 kcal/mol. Unlike the previous methods discussed, this method comes to the conclusion that all the intermolecular interactions are important and roughly equal with dispersion being the most important.

Another prominent energy decomposition scheme is the Kitaura-Morokuma energy decomposition analysis (EDA) developed in 1971.[53, 9] This EDA scheme has the advantage of being able to separate the four fundamental types of intermolecular interactions whereas the two previously mentioned schemes cannot. In this procedure, the major contribution arises from electrostatic interactions with smaller contributions from dispersion and charge transfer interactions.[54] The contribution from polarization is almost negligible giving an overall physical picture that is somewhat similar to results of SAPT. However, like the NBO-style methods, this scheme has a binding energy of -7 kcal/mol, overbinding the dimer by about 40% similar to the NBO schemes reflecting a small basis RHF calculation.

In the ALMO EDA scheme outlined above, the water dimer is bound mostly by electrostatic forces but all the other interactions are significant as well and can be seen in tables 5.3 and 5.4. The dispersive interactions are the smallest interactions but are only about 0.25 kcal/mol less than the polarization interaction. Therefore we can conclude that all of the interactions that are not the electrostatic interaction are essentially equivalent in strength. These conclusions are similar to those made when the ALMO EDA without correlation was initially applied to the water dimer using the B3LYP density functional.[55] It should be noted that the orbital distortion term for this system is small, essentially meaning that the orbital change from the frozen orbitals to ALMO orbitals coupled with the orbital change from the ALMO orbitals to the canonical orbitals is small. Finally, the dispersive interactions at the frozen level and at the ALMO level are essentially the same in the largest basis set, further emphasizing the point that the correlation energy is fairly invariant to the

different orbitals as is seen in the small orbital distortion term. In terms of comparison to the existing methods, the ALMO EDA method is most similar to the KM EDA, which is expected. However, the ALMO EDA method has the advantage of capturing the MP2 binding energy by definition, as well as variationally separating polarization contribution.

5.5 Conclusions

A new ALMO EDA method at the MP2 level has been proven to match physical intuition quantitatively for the test cases of the ethylene dimer and the He···BeO complex. For the water dimer, the ALMO EDA method predicts that the most significant interaction is the electrostatic interaction. All other interactions were found to be about half of this interaction, being about 1 kcal/mol energetically. The ALMO EDA scheme is also shown to be stable with respect to basis set size and with respect to the dissociation of a bound complex. The use of this partitioning is therefore recommended for characterizing other novel bonding motifs.

Bibliography

[1] Y. LEE, S. KUCHARSKI, and R. BARTLETT, *J. Chem. Phys.* **81**, 5906 (1984).

[2] S. XANTHEAS and T. DUNNING, *J. Chem. Phys.* **99**, 8774 (1993).

[3] K. KIM and K. JORDAN, *J. Phys. Chem.* **98**, 10089 (1994).

[4] P. JURECKA, J. SPONER, J. CERNY, and P. HOBZA, *Phys. Chem. Chem. Phys.* **8**, 1985 (2006).

[5] J. SPONER and P. HOBZA, *Chem. Phys. Lett.* **267**, 263 (1997).

[6] M. SINNOKROT, E. VALEEV, and C. SHERRILL, *J. Am. Chem. Soc.* **124**, 10887 (2002).

[7] R. A. DISTASIO, JR., G. VON HELDEN, R. P. STEELE, and M. HEAD-GORDON, *Chem. Phys. Lett.* **437**, 277 (2007).

[8] S. GRIMME, *J. Chem. Phys.* **118**, 9095 (2003).

[9] K. KITAURA and K. MOROKUMA, *Int. J. Quantum Chem.* **10**, 325 (1976).

[10] T. ZIEGLER and A. RAUK, *Inorg. Chem.* **18**, 1558 (1979).

[11] R. Z. KHALIULLIN, A. T. BELL, and M. HEAD-GORDON, *J. Chem. Phys.* **128**, 184112 (2008).

[12] P. MASLEN and M. HEAD-GORDON, *J. Chem. Phys.* **109**, 7093 (1998).

[13] Y. Shao, L. F. Molnar, Y. Jung, J. Kussmann, C. Ochsenfeld, S. T. Brown, A. T. B. Gilbert, L. V. Slipchenko, S. V. Levchenko, D. P. O'Neill, R. A. DiStasio, Jr., R. C. Lochan, T. Wang, G. J. O. Beran, N. A. Besley, J. M. Herbert, C. Y. Lin, T. Van Voorhis, S. H. Chien, A. Sodt, R. P. Steele, V. A. Rassolov, P. E. Maslen, P. P. Korambath, R. D. Adamson, B. Austin, J. Baker, E. F. C. Byrd, H. Dachsel, R. J. Doerksen, A. Dreuw, B. D. Dunietz, A. D. Dutoi, T. R. Furlani, S. R. Gwaltney, A. Heyden, S. Hirata, C.-P. Hsu, G. Kedziora, R. Z. Khalliulin, P. Klunzinger, A. M. Lee, M. S. Lee, W. Liang, I. Lotan, N. Nair, B. Peters, E. I. Proynov, P. A. Pieniazek, Y. M. Rhee, J. Ritchie, E. Rosta, C. D. Sherrill, A. C. Simmonett, J. E. Subotnik, H. L. Woodcock, III, W. Zhang, A. T. Bell, A. K. Chakraborty, D. M. Chipman, F. J. Keil, A. Warshel, W. J. Hehre, H. F. Schaefer, III, J. Kong, A. I. Krylov, P. M. W. Gill, and M. Head-Gordon, *Phys. Chem. Chem. Phys.* **8**, 3172 (2006).

[14] W. Koch, G. Frenking, J. Gauss, D. Cremer, and J. Collins, *J. Am. Chem. Soc.* **109**, 5917 (1987).

[15] P. Jurecka, J. Sponer, J. Cerny, and P. Hobza, *Phys. Chem. Chem. Phys.* **8**, 1985 (2006).

[16] S. Tsuzuki, K. Honda, T. Uchimaru, M. Mikami, and K. Tanabe, *J. Am. Chem. Soc.* **124**, 104 (2002).

[17] A. Reed, L. Curtiss, and F. Weinhold, *Chem. Rev.* **88**, 899 (1988).

[18] J. U. Reveles, P. Calaminici, M. R. Beltran, A. M. Koster, and S. N. Khanna, *J. Am. Chem. Soc.* **129**, 15565 (2007).

[19] M. Slipchenko, K. Kuyanov, B. Sartakov, and A. Vilesov, *J. Chem. Phys.* **124**, 241101 (2006).

[20] V. Vaida, J. Daniel, H. Kjaergaard, L. Goss, and A. Tuck, *Q. J. R. Meteorol. Soc.* **127**, 1627 (2001).

[21] J. U. Reveles, P. Calaminici, M. R. Beltran, A. M. Koster, and S. N. Khanna, *J. Am. Chem. Soc.* **129**, 15565 (2007).

[22] R. Barnett and U. Landman, *Phys. Rev. B* **48**, 2081 (1993).

[23] F. Sim, A. Stamant, I. Papai, and D. Salahub, *J. Am. Chem. Soc.* **114**, 4391 (1992).

[24] B. Marten, K. Kim, C. Cortis, R. Friesner, R. Murphy, M. Ringnalda, D. Sitkoff, and B. Honig, *J. Phys. Chem.* **100**, 11775 (1996).

[25] X. Wu, M. Vargas, S. Nayak, V. Lotrich, and G. Scoles, *J. Chem. Phys.* **115**, 8748 (2001).

[26] L. Curtiss and J. Pople, *J. Mol. Spectrosc.* **55**, 1 (1975).

[27] K. Asmis, N. Pivonka, G. Santambrogio, M. Brummer, C. Kaposta, D. Neumark, and L. Woste, *Science* **299**, 1375 (2003).

[28] T. Dyke, K. Mack, and J. Muenter, *J. Chem. Phys.* **66**, 498 (1977).

[29] L. Curtiss, D. Frurip, and M. Blander, *J. Chem. Phys.* **71**, 2703 (1979).

[30] K. Liu, J. Cruzan, and R. Saykally, *Science* **271**, 929 (1996).

[31] F. Huisken, M. Kaloudis, and A. Kulcke, *J. Chem. Phys.* **104**, 17 (1996).

[32] F. Keutsch and R. Saykally, *Proc. Natl. Acad. Sci. U. S. A.* **98**, 10533 (2001).

[33] E. Bieske and O. Dopfer, *Chem. Rev.* **100**, 3963 (2000).

[34] S. Clough, Y. Beers, G. Klein, and L. Rothman, *J. Chem. Phys.* **59**, 2254 (1973).

[35] M. Sinnokrot, E. Valeev, and C. Sherrill, *J. Am. Chem. Soc.* **124**, 10887 (2002).

[36] A. Reed, F. Weinhold, L. Curtiss, and D. Pochatko, *J. Chem. Phys.* **84**, 5687 (1986).

[37] E. Glendening, *J. Phys. Chem. A* **109**, 11936 (2005).

[38] E. Glendening and A. Streitwieser, *J. Chem. Phys.* **100**, 2900 (1994).

[39] Q. Wu, P. W. Ayers, and Y. Zhang, *J. Chem. Phys.* **131**, 164112 (2009).

[40] Q. Wu and W. Yang, *J. Chem. Phys.* **118**, 2498 (2003).

[41] S. Rybak, B. Jeziorski, and K. Szalewicz, *J. Chem. Phys.* **95**, 6576 (1991).

[42] T. Korona, H. Williams, R. Bukowski, B. Jeziorski, and K. Szalewicz, *J. Chem. Phys.* **106**, 5109 (1997).

[43] R. Bukowski, J. Sadlej, B. Jeziorski, P. Jankowski, and K. Szalewicz, *J. Chem. Phys.* **110**, 3785 (1999).

[44] H. Williams, K. Szalewicz, B. Jeziorski, R. Moszynski, and S. Rybak, *J. Chem. Phys.* **98**, 1279 (1993).

[45] A. Hesselmann, G. Jansen, and M. Schutz, *J. Chem. Phys.* **122**, 014103 (2005).

[46] A. Misquitta, R. Podeszwa, B. Jeziorski, and K. Szalewicz, *J. Chem. Phys.* **123**, 214103 (2005).

[47] R. Moszynski, P. Wormer, B. Jeziorski, and A. Vanderavoird, *J. Chem. Phys.* **101**, 2811 (1994).

[48] A. Milet, R. Moszynski, P. Wormer, and A. van der Avoird, *J. Phys. Chem. A* **103**, 6811 (1999).

[49] R. Moszynski, T. Heijmen, and B. Jeziorski, *Mol. Phys.* **88**, 741 (1996).

[50] M. Hodges and A. Stone, *Mol. Phys.* **98**, 275 (2000).

[51] A. J. Stone and A. J. Misquitta, *Chem. Phys. Lett.* **473**, 201 (2009).

[52] A. Stone, *Chem. Phys. Lett.* **211**, 101 (1993).

[53] K. Morokuma, *J. Chem. Phys.* **55**, 1236 (1971).

[54] D. G. Fedorov and K. Kitaura, *J. Comput. Chem.* **28**, 222 (2007).

[55] R. Z. Khaliullin, A. T. Bell, and M. Head-Gordon, *Chem.-Eur. J.* **15**, 851 (2009).

Chapter 6

Conclusion

6.1 Observations on the MP2 energy decomposition

Normally a recap of the enclosed chapter would be in this space but I would like to make some observations based on some unpublished work for the ALMO EDA method discussed in the previous chapter. One way used to describe the DIM method involves using excitation diagrams such as figure 5.1. Therefore, one might assume that one viable strategy in order to decompose the energy is to partition the MP2 energy into the different types of excitations instead of taking the computationally more difficult step of diagonalizing the pair energy matrix. However, we tried to implement this type of scheme with poor results. Specifically, we used a orthogonal occupied space together with a non-orthogonal virtual space. The types of interactions were split into the number of centers and the number of electrons transferred from one fragment to another fragment. For the water dimer there are only four types of excitations: one center zero electron (MP2 per fragment), two center zero electron (dispersive), one electron two center (ionic/charge transfer), and two center two electron (BSSE and dispersive exchange). The expectation would be that the one center zero electron excitation should be the largest in magnitude followed by two center zero electron, then the one electron two center, and finally the two center two electron. However when we did this type of decomposition we found that the ionic interaction was orders of magnitude larger than the dispersive interactions and in terms of actual contribution the ionic interaction was -12 kcal/mol. This interaction is almost the three times the binding energy of the water dimer. Clearly this approach is deeply flawed and it is necessary to conclude that this partitioning is invalid probably because of the non-orthogonal virtual space. One must be careful when applying principles used in canonical theories to schemes which involve non-orthogonal spaces.

6.2 Future Work

For the distannyne system, there is still an issue of why the experimental system adopts the **M**-type geometry (defined as the multiply-bonded motif) when the smaller model systems adopt the **S**-type geometry (defined as the singly-bonded motif). Based on some preliminary unpublished calculations, it was discovered that there might be some kind of intramolecu-

lar interaction between one of the periphery phenyl rings and the central π-system in the distannyne. However, there currently is not a satisfactory method to quantify this type of through-space interaction, likely dispersive. This system could be a large challenging case for an intramolecular energy decomposition scheme.

In chapter 3 the implications of breaking N-representability were discussed and the effects of this on physical properties were quantified. However, this problem should equally affect not just first-order properties but also second-order properties like IR frequencies. In fact some preliminary calculations found that many large errors for MP2 frequencies were due to the fact the N-representability was not maintained. It would then be logical to create a diagnostic for the MP2 method in order to warn the user when MP2 properties may be unreliable. However, there was not a large enough database of difficult problems to create reasonable cutoffs for what one would consider to be reliable, questionable, and incorrect. It is likely that if one were to do an extensive literature search and have over 150 examples, then the appropriate demarkations can be made.

Future work in the field of solitons could be quite varied. One possible project would be to investigate the electronic structure differences between the neutral soliton, which is very difficult to localize, and the positive soliton which is localized even in HF theory. Also an investigation into the effects of including a counter-ion like Li^+ and how the local charge would affect the localization in the neighboring chain would be interesting. Furthermore, one does not need to be limited to the polyacetylene chain and one should investigate smaller polyacenes or polythiols.

Immediate future work regarding the ALMO EDA scheme would be to first implement a fast algorithm for diagonalizing the pair energy matrix. Currently, the occupied space is orthogonal but the test code does not take advantage of this fact. Therefore the current code scales to the sixth order with the size of the largest fragment. Theoretically one should be able to reduce this scaling all the way down to possibly third order overall. Besides a fast implementation, this scheme can be extended to methods that include more accurate wave-function based approximations to the correlation energy, namely the coupled cluster methods. Cluster operators would need to be constructed that only included dispersive excitations, only on fragment excitations, and then all excitations. The extension of this theory to coupled cluster is promising because the inclusion of T_1 operator will provide approximate orbital invariance which is not present in MP2 theory. Therefore the orbital distortion term will become very small, which is desirable as they do not have a physical origin.